REPORT DOCUMENTATION PAGE

Form Approved
OMB No. 0704-0188

2. REPORT DATE	3. REPORT TYPE AND DATES COVERED
May 10, 1991	THESIS/[redacted]

4. TITLE AND SUBTITLE
An Aerocapture Attitude Control Systems Incorcporating Robustness and Vehicle Parameter Idéntification

5. FUNDING NUMBERS

6. AUTHOR(S)
James R. Bell, Captain

7. PERFORMING ORGANIZATION NAME(S) AND ADDRESS(ES)
AFIT Student Attending: Massachusetts Institute of Technology

8. PERFORMING ORGANIZATION REPORT NUMBER
AFIT/CI/CIA- 91-074

9. SPONSORING / MONITORING AGENCY NAME(S) AND ADDRESS(ES)
AFIT/CI
Wright-Patterson AFB OH 45433-6583

10. SPONSORING / MONITORING AGENCY REPORT NUMBER

11. SUPPLEMENTARY NOTES

12a. DISTRIBUTION / AVAILABILITY STATEMENT
Approved for Public Release IAW 190-1
Distributed Unlimited
ERNEST A. HAYGOOD, Captain, USAF
Executive Officer

12b. DISTRIBUTION CODE

13. ABSTRACT *(Maximum 200 words)*

14. SUBJECT TERMS

15. NUMBER OF PAGES
188

16. PRICE CODE

17. SECURITY CLASSIFICATION OF REPORT	18. SECURITY CLASSIFICATION OF THIS PAGE	19. SECURITY CLASSIFICATION OF ABSTRACT	20. LIMITATION OF ABSTRACT

An Aerocapture Attitude Control System Incorporating Robustness and Vehicle Parameter Identification

by

James R. Bell

Submitted to the Department of Aeronautics and Astronautics on May 10, 1991, in partial fulfillment of the requirements for the Degree of Master of Science.

ABSTRACT

A candidate attitude control system design is presented for an aerocapture vehicle capable of a wide range of mass properties. The control system consists of three main elements: a robust control law based on the nonlinear sliding mode control techniques, a linear programming jet selection algorithm adaptable to changing mass properties, and a mass property identification algorithm based on an extended Kalman filter design. The mass property identification algorithm is capable of accurately estimating unknown and changing vehicle mass properties. The estimated mass properties are fed back to the control law and the jet selection algorithm, extending the range of mass properties for which the control system is robust. A principal contribution of this thesis is the integration of these main elements into a viable attitude control system.

The control system is demonstrated for the Aeroassist Flight Experiment (AFE) vehicle via computer simulation.

Thesis Supervisor: Professor Walter M. Hollister
Title: Professor of Aeronautics and Astronautics, M.I.T.

Technical Supervisors: Edward V. Bergmann
Control and Dynamics Division
Charles Stark Draper Laboratory, Inc.

Lester L. Sackett
Control and Dynamics Division
Charles Stark Draper Laboratory, Inc.

CSDL-T-1085

AN AEROCAPTURE ATTITUDE CONTROL SYSTEM INCORPORATING ROBUSTNESS AND VEHICLE PARAMETER IDENTIFICATION

by
James R. Bell

June 1991

Master of Science Thesis
Massachusetts Institute of Technology

The Charles Stark Draper Laboratory, Inc.
555 Technology Square, Cambridge, Massachusetts 02139-3563

An Aerocapture Attitude Control System Incorporating Robustness and Vehicle Parameter Identification

by

James R. Bell

B.S., Electrical Engineering
U.S. Air Force Academy
(1986)

Submitted to the
Department of Aeronautics and Astronautics
in Partial Fulfillment of the Requirements
for the Degree of

Master of Science

at the

Massachusetts Institute of Technology

June, 1991

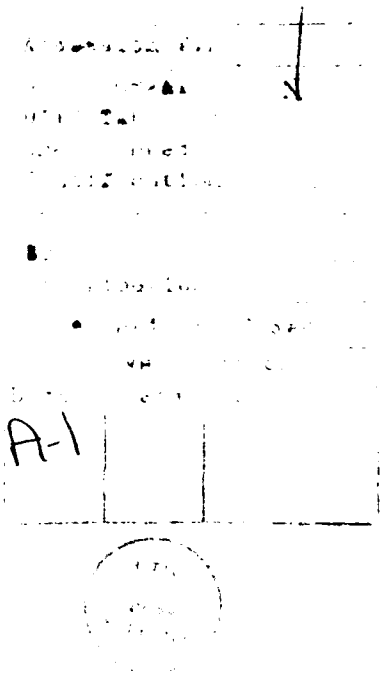

Signature of Author James R. Bell
Department of Aeronautics and Astronautics

Certified by Walter M. Hollister
Professor Walter M. Hollister, Thesis Advisor
Department of Aeronautics and Astronautics

Approved by Edward V. Bergmann
Edward V. Bergmann, Technical Supervisor
The Charles Stark Draper Laboratory, Inc.

Approved by Lester Sackett
Lester L. Sackett, Technical Supervisor
The Charles Stark Draper Laboratory, Inc.

Accepted by Harold Y. Wachman
Professor Harold Y. Wachman, Chairman
Department Graduate Committee

This report was prepared at The Charles Stark Draper Laboratory, Inc. under IR&D/CSR funding. Publication of this report does not constitute approval by The Charles Stark Draper Laboratory, Inc. or the Massachusetts Institute of Technology of the findings or conclusions contained herein. It is published solely for the exchange and stimulation of ideas.

I hereby assign my copyright of this thesis to The Charles Stark Draper Laboratory, Inc., Cambridge, Massachusetts.

James R. Bell

James R. Bell, Captain, USAF

Permission is hereby granted by The Charles Stark Draper Laboratory Inc. to the Massachusetts Institute of Technology to reproduce any or all of this thesis.

Table of Contents

List of Figures

List of Tables

spacecraft/payload mass properties. The second option is a control system that is robust over a smaller range of the possible mass properties but capable of estimating the mass properties and adapting to these changing estimates.

As a simple example from another type of control problem with similar demands, consider a robot arm capable of carrying objects weighing anywhere from 1 to 1000 lbs. The first approach to designing a controller for this robot arm may be a design robust to this full range. Though such a design may be possible, performance of this design may not be as accurate or timely as desired when attempting to control the arm with an object near one of the weight extremes. A more attractive approach may be a design robust only to a range of about 20 lbs but capable of estimating the weight to well within a few pounds. Suppose this approach were used for control of a robot arm carrying a mass of 953 lbs. If the control system could estimate the weight at 950 lbs, it could adapt to this estimate and provide robust control over a 20 lb range centered at this estimate. With the control system required to be robust over a much smaller range, it effectively has a more precise model of the process to be controlled and can, therefore, provide more precise and timely control.

This thesis employs the strategy of combining parameter identification with robustness in design of an attitude control system for a spacecraft with a wide range of mass properties performing an aerocapture maneuver in an environment with many unknowns. The control law, the first element of the attitude control system, is robust to a range of system unknowns smaller than the full possible

Chapter 1

Introduction

1.1 Motivation

When designing a control system for a particular process, a control system engineer must work with a mathematical model of that process. If the model cannot accurately predict the behavior of the process, design of an adequate control system may not be possible. The term "robustness" refers to a control system's exhibited degree of immunity to system uncertainties or changes. Control systems can be designed with a degree of robustness to these system uncertainties. A tradeoff, however, usually exists between the amount of robustness and the performance of the control system. Control systems designed to be robust over a great range of system uncertainties typically can't provide the desired accuracy or responsiveness. Much more accurate and efficient control can be provided when there is a small range of system unknowns.

Many times it is not possible to have a highly accurate mathematical model of the system to be controlled. For example, the mathematical model of a spacecraft capable of carrying varying payloads depends greatly on the mass properties of the unknown payload. There are two options for design of a control system for such a spacecraft with a wide range of possible payloads. The first is a control system robust over the full range of the combined

range. A parameter identification scheme, however, is employed to determine changes in these parameters real-time, and the control system is capable of adapting to the changing parameter estimates. This combination of robustness and parameter identification effectively extends the range of system unknowns for which attitude control is possible.

1.2 Mission Description

As a spacecraft approaches a planet on a hyperbolic trajectory, it must effect a large velocity reduction (ΔV) in order to enter a desired orbit about the planet. The usual method for performing such a ΔV has been to use rocket firing. Unfortunately, the required firing forces the spacecraft to carry a large mass of propellent for this purpose.

Studies [1] have investigated using an aeroassisted maneuver, called aerocapture, to generate most of the ΔV required to obtain a desired orbit. With aerocapture, the spacecraft descends into the upper portions of the planetary atmosphere as it passes by and uses the aerodynamic forces generated to reduce velocity. Ideally, the vehicle exits the atmosphere with the velocity required to reach a desired orbital altitude. Once the target altitude is reached, a comparatively small rocket firing is required to obtain the desired orbit characteristics (e.g., circularization).

The smaller propulsive ΔV required for a spacecraft employing aerocapture reduces the amount of fuel needed, allowing for a larger payload or smaller vehicle for the same mission. Even considering the added weight of an aeroshell and the thermal protection system

needed during atmospheric flight, the reduced weight of fuel can result in as much as twice the payload capacity of a similar all-propulsive vehicle [2]. This benefit has made aerocapture a likely element of many future missions.

Aerocapture at Mars has been advocated for future Martian missions along with Earth aerocapture for missions returning to Earth from high Earth orbits, the moon, and Mars [3]. To underscore the interest in aerocapture, the December 1990 report from the Advisory Committee on the Future of the U.S. Space Program headed by Mr. Norman Augustine recommends pursuing the technology of aerocapture [4]. Also, on March 12, 1991, Japan's Hiten satellite became the first spacecraft to demonstrate an Earth aerocapture after circling the Moon in 1990 [5].

1.3 Attitude Control System Requirements

The main disadvantage of an aerocapture maneuver relative to an all-propulsive maneuver is the difficulty in properly guiding and controlling the vehicle while in the atmosphere. Errors in the final orbit are highly sensitive to atmospheric exit conditions. Small errors in the exit velocity or flight path angle could cause large errors in the final orbit. Extra fuel would then be needed to correct to the desired orbit, reducing the original benefit of the aerocapture maneuver. Aerocapture guidance and control systems must be robust to a wide range of uncertainties to avoid these exit errors.

In simple terms, guidance determines where a vehicle must go in order to meet mission requirements, while control determines what the vehicle must do to get there. For the purposes of this

thesis, guidance is considered to be the determination of the commands needed to follow the trajectory required to meet the objectives of the aerocapture mission. Since the trajectory is dependent on the aerodynamic lift and drag acting on the vehicle, guidance consists of the calculation of the vehicle attitude needed to generate the required aerodynamic forces. Attitude control is the determination of how to employ the spacecraft's control actuators (e.g., jets, aerosurfaces, and control moment gyros) in a manner to achieve the attitude commanded by guidance. This thesis addresses the attitude control problem.

An aerocapture guidance law must be capable of guiding a vehicle through an atmosphere to ensure it exits the atmosphere with the proper energy to reach a desired orbit. Uncertainties that a guidance law must accommodate include atmospheric density fluctuations and aerodynamic prediction uncertainties. At Earth, density fluctuations of up to 30% off the nominal values can be expected [6]. At planets with lesser known atmospheres, such as Mars, larger fluctuations are considered possible. Little data is currently available, but densities ranging from -50% to +100% off present Martian density models are considered likely. Faulty guidance could cause a spacecraft to exit the atmosphere without the proper energy to reach the target orbit altitude. At one extreme, diving too deep could reduce the energy to the point that the spacecraft would not be able to exit, sending the vehicle crashing into the planet's surface. At the other extreme, going too shallow might cause the spacecraft to skip out of the atmosphere with too much energy to be captured into orbit about the planet.

Most current aerocapture guidance algorithms use vehicle bank angle ϕ as the only control (angle-of-attack, α, and sideslip angle, β, are assumed constant) [2,7,8,9]. For the purposes of this thesis, this set of angles (i.e., ϕ, α, and β) is called the "velocity angles". These angles are used to describe the attitude of the vehicle with respect to a frame containing the velocity vector as defined in Appendix A. In-plane guidance generates bank angle commands that vary the direction of the lift vector in order to fly a reference atmospheric trajectory which allows the spacecraft to reach the desired orbital altitude. Out-of-plane guidance periodically commands bank angle reversals in order to use out-of-plane lift to maintain the vehicle in the desired orbital plane. Future guidance systems may also vary angle-of-attack to regulate the total amount of lift, allowing in-plane guidance to be performed without generating any undesired out-of-plane lift. For the purpose of this thesis, only bank modulation will be considered.

The task of the attitude control system, then, is to implement the bank commands and periodic reversals while maintaining trim α and β. The attitude control system must perform this task in the presence of uncertainties. Variations in the vehicle mass properties (e.g., total mass, inertia, and location of the center of mass) can have a great impact on the effectiveness of control actuators. For generic "bus" vehicles capable of carrying and delivering several types of payloads, control must be performed over a wide range of mass properties. Rather than develop or modify a control system for each payload, a design capable of controlling over this range of mass properties is highly desirable. In addition, properties of the control

actuators themselves (e.g., jet thrust levels and directions, aerodynamic properties of control aerosurfaces) and atmospheric conditions (e.g., density) can vary, adding to the uncertainties with which the control system must contend.

1.4 Prior Work

Several guidance laws have been developed for two particular aerocapture missions [2,7,8,9]. Considerable work has gone into developing a guidance system for NASA's Aeroassist Flight Experiment (AFE). The AFE, expected to be flown in the later 1990's, consists of a small, blunt (lift-to-drag ratio ≈ 0.3) vehicle, sketched in

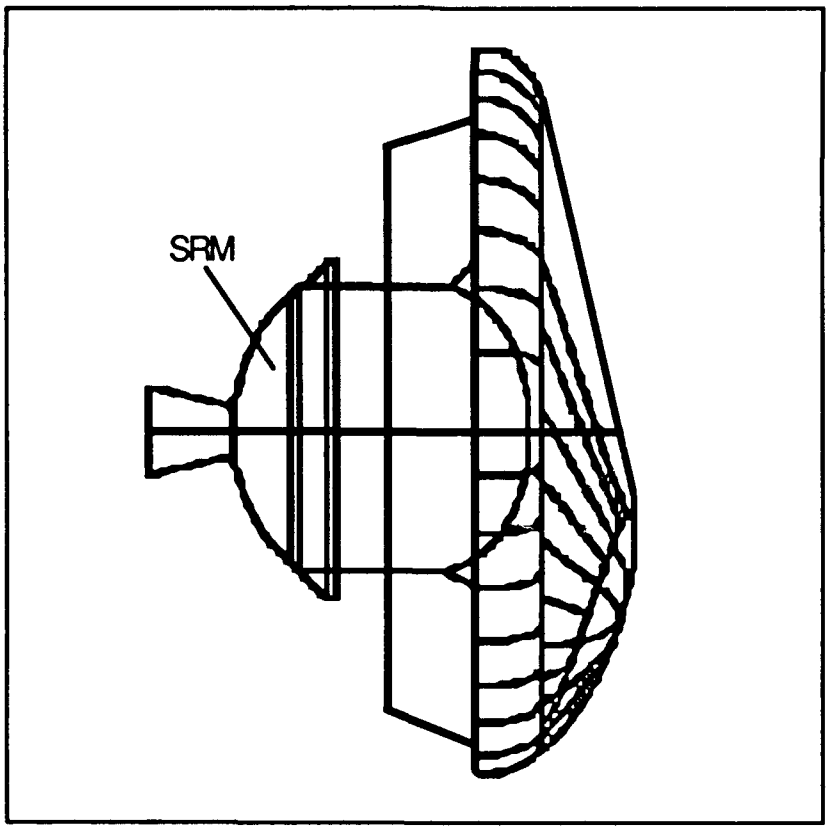

Figure 1.1. AFE Vehicle

Figure 1.1, to be deployed from the Space Shuttle with the objective of simulating a vehicle transferring from geosynchronous Earth orbit to a low Earth orbit using aerocapture. Once deployed from the Shuttle's cargo bay, the AFE vehicle will be propelled into the Earth's atmosphere by a solid rocket motor (SRM) burn, achieving entry interface conditions matching those of a vehicle returning from geosynchronous Earth orbit. After the atmospheric pass, the AFE orbit will be circularized with another rocket burn, allowing the vehicle to be retrieved by the Space Shuttle [10]. Figure 1.2 outlines the main events during the AFE flight.

The other mission that has received considerable attention is the Mars Rover Sample Return (MRSR) mission, studied during 1986-89 [11,12,13,14,15]. In this mission, an orbiter, lander, and rover, contained in an aeroshell, would aerocapture into a Martian orbit from which a landing, sample collection, and sample return to Earth would be accomplished. Since the president's speech on July 20, 1989 calling for a human expedition to Mars, the MRSR mission has been set aside. It is likely, however, that any resulting Martian exploration missions will include many of the elements of the MRSR mission, including aerocapture [4].

While there has been considerable effort in the development of aerocapture guidance laws, little effort has been focused on aerocapture attitude control system design. A simple system consisting of a proportional control law and a table look-up jet selection procedure has been developed for the AFE mission [16]. This attitude control system is adequate for the one-time, tightly

constrained AFE experiment where vehicle mass and actuator properties, as well as initial entry conditions, are well defined. Such a simple attitude control system, however, cannot provide the robustness required for a mission with vehicle and environmental properties varying over a wide range.

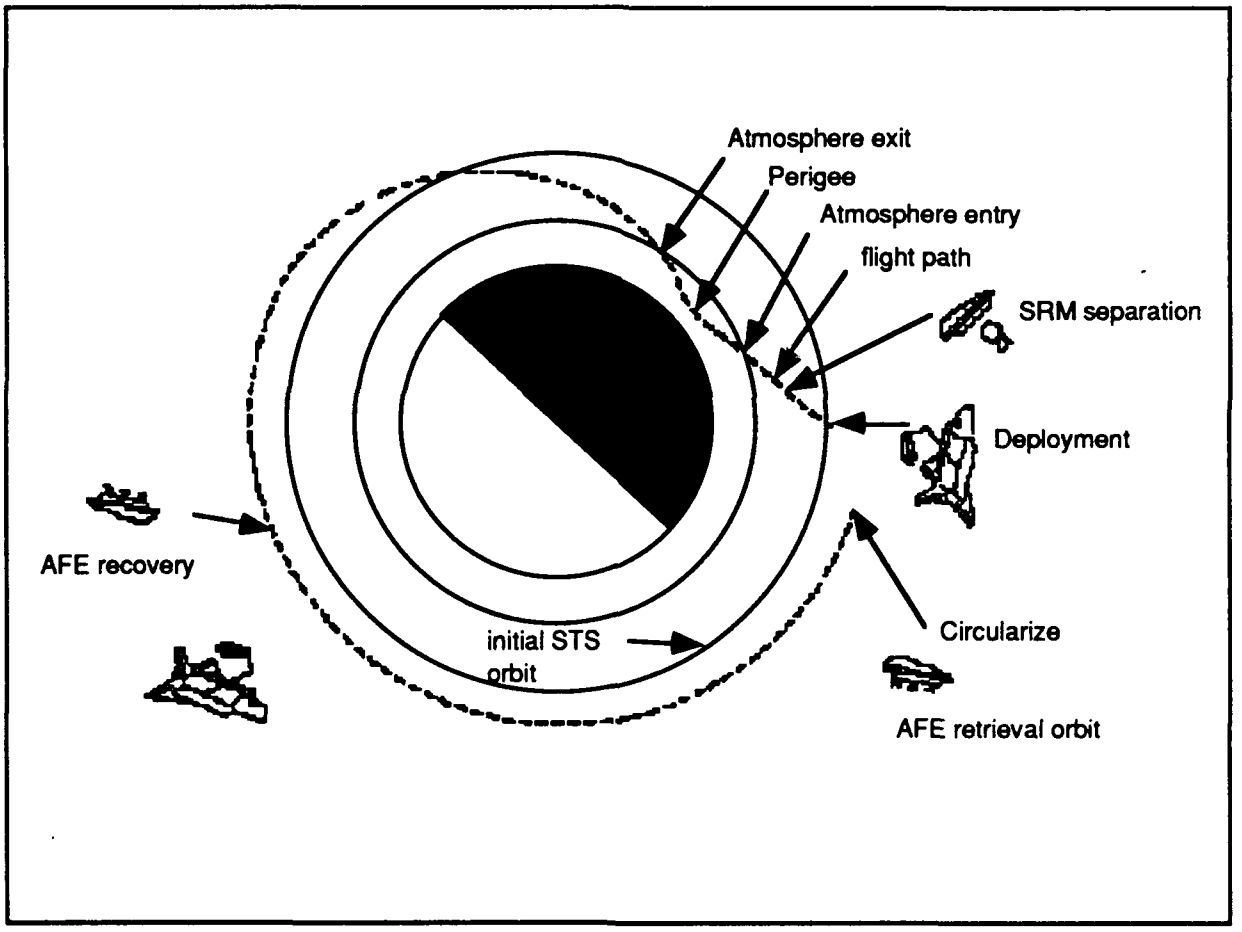

Figure 1.2. AFE Mission

1.5 Thesis Goal

1.5.1 Goal

The goal of this thesis is an attitude control system design applicable to aerocapture and capable of meeting some of the requirements outlined in Section 1.3 above. A desirable ultimate goal is a generic attitude control system for use with any aerocapture mission (e.g., at Earth or at Mars, with varying ranges of the atmospheric unknowns affecting the vehicle aerodynamics) and any vehicle (e.g., high vs. low lift-to-drag ratio, with jets and/or aerosurface control actuators, capable of carrying a single payload or a wide range of payloads). It is also desired that the system be able to control both variable bank angle and angle-of-attack and have the capability to identify any and all of the following: failed jets, reduced or misaligned jet thrust, changing vehicle mass properties, and changes in aerosurface effectiveness due to the aerosurface itself or to changes in atmospheric conditions.

This thesis addresses a subset of the ultimate goal. It develops a candidate attitude control system capable of performing attitude control during an aerocapture maneuver for a vehicle with a wide range of possible mass properties. Actuator properties (e.g., thrust levels and directions) are considered constant and known. Since the AFE vehicle and mission are presently the best defined for an aerocapture mission, the candidate control system has been designed for the AFE mission scenario (i.e., Earth aerocapture) and for a vehicle similar to the actual AFE vehicle but with a wider range of

possible mass properties. It is assumed that control is possible using the AFE's reaction control system (RCS) jets, the only type of control actuator employed for the AFE.

1.5.2 Assumptions

The following is a summary of the basic assumptions used throughout this thesis.

1. The control system is designed to provide attitude control for a vehicle performing an Earth aerocapture.

2. The attitude control system must implement bank angle commands while maintaining trim angle-of-attack and sideslip.

3. Control to within 2 degs of the commanded velocity angles is desired [17].

4. The vehicle to be controlled is rigid.

5. The aerocapture vehicle to be controlled has the same control actuators (i.e., RCS jets only) and aerodynamic properties as the AFE vehicle.

6. The aerocapture vehicle is capable of a much wider range of mass properties than the AFE vehicle.

7. Jet locations and thrust vectors are constant and known.

8. Sensors on the vehicle provide ideal, lag-free measurements of the vehicle attitude and rates.

9. The aerodynamic torques experienced by the vehicle during the aerocapture maneuver are small compared to the torques applied by the RCS jets.

1.5.3 Intended Contributions

The intended contributions of this thesis can be summarized as follows:

1. The development of a robust control law for attitude control of a vehicle with variable mass properties.

2. The combination of the control law with an adaptable jet selection algorithm to create a control system robust to a given range of mass properties but which is smaller than the full range possible.

3. The integration of a real-time mass property identification algorithm to extend the range of mass properties for which the candidate control system is robust.

1.6 Thesis Overview

The remaining chapters describe the candidate attitude control system design and its performance during computer simulation testing. Chapter 2 provides a system overview of the candidate design. The designs of the three main elements of the attitude control system, the control law, the actuator selection algorithm, and the mass property identification algorithm, are outlined in Chapters 3, 4, and 5, respectively. Chapter 6 then describes the integration of the main elements into a functional attitude control system.

Testing of the candidate design is accomplished using a 6 degree-of-freedom (6-DOF) FORTRAN computer simulation of an Earth aerocapture. This simulation and the testing results are discussed in Chapter 7.

The conclusions and contributions drawn from this research are summarized in Chapter 8 along with recommendations for future research.

Chapter 2

System Overview

2.1 Control System Structure

The candidate attitude control system consists of three main elements: the control law, the actuator selection algorithm, and the parameter identification algorithm as depicted in Figure 2.1.

The first element, the 3-dimensional attitude control law, compares the commanded velocity angles from the guidance law to the estimated velocity angles and determines the angular accelerations required to implement the guidance commands. It is designed to exhibit only the degree of robustness required for control over the range of possible values of the inertia matrix for the actual AFE vehicle as presented in Appendix B.

The required angular accelerations from the control law are the commanded inputs to the second main element, the actuator selection algorithm. This algorithm uses the control system's knowledge of the vehicle properties to determine the effectiveness of each actuator, and then calculates the actuator activity required to generate the commanded accelerations. Jet duty cycles and, for a more general design, aerosurface deflections are commanded by the actuator selection and implemented by the associated actuators.

The vehicle dynamics are determined by the moments and

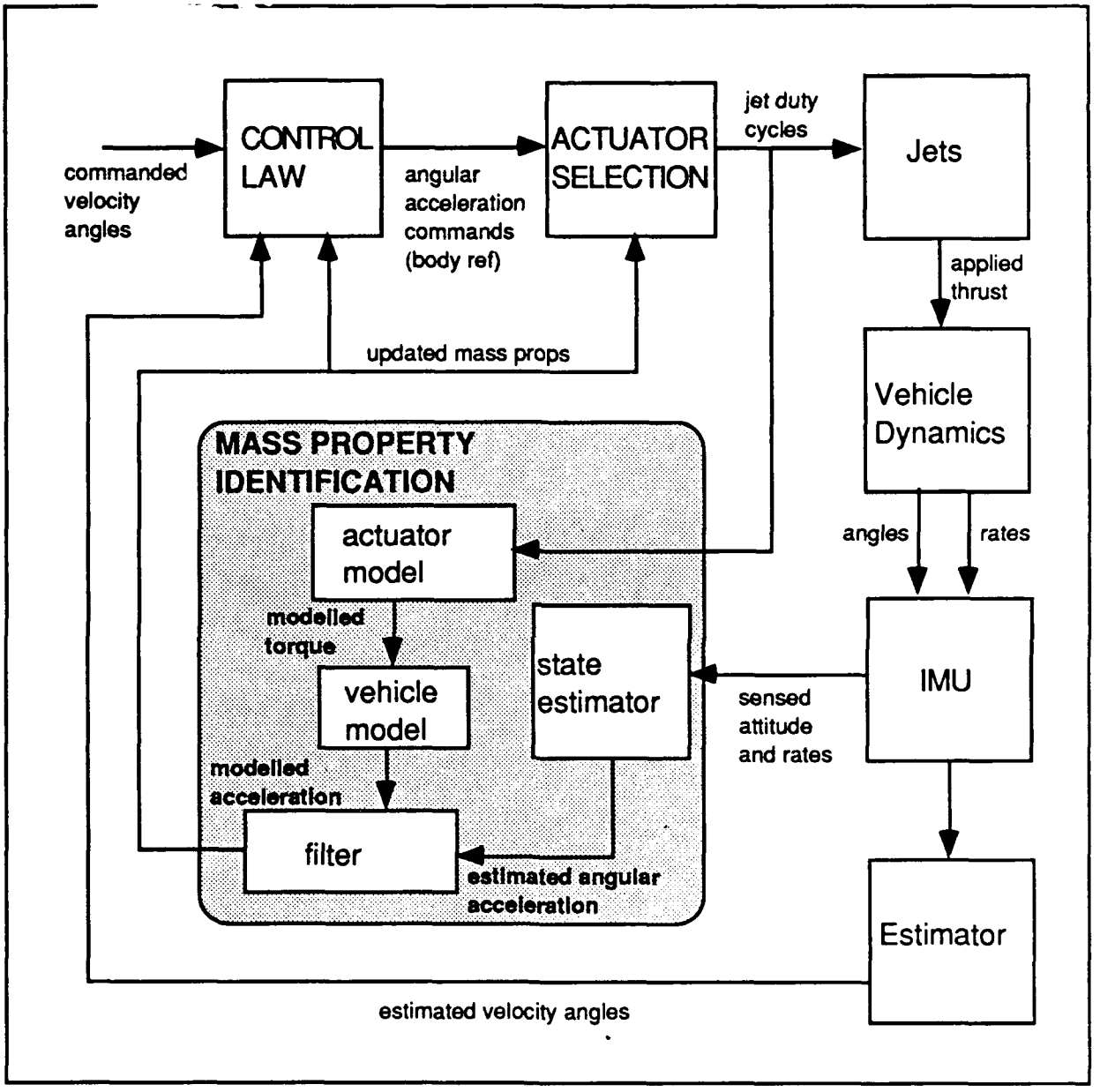

Figure 2.1. Aerocapture Control System Structure

forces acting on the vehicle. These moments and forces consist of those applied by the control system and those from the environment.

Lag-free measurements of the vehicle's attitude and rates are made by sensors in the vehicle's inertial measurement unit (IMU). The measured attitude is used to generate the velocity angle estimates used by the control law while the measured angular rates are used by the third main element of the control system, the mass property identification algorithm. This algorithm compares the vehicle's angular rate changes, determined from the IMU rate measurements, to the anticipated rate changes due to actuator activity predicted by models of the vehicle and its control actuators. This comparison is used to produce estimates of unknown and changing mass properties. Updated estimates are then supplied to the control law and the actuator selection algorithm, increasing the range of mass properties for which the attitude control system is usable.

The major elements of the attitude control system developed here have been adapted from previous works. The control law, the first main element, is a robust, nonlinear design based on the sliding mode control techniques outlined in references [18,19]. A variation of the actuator selection algorithm used previously for blended actuator selection [20,21] is used to create a jet selection algorithm capable of adjusting to changing mass property estimates. Mass property identification is performed using the second order, nonlinear filter design developed in references [22,23,24]. The main contribution of this thesis is the adaptation and integration of the

existing elements to form a viable attitude control system design with application to aerocapture.

2.2 Control Law

The candidate control system requires a control law that can determine the angular accelerations needed by the vehicle to track the velocity angles commanded by the guidance. Since the vehicle dynamics are affected by variable vehicle mass properties and atmospheric conditions, the control law must be robust to the anticipated ranges of these parameters.

Linear control design strategies such as H_∞, H_2, and μ synthesis [25,26,27] can be used for designing robust control laws. Sliding mode control, however, was chosen for this design. The dynamics of a spacecraft are inherently nonlinear. With sliding mode control, an extensive, linearized system model is not required. As long as bounds on parametric unknowns and unmodelled dynamics are known, a relatively simple, nonlinear model is all that's required. Sliding mode control then provides precise control robust over the range of bounded unknowns.

2.3 Actuator Selection

Once the control law calculates the angular accelerations required for the vehicle to implement the guidance commands, the actuator selection algorithm must determine which control actuators to activate, and to what extent, in order to generate the commanded accelerations. With only RCS jets available to the candidate system, the required jet selection algorithm must determine which jets to

fire, and with what duty cycle, to give the aerocapture vehicle the commanded angular accelerations.

In order for an actuator selection algorithm to perform its task, it must have accurate knowledge of the effectiveness of each of its control actuators. The effectiveness of an actuator depends on many things including the location of the center of mass, the moments of inertia of the vehicle, the location and orientation of the actuator, and the level of activity (e.g., amount of thrust of a jet) provided by the actuator.

For the one-time AFE mission with well defined mass and actuator properties, the effectiveness of each jet is calculated a priori and jet selection is performed via table look-up. For example, if the commanded roll acceleration is +5 deg/sec^2, then jets #1 and #2 are fired during the next time step. If the commanded yaw acceleration is -0.5 deg/sec^2, then jet #8 is fired (see Figure 4.1 in Chapter 4 for jet numbering and locations). A table look-up selection algorithm like this which uses a priori effectiveness calculations cannot always perform its task of implementing commanded angular accelerations when vehicle properties are not initially known or change during a mission. For the AFE vehicle with nominal moment arms of a little under 4 feet, a 2 foot change in the center of mass location greatly changes the effectiveness of the RCS jets. Without a method of identifying such a change, the table look-up jet selection algorithm must choose jet firings based on erroneous measures of jet effectiveness. Control would be inefficient at best, with the possibility of being unstable. For a mission where vehicle properties are unknown a priori or can change significantly, an actuator

selection algorithm that can adapt to the changing properties during the mission is required.

Several methods are available for design of an adaptable actuator selection algorithm. Included among those available are the dot product, control axes, pseudo inverse, and linear programming methods outlined in reference [28]. Being the most fuel optimal and adaptable of these methods, the linear programming approach was chosen to perform the actuator selection task for this thesis. This approach also has the benefit of having already been successfully flight tested in an experimental jet selection algorithm for the Space Shuttle on missions STS-51G (June 1985) and STS-61B (November 1985).

2.4 Parameter Identification

In order for the actuator selection algorithm to adapt to changing vehicle parameters and to increase the overall robustness of the attitude control system, a parameter identification algorithm capable of estimating and updating changing or unknown vehicle parameters is required.

For this thesis, the jet properties, such as thrust level and direction, are considered fixed and known, but the vehicle mass properties (i.e., the vehicle inertia matrix and location of the center of mass) are assumed to be initially unknown and subject to change. Mass property identification and estimation is accomplished using a second-order, nonlinear filter design resembling an extended Kalman filter [23,24]. The algorithm uses a model of the dynamics of a rigid spacecraft to predict the output of rate gyros and accelerometers due

to jet firings. Comparing its predictions to the measured output, revisions of mass property estimates are made.

This algorithm will be used to estimate the AFE mass properties using data gathered in flight. These estimates will be compared to actual measurements of the mass properties made on the ground prior to and after the AFE mission. Because of this association with the AFE, this algorithm is the chosen approach for mass property identification for this problem.

Chapter 3

Control Law Design

3.1 Introduction

The concepts of sliding mode control are used in designing a robust, nonlinear control law which determines the angular accelerations required to track the bank angle trajectory commanded by the guidance law while maintaining trim α and β. This chapter covers the development of this first element of the candidate attitude control system. The nonlinear stability analysis theory which provides the basis for sliding mode control is presented in Section 3.2. Section 3.3 develops the basic sliding mode concepts through the design of a control law for a simple single-input, single-output system. A further example of sliding mode control design for the single-input, single-output case is outlined in Section 3.4, while Section 3.5 describes the design of the sliding mode attitude control law for the multi-input, multi-output aerocapture vehicle.

3.2 Fundamentals of Lyapunov Theory

Sliding mode control originated from the stability theory for nonlinear systems introduced by the Russian mathematician A.M. Lyapunov in the late 1800's. Chapter 3 of reference [19] and chapter 3 of reference [29] provide good outlines of the fundamentals of

Lyapunov theory. The following is a summary of the main points presented in these references.

3.2.1 Stability

Before discussing Lyapunov stability theory, the basic definitions of stability first need to be discussed. Consider the basic nonlinear system of the form

$$\dot{\vec{x}}(t) = \mathbf{f}(\vec{x}, t) \tag{3.1}$$

An equilibrium state $\vec{x}_{eq}$ of this system is a state where once $\vec{x}(t) = \vec{x}_{eq}$, it remains equal to $\vec{x}_{eq}$ for all time. In mathematical terms, an equilibrium state satisfies $\vec{0} = \mathbf{f}(\vec{x}_{eq},t)$ for all time. An equilibrium state is considered stable if the system trajectory remains arbitrarily close to the equilibrium state when starting sufficiently close to it. Asymptotic stability implies not only that an equilibrium state is stable, but also that system trajectories starting sufficiently close to the equilibrium state actually converge to the equilibrium state as time goes to infinity. An equilibrium state which is stable but not asymptotically stable is often called marginally stable. Finally, global asymptotic stability of an equilibrium state means that asymptotic stability holds for any initial state.

3.2.2 Lyapunov's First Method

Lyapunov presented two methods for analyzing stability of nonlinear systems. With the first method of Lyapunov, the stability of an equilibrium state of a nonlinear system of the form of Equation

3.1 can be analyzed by first linearizing the system about the equilibrium state. Conclusions as to the stability of the nonlinear system can be drawn based on the stability of the linearized system. If the linearized system is strictly stable, the nonlinear system is stable at the equilibrium state. If the linearized system is unstable, the equilibrium state is also unstable. If the linearized system is marginally stable, no conclusions can be drawn as to the stability of the nonlinear system at the equilibrium state [19].

3.2.3 Lyapunov's Second Method

The basic approach of the second method of Lyapunov, also called Lyapunov's direct method, is to try to find a scalar function, based on the nonlinear system in question, that meets the criteria of a Lyapunov function. To be a Lyapunov function of a system, the function must exhibit two properties. The first is that the function $V(\vec{x})$ must be positive definite. For $V(\vec{x})$ to be positive definite, the following must be true:

(a) $V(\vec{x})$ must have continuous partial derivatives with respect to the components of $\vec{x}$

(b) $V(\vec{0}) = \vec{0}$

(c) $V(\vec{x}) > 0$ for $\vec{x} \neq \vec{0}$

The second property required of a Lyapunov function is the derivative of $V(\vec{x})$ must be negative definite inside a region R about the origin. To be negative definite, the same conditions as those for a

positive definite function must apply but with the inequality sign in condition (c) reversed.

Given these properties of a Lyapunov function, the theorem used in Lyapunov's second method of stability analysis simply states that the null solution to Equation 3.1 (i.e., the origin) is asymptotically stable in a region R around the origin if there exists a Lyapunov function of the system over the region R possessing the two properties described above. Further, if the function $V(\vec{x})$ satisfies the conditions of a Lyapunov function for all $\vec{x}$, the equilibrium state at the origin is globally asymptotically stable. This theorem provides only sufficient conditions for stability determination. Failure to find a Lyapunov function does not prove instability but only represents failure to prove stability [29].

The difficulty in applying Lyapunov theory to stability analysis of nonlinear systems is knowing what to choose as a possible Lyapunov function. For a given system, there may be many possible Lyapunov functions of the system; only one is needed to determine stability. The following example points to a typical source of a Lyapunov function for a mechanical system - the total mechanical energy.

3.2.4 Lyapunov Stability Analysis of a Simple Pendulum

As an illustration of the second method of Lyapunov, consider the pendulum in Figure 3.1 [19]. The dynamics of this simple pendulum are given by the nonlinear equation

$$mr^2\ddot{\theta} + k\dot{\theta} + mgr(\sin\theta) = 0 \qquad (3.2)$$

where m is the mass of the pendulum, r is the length of the pendulum, g is the acceleration due to gravity, k is the coefficient of friction, and θ is the angle defined in Figure 3.1.

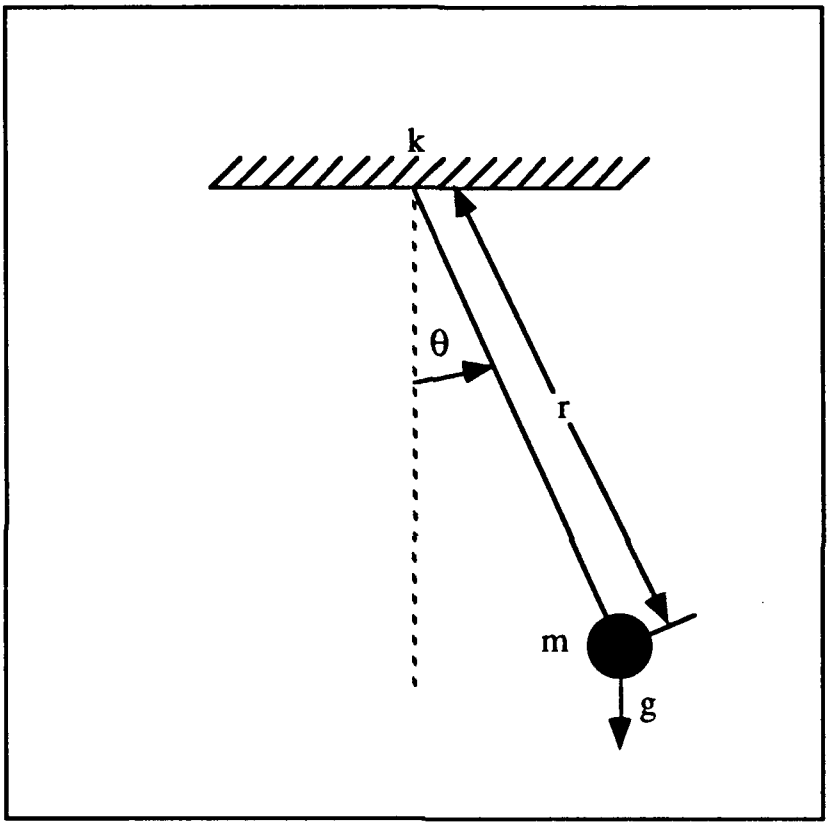

Figure 3.1. Simple Pendulum

Defining the state vector as $\vec{x} = [\ \theta \quad \dot{\theta}\ ]^T$, a stable equilibrium state of this system is at $\vec{x}_{eq} = [0 \quad 0]^T$ representing the pendulum at rest at the bottom of its arc. Starting the pendulum at this point with no velocity, the pendulum would stay at this point. Intuitively, this point is also asymptotically stable for all starting trajectories other than at $\vec{x}(0) = [\pi \quad 0]^T$ which represents the inverted pendulum at rest.

an unstable equilibrium state. As the pendulum is raised from $\theta = 0$, its potential energy is increased. When released, the pendulum swings back towards $\theta = 0$, trading potential energy for kinetic energy until it passes the bottom of its arc and begins swinging back upward, trading kinetic energy for potential energy. For a pendulum with no dissipative friction (i.e., $k = 0$), the total mechanical energy of the system (i.e., kinetic + potential) remains constant with the pendulum swinging back and forth, always returning to the height from which it was released. With friction, however, the total mechanical energy of the pendulum is dissipated and each upward swing of the pendulum will not reach the height of its previous swing. Eventually, the pendulum will slow down and come to rest at the bottom of its arc, representing the equilibrium point $\vec{x}_{eq} = [0\ 0]^T$.

Before coming to rest, the pendulum possesses positive total mechanical energy. Since the friction causes the total mechanical energy to dissipate, the total mechanical energy can be thought of as having a negative derivative. These two characteristics of the total mechanical energy (i.e., positive with negative derivative) are the desired characteristics of a Lyapunov function suggesting the possibility of a Lyapunov function based on the total mechanical energy of the system.

The total mechanical energy of the pendulum is given by the function

$$V(\vec{x}) = \frac{1}{2} mr^2\dot{\theta}^2 + mgr(1 - \cos\theta) \qquad (3.3)$$

representing the combined kinetic and potential energy. Applying the second method of Lyapunov, $V(\vec{x})$ meets the two criteria required of a Lyapunov function for all states except $\vec{x} = [\pi \ 0]^T$:

1. $V(\vec{x})$ is positive definite

   (a) $V(\vec{x})$ has continuous partial derivatives with respect to the components of $\vec{x}$
   (b) $V(\vec{0}) = \vec{0}$
   (c) $V(\vec{x}) > 0$ for $\vec{x} \neq \vec{0}, [\pi \ 0]^T$

2. Differentiating $V(\vec{x})$ and substituting in for $\ddot{\theta}$ from Equation 3.2, $\dot{V}(\vec{x})$ is shown to be negative definite:

$$\dot{V}(\vec{x}) = mr^2 \ddot{\theta}\dot{\theta} + mgr \sin\theta \, \dot{\theta}$$
$$= mr^2 \left(-\frac{k}{mr^2}\dot{\theta} - \frac{g}{r}\sin\theta\right)\dot{\theta} + mgr \sin\theta \, \dot{\theta}$$
$$\dot{V}(\vec{x}) = -k\dot{\theta}^2 < 0, \dot{\theta} \neq 0$$

The function $V(\vec{x})$ is a Lyapunov function of the simple pendulum for all $\vec{x}$ except $\vec{x} = [\pi \ 0]^T$. For the simple pendulum, the equilibrium point at the origin is asymptotically stable everywhere except for the single state $\vec{x} = [\pi \ 0]^T$, the result expected from intuition.

3.3 Fundamentals of Sliding Mode Control

This section outlines the basics of sliding mode control as presented in chapter 7 of reference [19]. The concept of robust sliding mode control stems from the second method of Lyapunov outlined above. The basic idea is to design a feedback control law such that a function based on the closed loop system can be defined

that exhibits the properties of a Lyapunov function for any state. If such a Lyapunov function can be defined, the closed loop system will be globally asymptotically stable. To be a robust control law, the Lyapunov function must also maintain the properties of a Lyapunov function over the range of expected system unknowns.

Sliding mode controllers are robust to both parametric uncertainties (e.g., imprecision on the mass properties) and the presence of unmodelled dynamics (e.g., structural resonant modes). System models are not required to be extensive as long as the bounds on the uncertainties are known. Also, the less dominant dynamics are not required to be modelled with high precision. Instead, they can be treated as disturbances as long as the upper bounds on their magnitudes are known. For an aerocapture vehicle, for example, the accelerations due to aerodynamic torques are assumed to be significantly smaller in magnitude than the accelerations due to the control actuators. Being less dominant, these aerodynamic accelerations can be treated as disturbances and an extensive aerodynamic model is not required. As long as there are known bounds on the system unknowns, a globally stable sliding mode control law can be designed which is robust over the bounded range of system unknowns.

3.3.1 Single-Input, Single-Output System Model

To best understand the sliding mode concepts and for ease of explanation, first consider a general, single-input system [18] with dynamics described by the equation

$$x^{(n)} = f(\vec{x}) + b(\vec{x})\, u + d(t) \qquad (3.4)$$

where the scalar x is the output to be controlled (e.g., position of a body in one dimension), $x^{(n)}$ denotes the n-th derivative of x, u is the control input (e.g., imposed force or acceleration), and $\vec{x} = [x, \dot{x},..., x^{(n-1)}]^T$ is the state vector. With parametric unknowns having bounded limits, the typically nonlinear function, $f(\vec{x})$, and the control gain, $b(\vec{x})$, are not exactly known, but upper bounds on the magnitude of the imprecision in $f(\vec{x})$ and $b(\vec{x})$ are known. Unmodelled dynamics are accounted for in the disturbance term, d(t), whose magnitude is also unknown but upper bounded by a known continuous function of $\vec{x}$ and t. The control problem, then, is to track a desired time-varying state $\vec{x}_d = [x_d, \dot{x}_d,..., x_d^{(n-1)}]^T$ despite the uncertainties in $f(\vec{x})$, $b(\vec{x})$, and d(t).

As an example, again consider the simple pendulum of the previous section. Suppose a perpendicular controlling force u, as shown in Figure 3.2, is used to assist in bringing the pendulum to rest at $\theta = 0$ (Section 3.4 presents the case where the desired state is not a single stable equilibrium state, but rather a time-varying state). The dynamics of the system are now defined by

$$mr^2\ddot{\theta} + k\dot{\theta} + mgr(\sin\theta) - ru = 0 \qquad (3.5)$$

or in the form of Equation 3.4

$$\ddot{\theta} = f(\vec{x}) + bu + d(t) \qquad (3.6)$$

where $x = \theta$ is the output to be controlled, the state vector is $\vec{x} = [\theta \ \dot{\theta}]^T$, d(t) is a disturbance term consisting of any unmodelled dynamics, b = r, and

$$f(\vec{x}) = -\frac{k}{mr^2}\dot{\theta} - \frac{g}{r}\sin\theta \qquad (3.7)$$

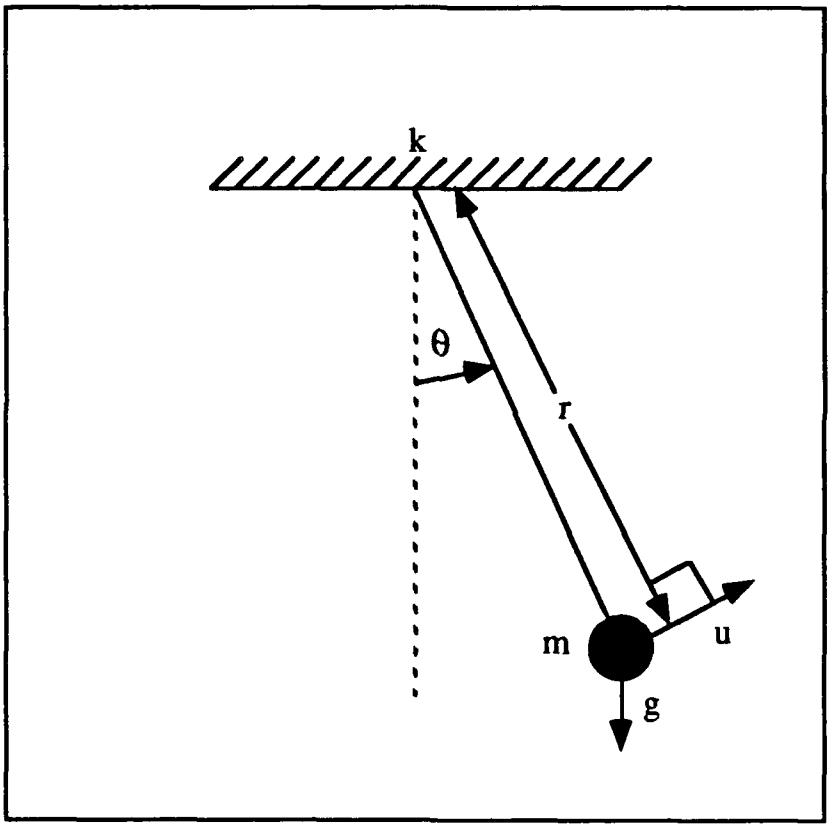

Figure 3.2. Controlled Pendulum

Sliding mode control requires known bounds on the imprecision on $f(\vec{x})$, b, and d(t). For this example, assume the following parameters are not exactly known but fall within the given ranges:

$$1.0 \text{ ft} \leq r \leq 1.3 \text{ ft}$$

$$1.0 \frac{\text{slug}\cdot\text{ft}^2}{\text{sec}} \leq k \leq 2.0 \frac{\text{slug}\cdot\text{ft}^2}{\text{sec}}$$

$$1.0 \text{ slug} \leq m \leq 2.0 \text{ slug}$$

$$-0.5 \frac{\text{rad}}{\text{sec}^2} \leq d \leq 0.5 \frac{\text{rad}}{\text{sec}^2}$$

Gravitational acceleration is a known constant 32 ft/sec^2. Given these ranges, the bounds on $f(\vec{x})$ can be calculated from Equation 3.7 as

$$\left(-2.0\,\dot{\theta} - 32.0 \sin\theta\right) \frac{\text{rad}}{\text{sec}^2} \leq f(\vec{x}) \leq \left(-0.3\,\dot{\theta} - 24.6 \sin\theta\right) \frac{\text{rad}}{\text{sec}^2}$$

3.3.2 Sliding Surface

Sliding mode control design begins by reducing the tracking problem to a first order stabilization problem. A time varying "sliding surface" is defined in the state-space by the scalar equation

$$s(\vec{x},t) = \left(\frac{d}{dt} + \lambda\right)^{n-1} \tilde{x} = 0 \qquad (3.8)$$

where the scalar $\tilde{x}$ represents the tracking error in x (i.e., $\tilde{x} = x - x_d$), d/dt is the derivative operator, and λ is a positive constant with units of 1/time. Equation 3.8 suggests that once on the sliding surface, the tracking error moves exponentially to zero with a time constant $(n-1)/\lambda$. While on this surface, the system is said to be behaving in the "sliding mode".

For the second-order (i.e., n=2) pendulum example, the sliding surface is defined by the equation

$$s(\vec{x},t) = \left(\frac{d}{dt} + \lambda\right)\tilde{\theta} = 0 \qquad (3.9)$$
$$= \dot{\tilde{\theta}} + \lambda\tilde{\theta} = 0$$
$$= \dot{\theta} - \dot{\theta}_d + \lambda(\theta - \theta_d) = 0$$

For the simple problem of bringing the pendulum to rest at the bottom of its arc, $\dot{\theta}_d = \theta_d = 0$ so that the sliding surface is given by

$$s(\vec{x},t) = \dot{\theta} + \lambda\theta = 0 \qquad (3.10)$$

With λ a positive constant, Equation 3.10 is the equation of a line in the phase plane passing through the origin as shown in Figure 3.3. The general solution of this simple differential equation is of the form

$$\theta(t) = \theta_o e^{-\lambda t}$$

so that

$$\dot{\theta}(t) = -\theta_o \lambda e^{-\lambda t}$$

These solutions suggest that when the state trajectory is on the sliding surface, it will decay exponentially towards the desired state $\vec{x}_d = [0 \;\; 0]^T$ with a time constant $1/\lambda$.

Since the behavior on the sliding surface is for a state trajectory to move exponentially towards its desired state, the task

of sliding mode control is to drive the state trajectory to this sliding surface, and once on it, to maintain it on the sliding surface. To accomplish its task, sliding mode control attempts to design a control law so that a Lyapunov function based on the closed loop system dynamics can be defined to show that the sliding surface is asymptotically stable.

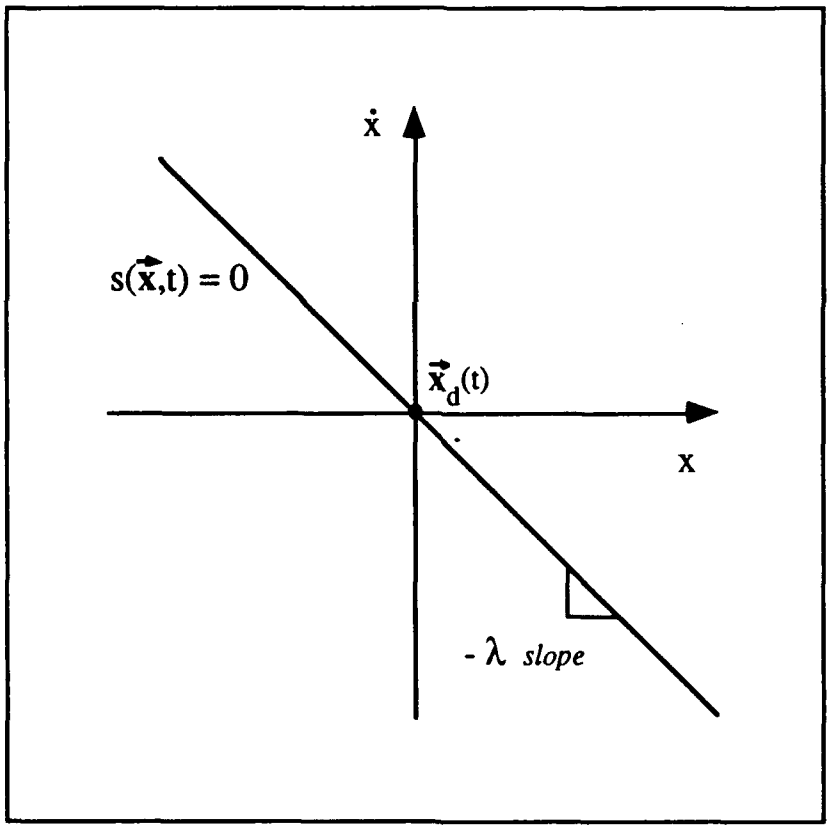

Figure 3.3. Sliding Surface Through Origin

As presented in references [18,19], the Lyapunov function used in sliding mode control is the positive definite function s^2 with $s = s(\vec{x},t)$ as defined in Equation 3.8. To be a Lyapunov function, the derivative of s^2 must be negative despite system uncertainties. This is guaranteed when the "sliding condition"

$$\frac{1}{2}\frac{d}{dt}s^2 \leq -\eta |s| \tag{3.11}$$

is satisfied where η is a positive constant. This particular inequality also guarantees that if initially the system is not on the sliding surface (i.e., $s \neq 0$), the surface will be reached in a finite time less than

$$t_{reach} < \frac{|s(\vec{x}(0), 0)|}{\eta} \tag{3.12}$$

With the sliding condition (Equation 3.11) met, s^2 is a Lyapunov function of the closed loop dynamics and the sliding surface is attractive. Equation 3.11 ensures all trajectories point toward the sliding surface, as illustrated in Figure 3.4, and that once on the surface, the state trajectory stays on the surface.

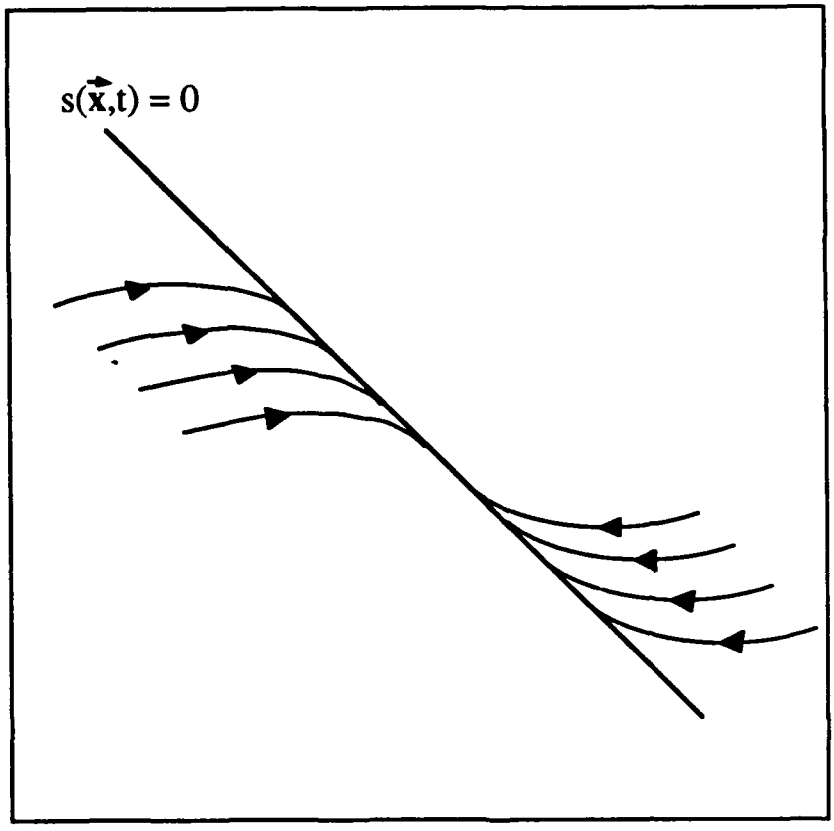

Figure 3.4. Attractive Sliding Surface

A typical state trajectory for a second-order system, such as the pendulum, satisfying the sliding condition (Equation 3.11) is depicted in Figure 3.5. From an initial condition off the sliding surface, the trajectory reaches the surface in a finite time less than that specified by Equation 3.12, and then slides exponentially along the surface to $\vec{x}_d$ with a time constant of $1/\lambda$.

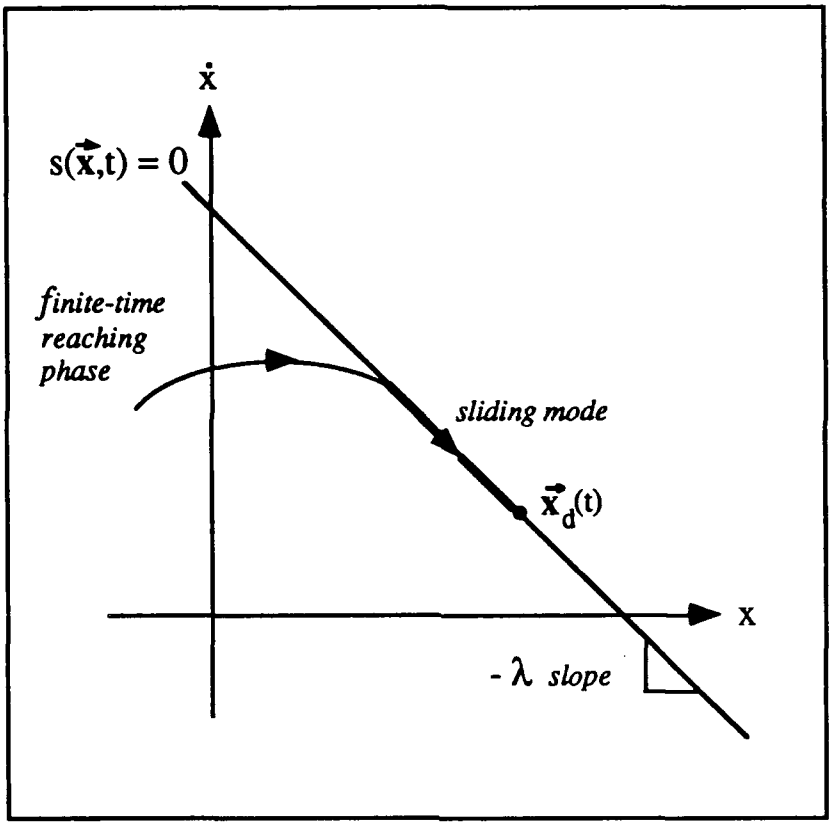

Figure 3.5. Typical State Trajectory

3.3.3 Switching Sliding Mode Control

The desired sliding mode control law for the general single-input case is a switching (i.e., discontinuous) design of the form

$$u = \frac{1}{\hat{b}}\left[\hat{u} - k\,\mathrm{sgn}(s)\right] \qquad (3.13)$$

where the sign function sgn(s) is defined by

$$\mathrm{sgn}(s) = -1 \quad \text{for } s < 0$$

$$\mathrm{sgn}(s) = +1 \quad \text{for } s \geq 0$$

In Equation 3.13, $\hat{u}$, to be derived below for the pendulum, is the best approximation of a continuous control law that would maintain the system trajectory on the sliding surface, while the discontinuous term k·sgn(s) satisfies the sliding condition (i.e., Equation 3.11) despite the system uncertainties, thus ensuring state trajectories off the sliding surface are driven back to the surface. The remainder of this section will be used to show how sliding mode control design is accomplished by designing a control law of the form of Equation 3.13 for the simple pendulum example.

Since the control gain $b(\vec{x})$ is multiplicative in the dynamics, the estimated control gain, $\hat{b}$, is typically chosen as the geometric mean of the bounds on $b(\vec{x})$

$$\hat{b} = \sqrt{b_{min}\, b_{max}} \tag{3.14}$$

For the pendulum,

$$\hat{b} = \sqrt{(1.0)\cdot(1.3)} = 1.14 \text{ ft}$$

The estimated control $\hat{u}$ is chosen to maintain $s(\vec{x},t) = 0$ which means the derivative of $s(\vec{x},t)$ must also equal zero. Differentiating Equation 3.10 yields

$$\dot{s}(\vec{x},t) = \ddot{\theta} + \lambda\dot{\theta} = 0$$

Substituting the expression for the estimated closed loop dynamics of the pendulum from Equation 3.6 gives

$$\dot{s}(\vec{x},t) = \left(\hat{f} + \hat{b}\,\hat{u} + \hat{d}\right) + \lambda\dot{\theta} = 0 \qquad (3.15)$$

Solving Equation 3.15, $\hat{u}$ for the pendulum is found to be

$$\hat{u} = -\hat{f} - \hat{d} - \lambda\dot{\theta} \qquad (3.16)$$

where $\hat{b}$ has been accounted for in the overall control law, Equation 3.13. The estimates $\hat{f}$ and $\hat{d}$ are selected as the average of their given bounds:

$$\hat{f} = \frac{1}{2}\left(-2.0\,\dot{\theta} - 32.0\sin\theta - 0.3\,\dot{\theta} - 24.6\sin\theta\right)$$

$$\hat{f} = -1.15\,\dot{\theta} - 28.3\sin\theta$$

and

$$\hat{d} = \frac{1}{2}\left(-0.5 + 0.5\right) = 0$$

The choice of λ depends on the type and characteristics of the system to be controlled. From reference [19], for a mechanical system λ must be smaller than all of the following: the frequency of the lowest unmodelled resonant mode, the sampling frequency, and the inverse of the largest unmodelled time delay. For this pendulum example, assume the sampling frequency drives the strictest criteria. A general rule of thumb for choosing λ based on the sampling frequency is

$$\lambda = \frac{\text{sampling rate}}{5}$$

For a sampling rate of 100 hz, $\lambda = 20$.

The gain k in Equation 3.13 must be large enough to satisfy the sliding condition, Equation 3.11. As derived in reference [19], a gain that guarantees the sliding condition will be satisfied can be calculated from

$$k(\vec{x}) = \beta (F + D + \eta) + (\beta - 1)|\hat{u}| \tag{3.17}$$

where

$$\begin{aligned} F &= \max|\hat{f} - f| \\ D &= \max|\hat{d} - d| \end{aligned} \tag{3.18}$$

are the maximum deviations of $f(\vec{x})$ and d(t) from their estimates, $\hat{f}$ and $\hat{d}$. In Equation 3.17, β is considered the gain margin and is calculated by

$$\beta = \sqrt{\frac{b_{max}}{b_{min}}} \tag{3.19}$$

For the pendulum example,

$$\begin{aligned} \beta &= \sqrt{1.3} = 1.14 \\ F &= 0.85|\dot{\theta}| + 3.7|\sin\theta| \\ D &= 0.5 \end{aligned}$$

The only requirement on the selection of η is that it be a positive constant. It may be selected to provide a desired reach time according to Equation 3.12. For this pendulum example, $\eta=20$.

With the switching control law complete, a simulation of the pendulum is now run. To demonstrate the control law's robust performance in the presence of unknowns and disturbances, the actual values of r, k, m, and d are varied over their full possible ranges. Releasing the pendulum from an angle of 45 deg, the control law, Equation 3.13, attempts to assist the pendulum in coming to rest at $\theta=0$. Figure 3.6 plots the trajectory of the pendulum vs. time. The pendulum achieves $\theta=0$ in less than 0.5 sec and stays close to $\theta=0$. Figure 3.7 plots the value of the sliding variable $s(\vec{x},t)$ vs. time. The state trajectory of the pendulum is initially off the sliding surface, $s(\vec{x},0) \neq 0$, but the sliding surface is reached in 0.4 sec, agreeing with the criteria set by Equation 3.12:

$$t_{reach} < \frac{|s(\vec{x},0)|}{\eta} = \frac{|\lambda(\theta - \theta_d)|}{\eta} = \frac{20}{20}\left(45 \cdot \frac{\pi}{180}\right) \approx 0.8 \text{ sec}$$

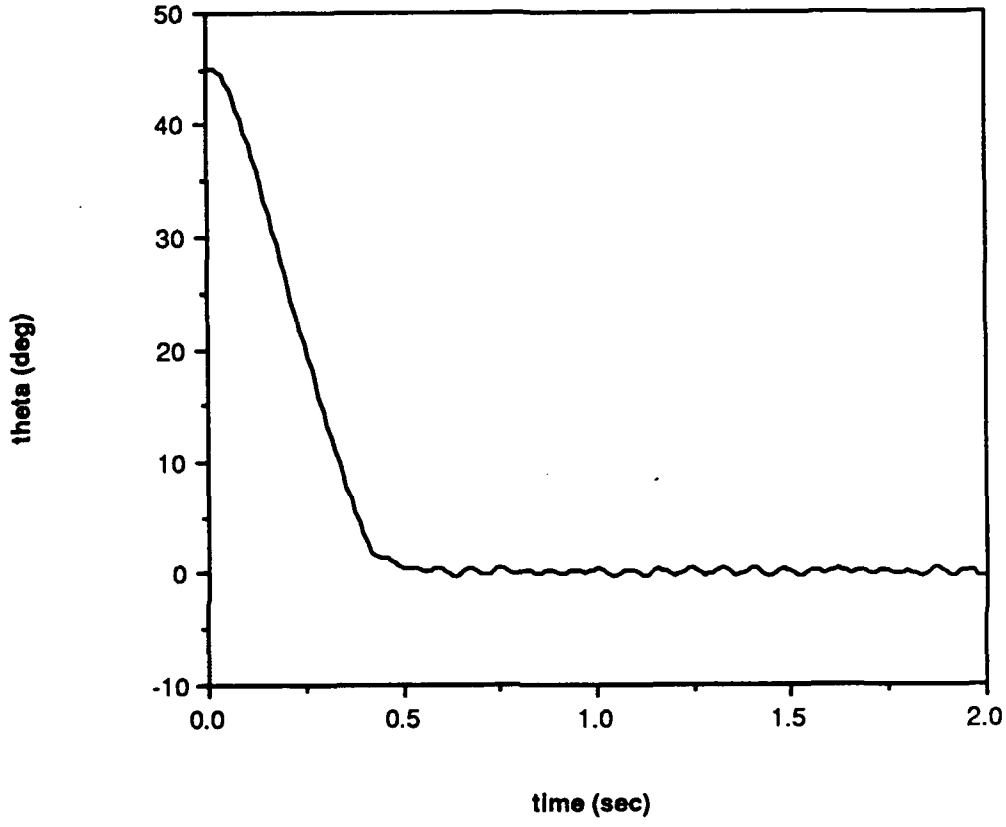

Figure 3.6. Pendulum Trajectory with $\theta_d = 0$ (Switching Control Law)

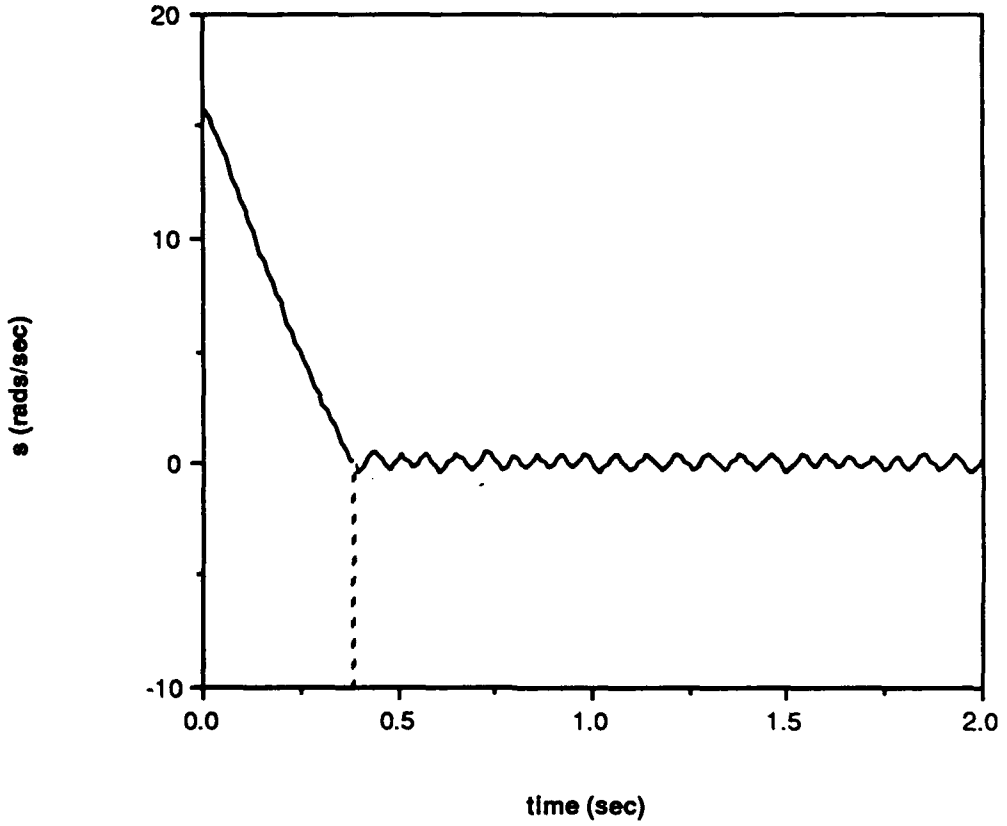

Figure 3.7. Sliding Variable vs. Time (Switching Control Law)

3.3.4 Continuous Approximation of the Switching Sliding Mode Control Law

Taking a closer look at Figure 3.7, Figure 3.8 shows the behavior of $s(\vec{x},t)$ near the sliding surface. Since the second term of the sliding mode control law, Equation 3.13, is discontinuous across the sliding surface, control chattering is encountered during its implementation.

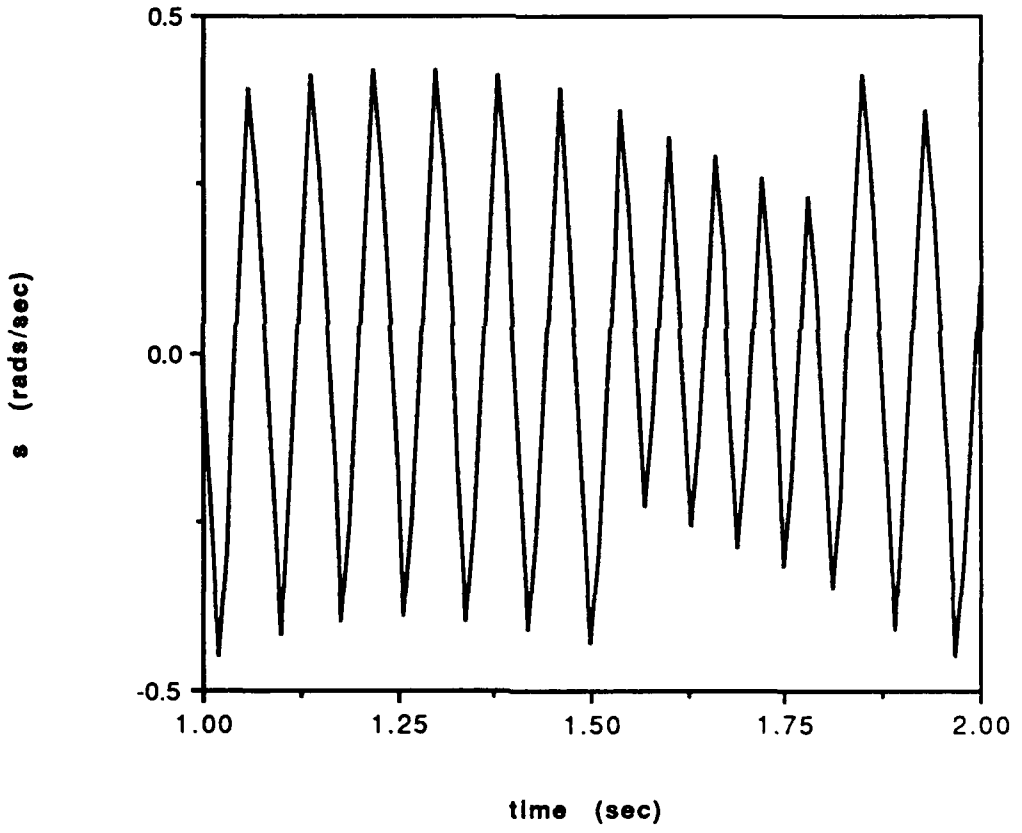

Figure 3.8. Sliding Variable vs. Time (Expanded View)

Such chattering is undesirable since it results in a large amount of control activity, as illustrated in Figure 3.9, and may excite high frequency dynamics neglected in the course of modelling.

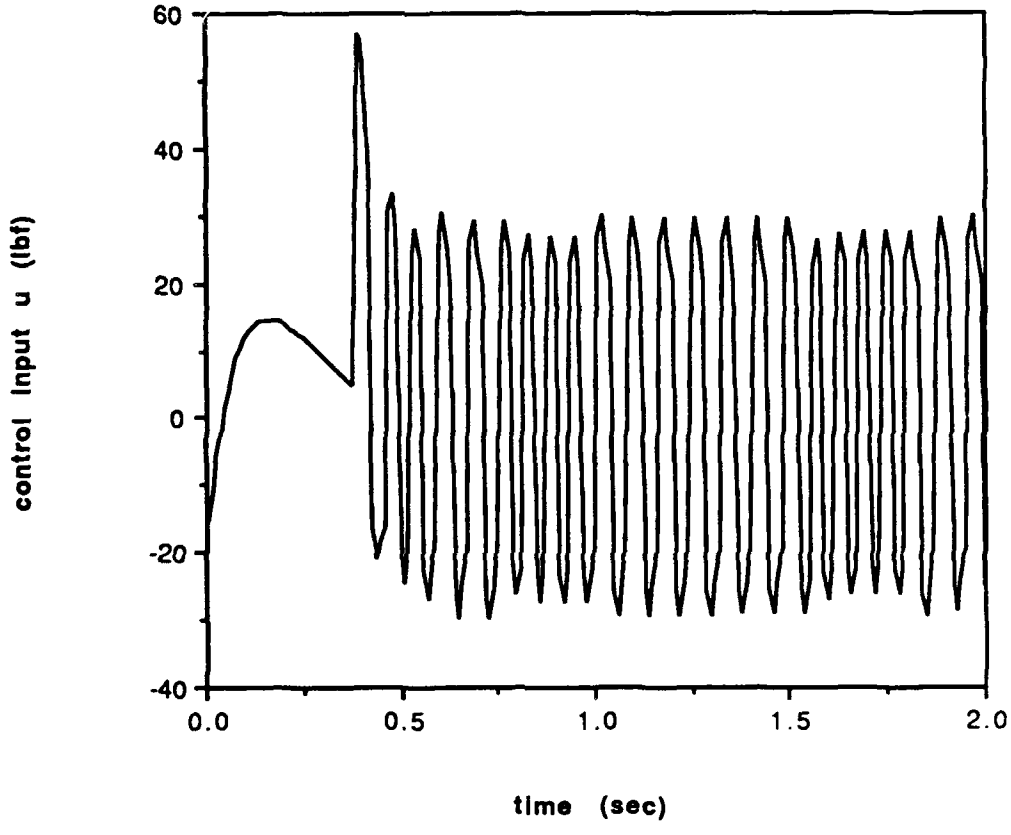

Figure 3.9. Control Activity (Switching Control Law)

Chattering can be eliminated, however, with a continuous approximation of Equation 3.13. A thin boundary layer about the sliding surface is introduced such that outside the boundary layer, the control law is as in Equation 3.13, guaranteeing the boundary layer is attractive. Inside the boundary layer, a continuous function is required in place of sgn(s) to make a smooth transition across the

sliding surface. These characteristics are achieved by replacing the sgn(s) term in Equation 3.13 with the saturation function sat(s/Φ) where Φ is the boundary layer thickness and sat(s/Φ) is defined by

$$\begin{aligned} sat(s/\Phi) &= s/\Phi \qquad \text{for } |s/\Phi| \le 1 \\ sat(s/\Phi) &= sgn(s/\Phi) \qquad \text{otherwise} \end{aligned} \tag{3.20}$$

Figure 3.10 graphically illustrates the definition of sat(s/Φ).

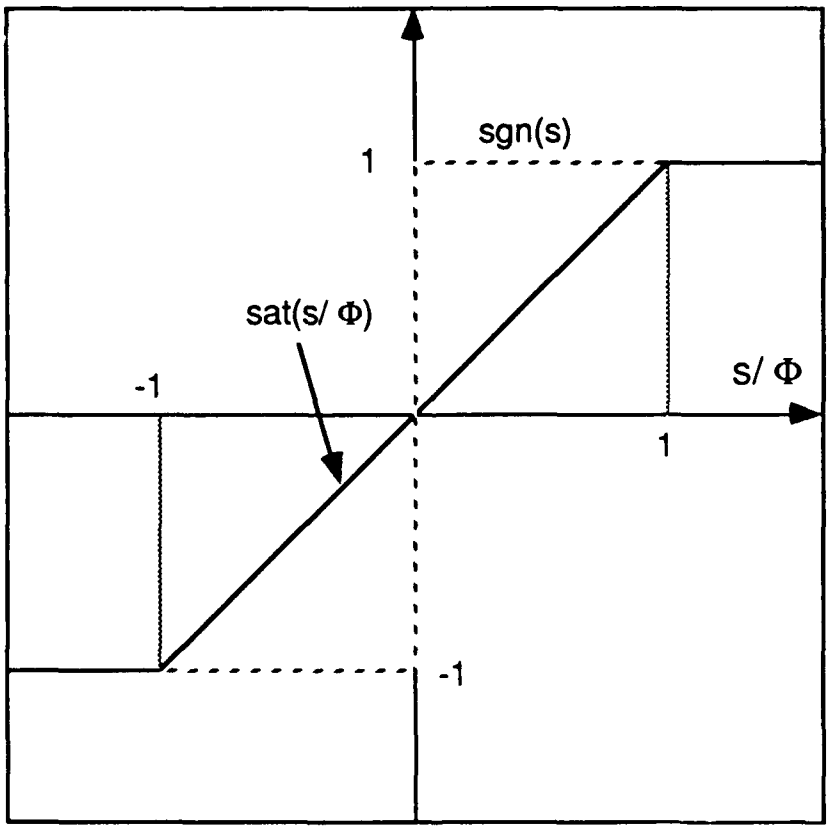

Figure 3.10. Saturation Function, sat(s/Φ)

From the derivation presented in section 7.2 of reference [19], the sliding condition can be met by choosing $\Phi(t)$ as the solution to the appropriate differential equation from

$$\dot{\Phi}(t) = -\lambda\Phi + \beta\, k(\vec{x}_d) \quad \text{if } k(\vec{x}_d) > \frac{\lambda\Phi}{\beta} \qquad (3.21)$$

$$\dot{\Phi}(t) = \frac{-\lambda\Phi}{\beta^2} + \frac{k(\vec{x}_d)}{\beta} \qquad \text{otherwise}$$

with initial condition

$$\Phi(0) = \beta\, \frac{k(\vec{x}_d)}{\lambda}$$

The new, continuous control law is then

$$u = \frac{1}{\hat{b}}\left[\hat{u} - k'(\vec{x})\, \mathrm{sat}(s/\Phi)\right] \qquad (3.22)$$

where the scalar gain on the saturation term is found from

$$k'(\vec{x}) = k(\vec{x}) - k(\vec{x}_d) + \frac{\lambda\Phi}{\beta} \qquad (3.23)$$

and $k(\vec{x})$ and $k(\vec{x}_d)$ are calculated from Equation 3.17. The continuous control law (Equation 3.22) is essentially the same as the switching control law (Equation 3.13) outside the boundary layer. Inside the boundary layer, Equation 3.22 is basically a proportional control law.

Using this continuous approximation to the control law for the pendulum example, Figure 3.11 shows the behavior of the pendulum for a repeat of the previous simulation. The effort to eliminate

chattering results in the continuous sliding mode control law (Equation 3.22) with tracking to within the boundary layer rather than the "perfect" tracking of the switching sliding mode control law. Figure 3.12 shows the behavior of $s(\vec{x},t)$ without chattering near the sliding surface while Figure 3.13 shows the reduced smooth control activity required.

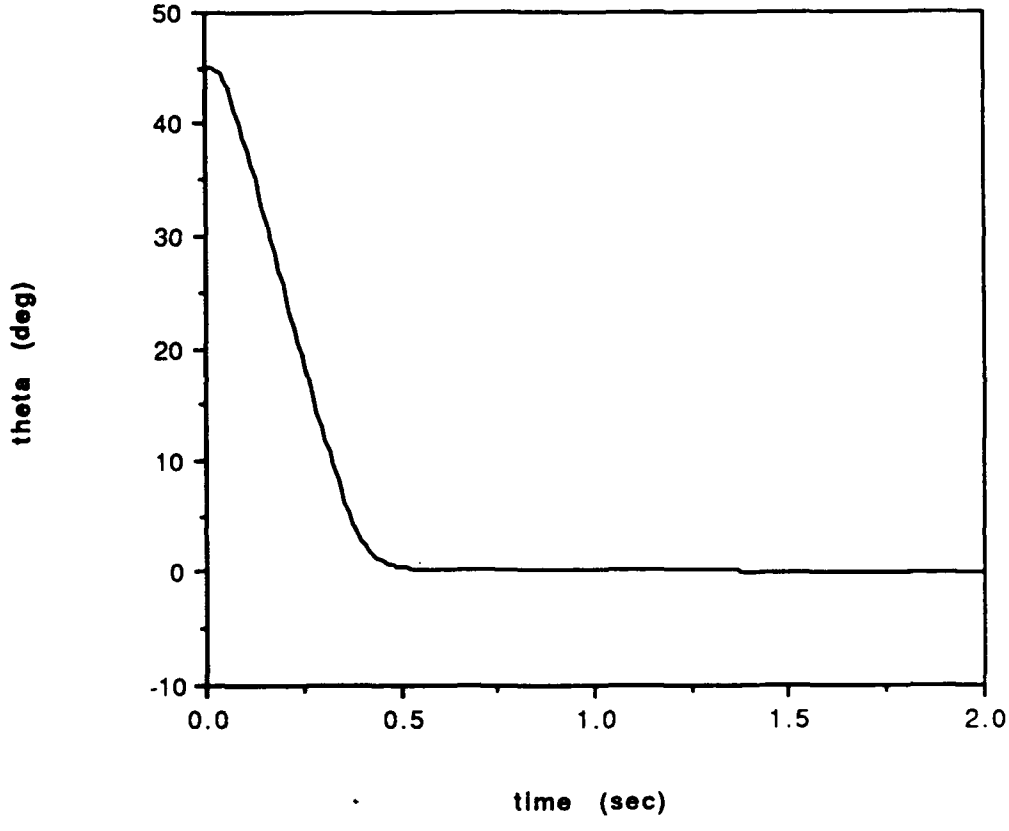

Figure 3.11. Pendulum Trajectory with $\theta_d = 0$ (Continuous Control Law)

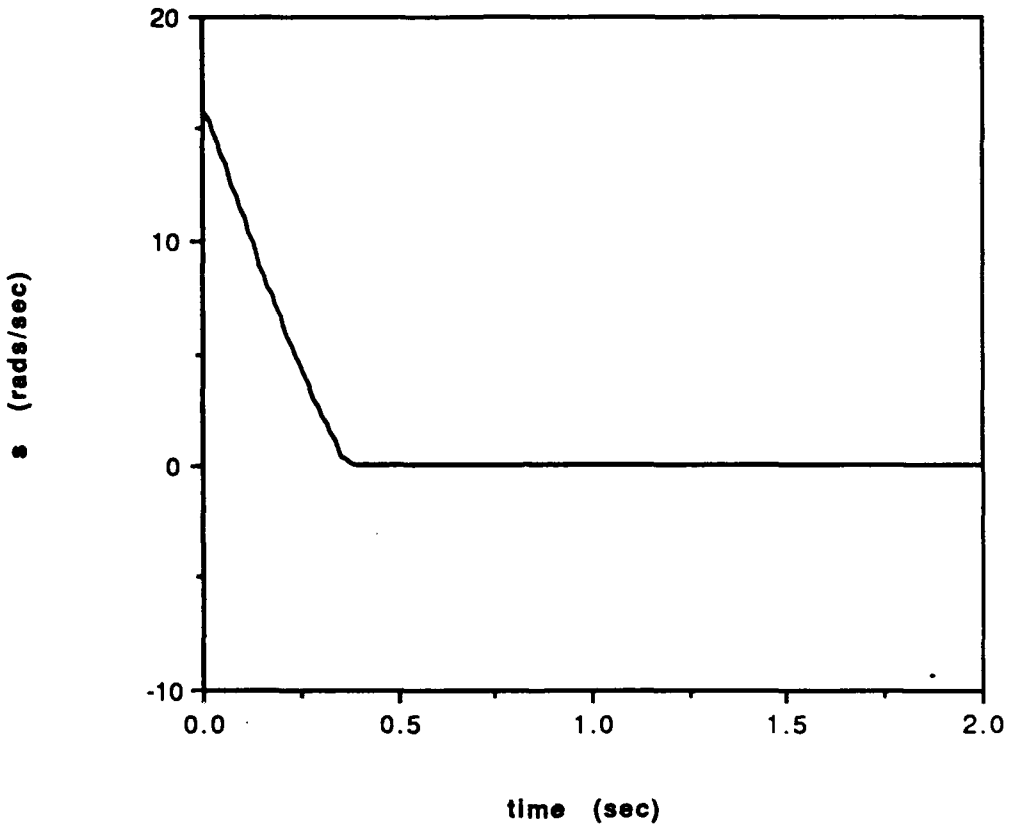

Figure 3.12. Sliding Variable vs. Time (Continuous Control Law)

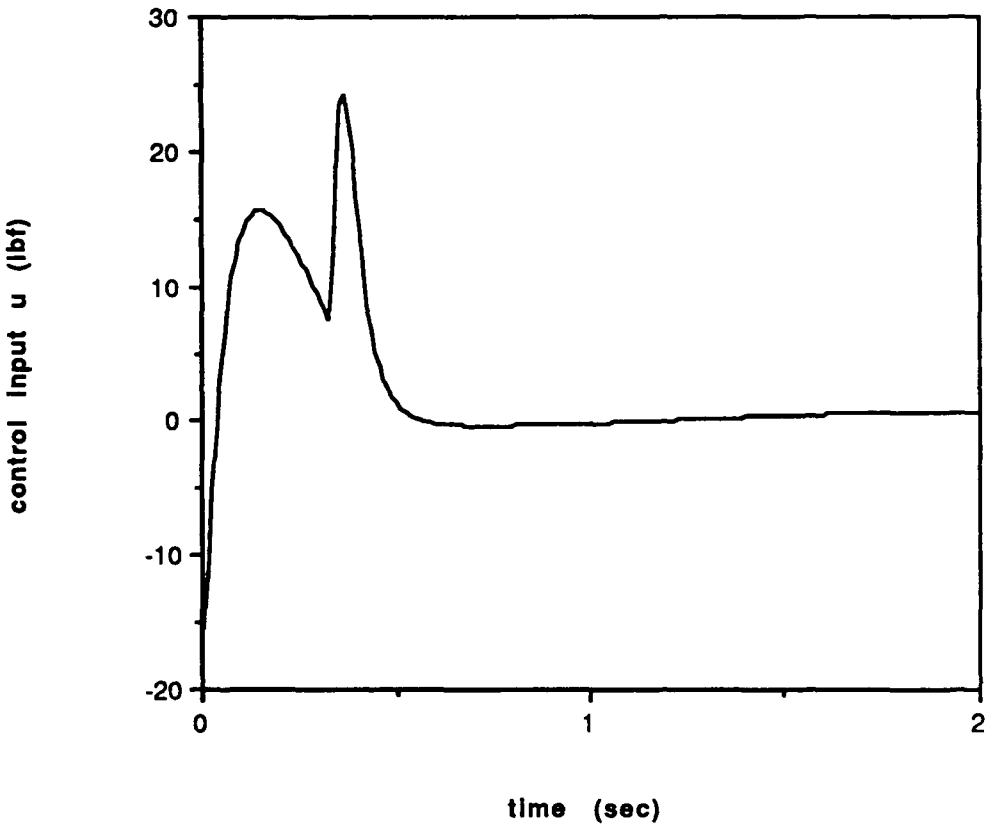

Figure 3.13. Control Activity (Continuous Control Law)

The state trajectory in the phase plane is shown in Figure 3.14. The line through the origin with a slope of -20 represents the sliding surface. The trajectory reaches the sliding surface asymptotically and then slides along the surface to the origin.

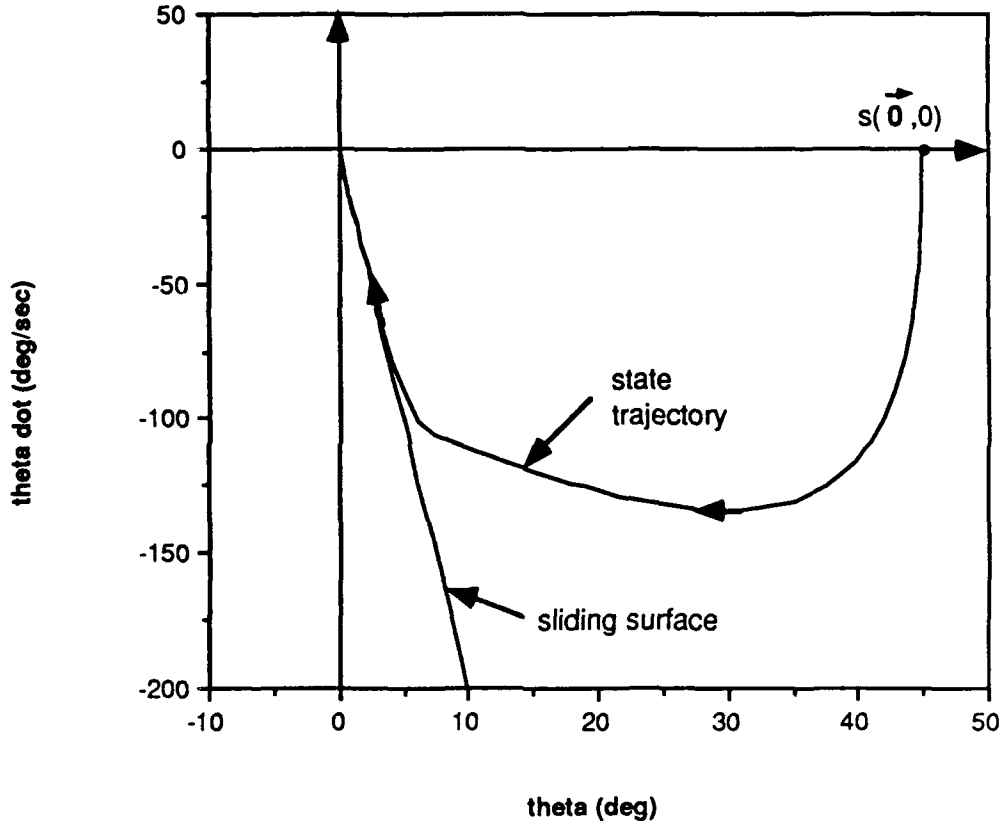

Figure 3.14. State Trajectory in Phase Plane (Continuous Control Law)

3.4 The Pendulum Example Continued

In the previous section, sliding mode control was used to assist the pendulum in achieving a stable, equilibrium condition (i.e., $\vec{x}_d = [0 \;\; 0]^T$). The effect of the control law was, essentially, to enhance the damping on the pendulum so that it reached the equilibrium state sooner than it would without the control. Rarely does the desired state of a system correspond to a single equilibrium state. The goal of any control law design is to make a system perform in a desired behavior whether that behavior is natural for the system or not. In this section, therefore, sliding mode control is used to control the pendulum to track a varying trajectory.

Though the desired state, $\vec{x}_d = [\theta_d(t) \;\; \dot{\theta}_d(t)]^T$, does not represent a single stable state as in the previous section, with the correct control law, the time varying sliding surface does represent an asymptotically stable surface. All state trajectories lead to the surface, and once on the surface, the trajectory slides exponentially along the sliding surface to the desired state.

For this example, the pendulum is started at rest at the bottom of its arc, $\vec{x}(0) = [0 \;\; 0]^T$. The desired trajectory is given by the equation

$$\theta_d(t) = \frac{\pi}{4} \cos\left(\frac{\pi}{5} t\right) \tag{3.24}$$

so that the pendulum must track a slow swing from $\theta_d(0)$ = +45 deg to θ_d(5 sec) = -45 deg and back to θ_d(10 sec) = +45 deg.

The desired control law is still of the form of Equation 3.22, with the estimates $\hat{b}$, $\hat{f}$, $\hat{d}$ and the parameters β, F, D, λ, and η the same as before. The sliding surface is defined by

$$s(\vec{x},t) = \dot{\tilde{\theta}} + \lambda\tilde{\theta} = 0 \qquad (3.25)$$

as before, but since $\vec{x}_d$ is now time varying, the sliding surface no longer passes through the origin of the phase plane, but rather is a time varying line through $\vec{x}_d$ with slope $-\lambda = -20$.

The best approximation $\hat{u}$ of a continuous control law that would maintain the state trajectory on the sliding surface is again found by requiring the derivative of $s(\vec{x},t)$ to be zero. Differentiating Equation 3.25,

$$\begin{aligned} \dot{s}(\vec{x},t) &= \ddot{\tilde{\theta}} + \lambda\dot{\tilde{\theta}} = 0 \\ &= \ddot{\theta} - \ddot{\theta}_d + \lambda(\dot{\theta} - \dot{\theta}_d) \end{aligned}$$

Substituting the equation for the estimated closed loop dynamics of the pendulum for $\ddot{\theta}$,

$$\dot{s}(\vec{x},t) = (\hat{f} + \hat{b}\,\hat{u} + \hat{d}) - \ddot{\theta}_d + \lambda(\dot{\theta} - \dot{\theta}_d) \qquad (3.26)$$

Solving Equation 3.26 for $\hat{u}$ results in

$$\hat{u} = -\hat{f} - \hat{d} + \ddot{\theta}_d - \lambda(\dot{\theta} - \dot{\theta}_d) \qquad (3.27)$$

with $\hat{b}$ accounted for in the overall control law. Differentiating Equation 3.24 twice, the desired angular velocity and acceleration are

$$\dot{\theta}_d(t) = -\frac{\pi^2}{20}\sin\left(\frac{\pi}{5}t\right) \qquad (3.28)$$
$$\ddot{\theta}_d(t) = -\frac{\pi^3}{100}\cos\left(\frac{\pi}{5}t\right)$$

and all terms in Equation 3.27 are known. With the second term of Equation 3.22 calculated as in the previous section, the continuous sliding mode control law design is complete. Figure 3.15 shows the tracking response of the pendulum using this sliding mode control law.

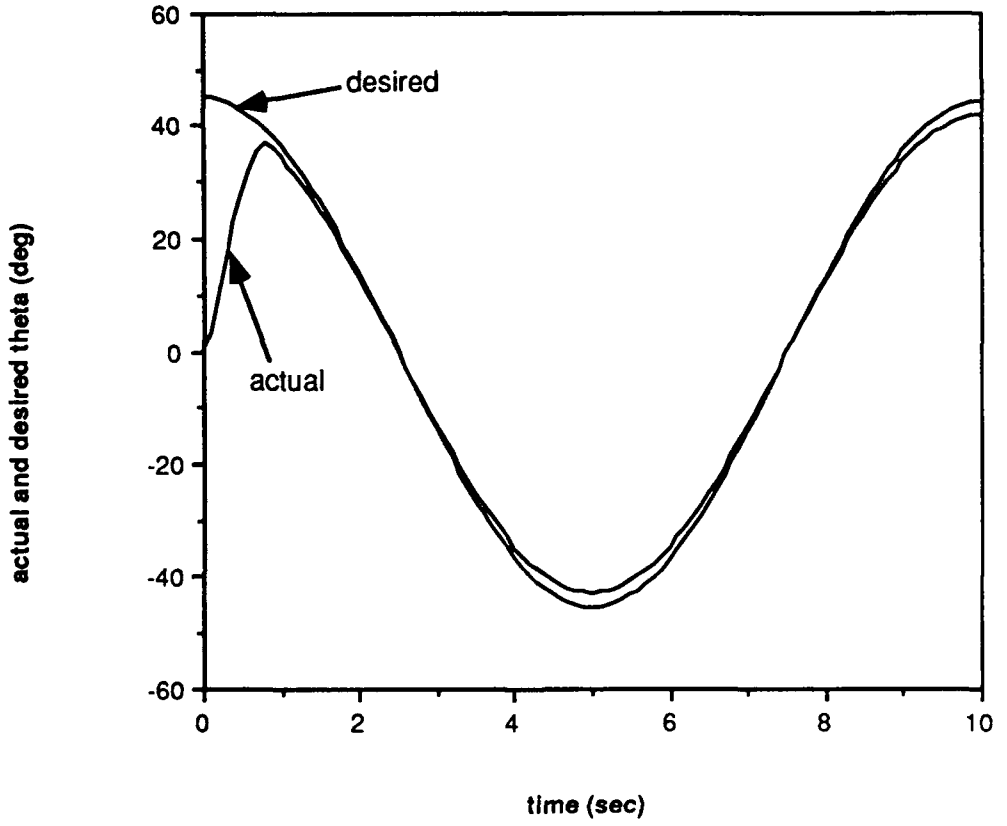

Figure 3.15. Pendulum Trajectory with Varying θ_d (Continuous Control Law)

Figure 3.16 shows the sliding surface was reached in 0.7 sec, again in agreement with Equation 3.12, with tracking to within the boundary layer after reaching the sliding surface.

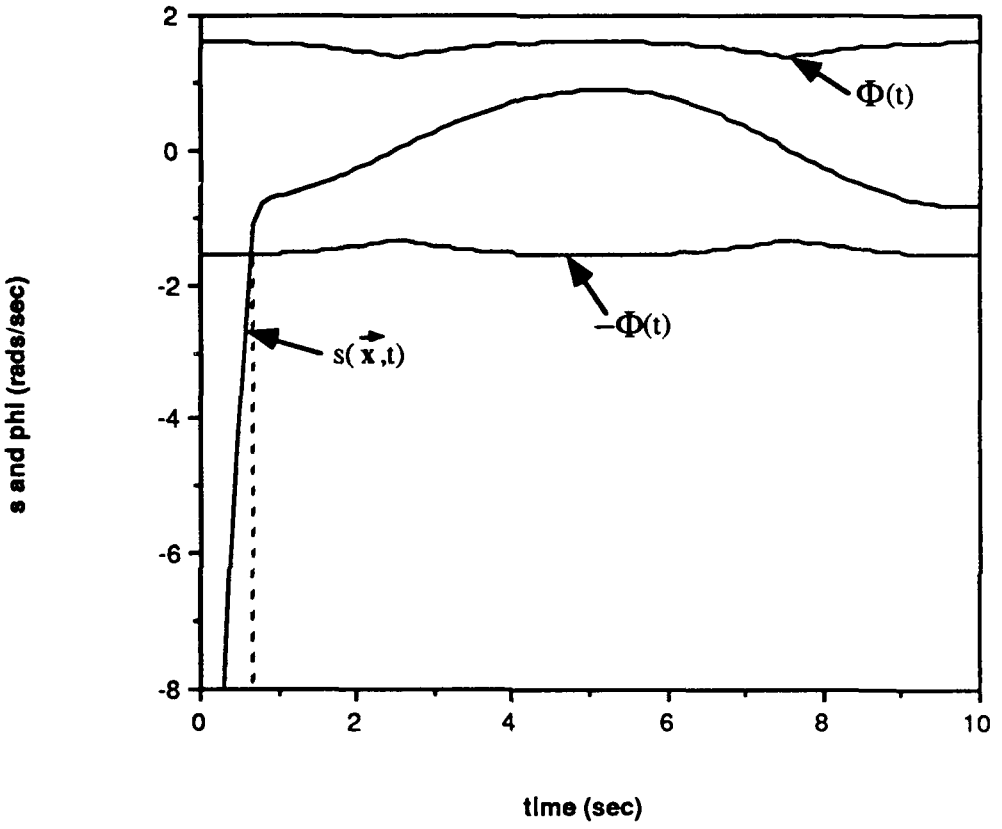

Figure 3.16. Sliding Variable and Boundary Layer vs. Time

3.5 Application of Sliding Mode to Attitude Control for Aerocapture

Sliding mode techniques can be applied directly to multi-input systems with differences from the single-input case due only to the increased mathematical complexity. The general form of a multi-input, multi-output sliding mode control law is presented in Section

3.5.1. A system model for the AFE vehicle in a form suitable for application of sliding mode techniques is developed in Section 3.5.2 along with the design of the desired control law.

3.5.1 Multi-Input, Multi-Output Sliding Mode Control

A general multi-input, multi-output dynamical system can be modelled by the system of equations

$$x_i^{(n_i)} = f_i(\vec{x}) + \sum_{j=1}^{m} b_{ij}(\vec{x})\, u_j + d_i(t) \qquad (3.29)$$
$$i = 1, \cdots, m$$

where the state vector $\vec{x}$ is composed of the x_i's and their first (n_i-1) derivatives, $d_i(t)$ is the disturbance component associated with x_i, $\vec{u}$ is the control input vector of components u_j, and all the b_{ij}'s form the input matrix **B**. Uncertainty on the elements of the input matrix are indicated by writing **B** in the form

$$\mathbf{B} = (\mathbf{1} + \Delta)\,\hat{\mathbf{B}} \qquad (3.30)$$

where $\mathbf{1}$ is the m x m identity matrix, $\hat{\mathbf{B}}$ is the estimated input matrix, and the matrix Δ is a measure of the uncertainty.

Following the logic presented in Section 3.3 for the development of the control law for the single-input case, a discontinuous switching control law is first sought for the multi-input, multi-output system that verifies the sliding conditions

$$\frac{1}{2}\frac{d}{dt}s_i^2 \le -\eta_i |s_i|, \quad \eta_i > 0 \tag{3.31}$$

where each s_i is a component of a vector $\vec{s}$ and is defined by

$$s_i(\vec{x},t) = \left(\frac{d}{dt} + \lambda_i\right)^{n_i - 1} \tilde{x}_i \tag{3.32}$$

similar to Equation 3.8 for single-input systems. By allowing $\vec{k}sgn(\vec{s})$ to be the vector of components $k_i sgn(s_i)$, the desired switching control law can be written in the form

$$\vec{u} = \hat{B}^{-1}\left[\vec{\hat{u}} - \vec{k}\, sgn(\vec{s})\right] \tag{3.33}$$

where, similar to $\hat{u}$ in Equation 3.13, $\vec{\hat{u}}$ represents the best approximation of a continuous control law that would maintain the sliding mode for each dimension. The gains $\vec{k}$ are found by solving the system of equations

$$(1 - D_{ij})\, k_i + \sum_{j \ne i} D_{ij}\, k_j = F_i + \sum_{j=1}^{n} D_{ij} \left| x_{ri}^{(n_i)} - \hat{f}_j \right| + \eta_i + d_{i_{max}} \tag{3.34}$$

where each F_i can be calculated from Equation 3.18, $d_{i_{max}}$ is the magnitude of the maximum disturbance, the elements D_{ij} are determined from

$$D_{ij} = \max |\Delta_{ij}| \tag{3.35}$$

and

$$x_{r_i}^{(n_i)} = x_{d_i}^{(n_i)} - \lambda_i \tilde{x}_i^{(n_i)} \tag{3.36}$$

As for the single-input case, a continuous approximation to the control law (Equation 3.33) is required to eliminate chattering upon implementation of the multi-input, multi-output control law. The desired form is

$$\vec{u} = \hat{B}^{-1} \left[\dot{\vec{\hat{u}}} - \vec{k} \, \text{sat}\left(\frac{\vec{s}}{\vec{\Phi}} \right) \right] \tag{3.37}$$

where the term $\vec{k}$ sat($\vec{s}/\vec{\Phi}$) represents a vector containing the components $k_i \text{sat}(s_i/\Phi_i)$ with the saturation function defined as in Section 3.3 and each boundary layer thickness Φ_i determined by the desired tracking precision. The aerocapture attitude control law design outlined below presents one method of determining the Φ_i's.

3.5.2 Aerocapture Attitude Control

The first step in designing a control law of the form of Equation 3.37 for a multi-input, multi-output system is to develop a dynamics model in the form of Equation 3.29 with the input matrix **B** defined by Equation 3.30. Once an appropriate system model is developed and bounds on the unknowns are determined, the equations presented in the previous section can be used directly to complete the control law design.

Ignoring aerodynamic interaction, the dynamics of an aerocapture vehicle like the one to be used in the AFE can be described by

$$\vec{\tau} = \frac{d\mathbf{H}}{dt} = \frac{\partial \mathbf{H}}{\partial t} + \vec{\omega} \times \mathbf{H} \tag{3.38}$$

where $\vec{\tau}$, $\mathbf{H}$, and $\vec{\omega}$ represent the three-dimensional torque due to the actuators, the angular momentum, and the angular velocity vector, respectively, with the angular velocities measured with respect to the body referenced system. Appendix A compares the body referenced system to the velocity vector referenced system (i.e., velocity angles). Angular momentum about the center of mass can be expressed by $\mathbf{H}=\mathbf{I}\vec{\omega}$ [30] where $\mathbf{I}$, the inertia matrix of the vehicle, is of the form

$$\mathbf{I} = \begin{bmatrix} I_{xx} & I_{xy} & I_{xz} \\ I_{xy} & I_{yy} & I_{yz} \\ I_{xz} & I_{yz} & I_{zz} \end{bmatrix} \tag{3.39}$$

Assuming $\mathbf{I}$ changes slowly enough to be considered constant over the interval of interest,

$$\frac{\partial(\mathbf{I}\vec{\omega})}{\partial t} = \mathbf{I}\,\frac{\partial \vec{\omega}}{\partial t}$$

and Equation 3.38 can be rewritten as

$$\vec{\tau} = \mathbf{I}\dot{\vec{\omega}} + (\vec{\omega} \times \mathbf{I}\vec{\omega}) \tag{3.40}$$

The goal of the attitude control system is to control the vehicle's velocity angles which are used to define the vector

$$\vec{\theta} = [\phi \;\; \alpha \;\; \beta]^T$$

so that $\vec{\omega} = \mathbf{R}^{-1}\dot{\vec{\theta}}$ and $\dot{\vec{\omega}} = \mathbf{R}^{-1}\ddot{\vec{\theta}}$ where

$$\mathbf{R} = \begin{bmatrix} \cos\beta\cos\alpha & -\sin\beta & \cos\beta\sin\alpha \\ \sin\beta\cos\alpha & \cos\beta & \sin\beta\sin\alpha \\ -\sin\alpha & 0 & \cos\alpha \end{bmatrix} \tag{3.41}$$

is the rotation matrix, calculated in Appendix A, that is required to convert from a body referenced system to a velocity angle referenced system. Substituting the expressions for $\vec{\omega}$ and $\dot{\vec{\omega}}$ into Equation 3.40 and rearranging yields the second-order system

$$\ddot{\vec{\theta}} = -\mathbf{R}\,\mathbf{I}^{-1}\left(\mathbf{R}^{-1}\dot{\vec{\theta}} \times \mathbf{I}\mathbf{R}^{-1}\dot{\vec{\theta}}\right) + \mathbf{R}\,\mathbf{I}^{-1}\vec{\tau}_{in} + \vec{\mathbf{d}}(t) \tag{3.42}$$

where $\vec{\mathbf{d}}(t)$ has been added to represent the disturbances due to unmodelled dynamics and $\vec{\tau}_{in}$ is the torque due to the control inputs (i.e., jet firings). With the acceleration due to dynamic coupling already included in the first term of Equation 3.42, the acceleration due to control inputs can be assumed to be $\vec{\mathbf{u}} = \hat{\mathbf{I}}^{-1}\vec{\tau}_{in}$, which represents the desired control (i.e., the body referenced angular acceleration commands to be used by the actuator selection

algorithm). Rearranging, Equation 3.42 can be written in the desired form

$$\ddot{\vec{\theta}} = \vec{f} + B\vec{u} + \vec{d} \tag{3.43}$$

where

$$\vec{f} = -R\, I^{-1}\left(R^{-1}\,\dot{\vec{\theta}} \times IR^{-1}\,\dot{\vec{\theta}}\right) \tag{3.44}$$

and

$$B\vec{u} = R\, I^{-1}\,\vec{\tau}_{in}$$

From Equation 3.30, the desired form of **B** is $\mathbf{B} = (\underline{1} + \Delta)\hat{\mathbf{B}}$ with $\underline{1}$ the 3 x 3 identity matrix. The rotation matrix **R** is strictly a function of the velocity angles. Assuming accurate knowledge of these angles, **R** can be assumed known. The mass properties, however, are unknown, and the actual inertia matrix is written as $\mathbf{I} = \hat{\mathbf{I}} + \delta\mathbf{I}$ where $\hat{\mathbf{I}}$ is the current estimate and $\delta\mathbf{I}$ represents the error or difference between the actual and estimated inertia matrix. **B** can then be put in the desired form with

$$\begin{aligned} \hat{\mathbf{B}} &= \underline{1} \\ \Delta &= R\left(\hat{\mathbf{I}} + \delta\mathbf{I}\right)^{-1}\hat{\mathbf{I}} - \underline{1} \end{aligned} \tag{3.45}$$

With an appropriate system model established as Equation 3.43, a discontinuous 3-dimensional control law for this second-order system of the form of Equation 3.33 can be designed. Following the

single-input, second-order example presented in Section 3.4, $\vec{\hat{\mathbf{u}}}$ is found to be

$$\vec{\hat{\mathbf{u}}} = \vec{\dot{\theta}}_r - \vec{\hat{\mathbf{f}}} - \vec{\hat{\mathbf{d}}} \tag{3.46}$$

with

$$\vec{\dot{\theta}}_r = \vec{\dot{\theta}}_d - \Lambda\vec{\tilde{\theta}} \tag{3.47}$$

where Λ is a diagonal matrix containing the λ_i's from Equation 3.32, and $\vec{\dot{\theta}}_d$ represents the desired velocity angle accelerations. All that remains to finish the switching control law design is to calculate estimates and bounds for $\mathbf{I}$, $\mathbf{B}$, and $\vec{\mathbf{d}}(t)$ based on the expected atmospheric densities and vehicle properties for the given aerocapture mission and vehicle. Calculations for these estimates and bounds for an Earth aerocapture using the AFE vehicle are presented in Appendix B.

The final attitude control law design in the continuous form of Equation 3.37 can now be completed by selecting the thickness of the boundary layers. The elements of the vector

$$\vec{\Phi} = [\Phi_\phi \; \Phi_\alpha \; \Phi_\beta]^T$$

represent the boundary layer thickness about the sliding surfaces corresponding to each of the velocity angles. For simplicity, a constant thickness is chosen for each Φ_i. For this design, the choice of each Φ_i is based on the desire to track the velocity angles to

within 2 degs of the commanded angles. Since this is a second-order system, from Equation 3.32

$$s_i(\vec{x},t) = \dot{\tilde{\theta}}_i + \lambda_i \tilde{\theta}_i$$

As in the example in Section 3.3, the sampling rate is assumed to provide the strictest criteria on the choice of each λ_i. With a sampling rate of 25 hz, $\lambda_i = 5$. Assuming $\dot{\tilde{\theta}}_i$ is negligible with respect to $\lambda_i \tilde{\theta}_i$ and angular tracking is desired to be within 2 deg $(|\tilde{\theta}_i| \leq 0.035 \text{ rads})$, after each sliding surface is reached s_i should be within the range $|s_i| \leq 0.17$. The thickness of each boundary, Φ_i, is therefore selected to be 0.17, or

$$\Phi = \begin{bmatrix} 0.17 \\ 0.17 \\ 0.17 \end{bmatrix} \frac{\text{rads}}{\text{sec}}$$

With selection of Φ, design of the first element of the aerocapture attitude control system, the control law, is complete.

The same steps described above can be used to design the control law for any aerocapture mission or vehicle. The only differences from one mission or vehicle to the next are the estimates and bounds on $\mathbf{I}$, $\mathbf{B}$, and $\vec{\mathbf{d}}(t)$ and the choice of each λ_i and Φ_i. Estimates and bounds on $\mathbf{I}$, $\mathbf{B}$, and $\vec{\mathbf{d}}(t)$ are dependent on the atmosphere and vehicle properties for a given mission, while λ_i and Φ_i are based on the system cycling rates and desired tracking response.

Chapter 4

Actuator Selection

4.1 Introduction

The task of the actuator selection algorithm is to determine which actuators to employ, and to what extent, in order to generate the angular accelerations commanded by the control law. In order for the algorithm to make the proper selection, accurate knowledge of the effectiveness of each actuator is required. The selection algorithm must also be able to adapt to updated knowledge of those parameters which affect the control authority of the actuators (e.g., vehicle mass properties).

Section 4.2 presents the general actuator selection problem as a linear system of equations whose solution is the optimal mix of actuator activity that generates the commanded angular accelerations. Section 4.3 describes how linear programming is used with the simplex method to solve the actuator selection problem.

4.2 Actuator Selection Problem as a Linear System of Equations

The actuator selection problem can be represented as the problem of finding a solution to a system of linear equations equal to the requested angular accelerations. In addition, it may be desirable to find the solution that minimizes a linear cost function

corresponding to fuel usage. Such a problem can be summarized as the minimization of the cost function

$$z = \sum_{j=1}^{n} c_j x_j \tag{4.1}$$

subject to

$$\sum_{j=1}^{n} \vec{a}_j x_j = \Delta \mathbf{R} \tag{4.2a}$$

$$0 \leq x_j \leq u_j^+ \tag{4.2b}$$

where

n = # of actuators available
c_j = cost factor associated with use of actuator #j
x_j = decision variable indicating amount of action selected for actuator #j
u_j^+ = upper bound on the decision variable for actuator #j
$\vec{a}_j$ = activity vector specifying control authority of actuator #j
$\Delta \mathbf{R} = [\dot{p}_c \;\; \dot{q}_c \;\; \dot{r}_c \;]^T$ = commanded angular accelerations.

This formulation of the actuator selection problem can be applied to more than one type of actuator. Each $\vec{a}_j$ represents the acceleration provided by actuator #j per unit amount of its employment. The solution $\vec{x}$ to the linear program is the vector containing the decision variables x_j specifying the amount of corresponding actuator action required to generate the commanded acceleration. For aerosurface control actuators, decision variables may represent aerosurface deflection angles. For RCS jets, the

decision variables represent the duty cycle (i.e., the ratio of jet on time to off time), ranging from 0 to 1, defining the fraction of maximum acceleration required of a particular jet. The cost c_j of using actuator #j is defined by the user and can vary greatly depending on the type of actuator and the mission profile. The cost of employing an aerosurface relative to the cost of an RCS jet may be higher at high altitudes where aerosurfaces are less effective than jets, but may be lower at the lower attitudes where they are effective and reduce the fuel expenditure due to firing jets.

For the AFE-like vehicle used in this thesis, the only actuators used for attitude control are RCS jets. When new angular accelerations are commanded by the control law, a new optimization problem of the form of Equations 4.1 and 4.2 must be solved to determine the optimal jet duty cycles. The scheduling of jet firings is then determined based on the chosen duty cycles as will be discussed in Chapter 6. To perform this jet selection task, an activity vector $\vec{\mathbf{a}}_j$ for each jet must first be calculated.

The activity vector of each jet is determined from the equation

$$\vec{\mathbf{a}}_j = \mathbf{I}^{-1}\left(\vec{\mathbf{r}}_j \times \vec{\mathbf{T}}_j\right) \tag{4.3}$$

where $\mathbf{I}$ is the vehicle inertia matrix, $\vec{\mathbf{r}}_j$ is the position of jet #j witn respect to the center of mass of the vehicle, and $\vec{\mathbf{T}}_j$ is the thrust of jet #j. Figure 4.1 is a rear view of the AFE vehicle used in this thesis diagraming the positioning of the RCS jets. Jets #1 - #8 all provide

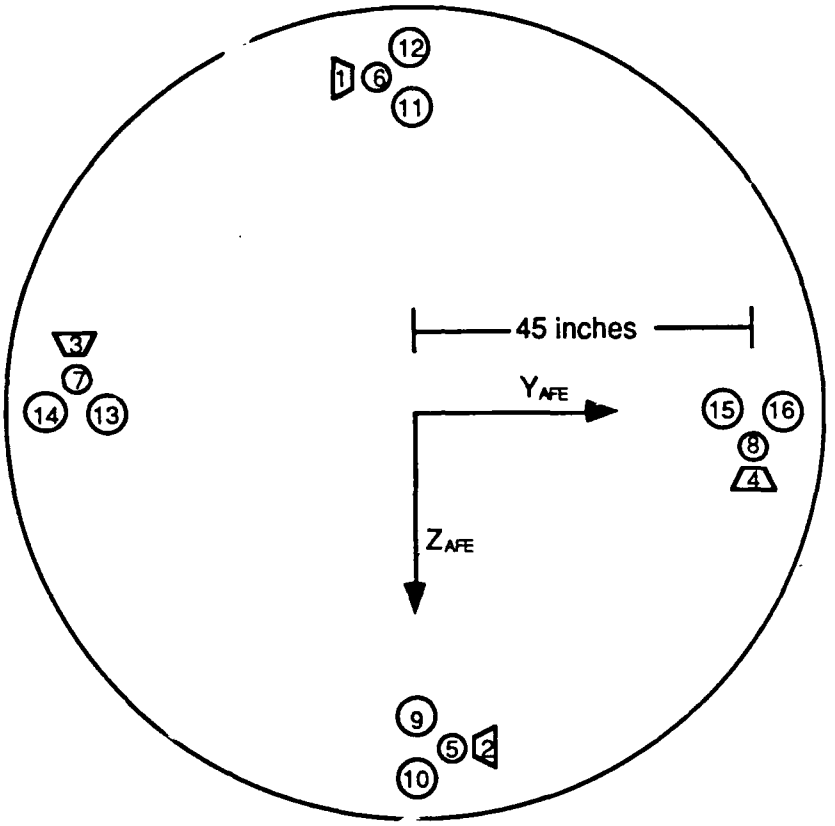

Jet #	Direction of thrust
1	+Y
2	- Y
3	+Z
4	- Z
5 - 16	+X

Figure 4.1. Aft View of AFE Vehicle (+X axis into page)

30 lbf of thrust while jets #9 - #16 provide 125 lbf of thrust [31]. Assuming known position and thrust of each jet, accurate estimates of the vehicle inertia and center of mass location are required to properly calculate jet activity vectors. Estimation of these mass

properties is accomplished outside of the actuator selection algorithm (i.e., by the mass property identification algorithm discussed in Chapter 5). Whenever updated estimates are provided, the activity vectors are recalculated.

All that remains to complete the formulation of the jet selection problem is the definition of the costs associated with the use of each jet. For the candidate control system, each c_j is assigned as a constant representing the rate of fuel consumption during firing of jet #j. Assuming a constant ratio between the amount of fuel used and the amount of thrust provided, the 125 lbf jets are assigned a cost of 4.2 while the 30 lbf jets are assigned a cost of 1.

Several algorithms surveyed in reference [28] can be used to solve the system represented by Equation 4.2. Of these, only the linear programming approach solves Equation 4.2 while minimizing Equation 4.1. Because of this, linear programming was chosen for the jet selection element of the candidate aerocapture attitude control system.

4.3 Linear Programming and the Simplex Method

The use of linear programming has been shown [32] to perform the task of adaptable jet selection quite well. It is especially well suited for hybrid actuator selection for which the optimal blend of different types of actuators (e.g., RCS jets and aerosurfaces) is chosen from a common pool of actuators [20,21]. RCS jets are the only attitude control actuators available to the actual AFE vehicle. For the current effort, they also represent the only type of actuators available to the candidate design. As an actuator selection algorithm

for jets only, linear programming is still attractive, having been shown in flight test to select the most fuel efficient mix of jet firings that implements the commanded angular accelerations. Also, by employing linear programming for jet selection for this example, this attitude control system can easily be used for control of a vehicle with varied actuators without changing the system structure.

The combination of Equations 4.1 and 4.2 is the formulation of a general linear programming problem. To solve this problem, an upper bounding simplex method is employed. Section 4.3.1 outlines the basic simplex method for a general linear programming problem. Section 4.3.2 describes how the simplex method is altered when the decision variables (i.e., amounts of actuator activity) are upper bounded as in the actuator selection problem.

4.3.1 Basic Linear Programming Problem and Simplex Method

Like the actuator selection problem presented in Section 4.2, the typical linear programming problem is to find the one solution to an underdetermined system of linear equations having many possible solutions which minimizes a linear cost function. In equation form [33], the problem is to minimize $z = \vec{c}^T \vec{x}$ subject to

$$\mathbf{A}\vec{x} = \vec{b}\,, \; x_j \geq 0 \tag{4.4}$$

where $\vec{x}$ is the solution vector having n components, $\vec{c}$ is a vector having n cost components, $z = c_1x_1 + \ldots + c_nx_n$ is the cost function to be minimized, $\mathbf{A}$ is an m by n matrix with $m \leq n$, and $\vec{b}$ is a column

vector of m components. Comparing this formulation to Equations 4.1 and 4.2, the columns of the matrix **A** are the activity vectors associated with each decision variable x_j, and $\vec{\mathbf{b}}$ is the requested output $\Delta\mathbf{R}$. The main difference between the two formulations is that the x_j's are not upper bounded in Equation 4.4 as they are in Equation 4.2.

An important property of the solution vector $\vec{\mathbf{x}}$ that minimizes the cost function is that at least $n - m$ of its components are zero [33]. To illustrate this property, consider the simple problem of minimizing the cost function $z = 2x_1 + x_2$ subject to the equation $x_1 + 2x_2 = 4$. Written in the form of Equation 4.4, the problem is:

minimize

$$z = 2x_1 + x_2 \tag{4.5a}$$

subject to

$$\begin{bmatrix} 1 & 2 \end{bmatrix} \begin{bmatrix} x_1 \\ x_2 \end{bmatrix} = 4 \tag{4.5b}$$

with $m = 1$, $n = 2$ ($m < n$). In Figure 4.2, the line segment PQ represents the "feasible set" of all possible solutions to the equality constraint (Equation 4.5b) with the additional constraint of $x_i \geq 0$. For a cost of z=0, Figure 4.2 shows that the line of constant cost does not intersect the feasible set. The first intersection occurs at point P when the cost is increased to 2. This intersection point, corresponding to $\vec{\mathbf{x}} = [0\ 2]^T$, represents the solution to the equality constraints that minimizes the cost function and, therefore, the desired solution to the linear program. The solution also agrees with

the property of having $n - m = 1$ components equal to zero. This property holds for problems of higher dimension.

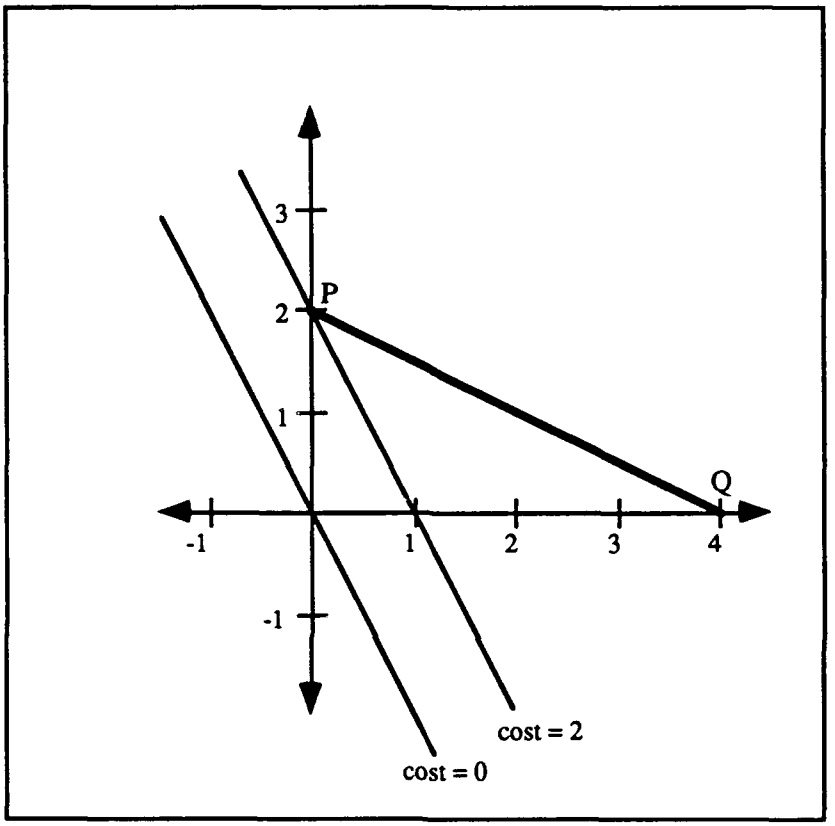

Figure 4.2. Feasible Set and Cost Curves

As outlined in reference [33], the simplex method can be used to solve the linear programming problem. Given the property discussed above, the task of the simplex method is to determine where the zeros belong in the solution. The feasible set of solutions can be imagined to be a polyhedron of many edges and faces with the corners representing a solution to the equality constraints in Equation 4.4 with only m nonzero components. The basic approach

of simplex is to start at an extreme point or corner of the feasible set. Since this starting point probably does not minimize the cost function, the next step in simplex is to move to a neighboring corner of the feasible set where the cost is lower. To find a neighboring corner, one of the zero components of $\vec{x}$ is allowed to become positive while the remaining zero components are unchanged. As the selected component is increased, the original nonzero components must adjust in order for the equality constraints in Equation 4.4 to still hold. During the adjustment, some of these components may decrease toward zero. Once the new component of $\vec{x}$ is increased to the point where one of the original nonzero components becomes zero, a neighboring corner has been found and the cost can be evaluated to determine if it has been reduced. Since there is a finite number of corners to a feasible set, a smaller finite number of steps is required until the cost is reduced to its minimum and the optimal solution is found.

As an example illustrating the basic approach of simplex, consider the following simple minimization problem:

$$\text{minimize} \qquad z = [3 \;\; 4 \;\; 1]\,\vec{x} \tag{4.6a}$$

$$\text{subject to} \qquad [1 \;\; 1 \;\; 1]\,\vec{x} = 1 \;,\; x_i \geq 0 \tag{4.6b}$$

The shaded region in Figure 4.3 represents the feasible set of solutions to the equality constraints in Equation 4.6b.

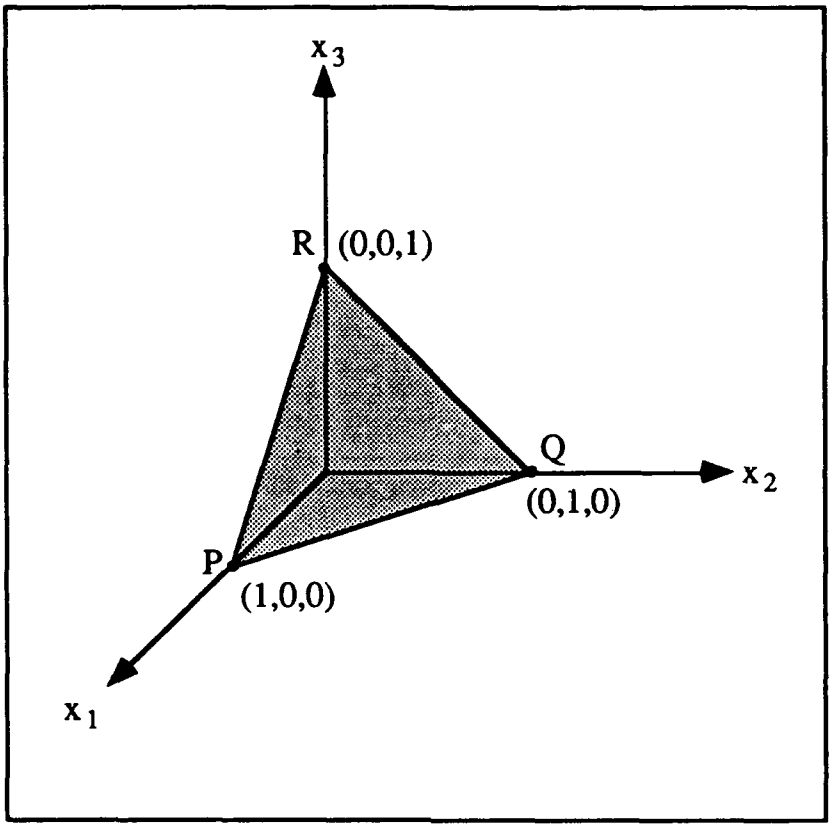

Figure 4.3. 3-D Feasible Set for Example Problem

Point P represents a corner of the feasible set with $m = 1$ positive components and $n - m = 2$ zero components. Beginning at P (i.e., $\vec{x} = [1\ 0\ 0]^T$), simplex must find a neighboring corner with a cost lower than $z(P) = 3$. The decision as to which zero component to allow to become positive must be made. If x_2 is increased while keeping $x_3=0$, then Equation 4.6b requires

$$x_1 = 1 - x_2 \tag{4.7a}$$

and the cost function is

$$z=3(1 - x_2) + 4x_2 = 3 + x_2 \tag{4.7b}$$

so that the cost is increased as x_2 is increased. If, however, x_3 is increased while x_2 is held at zero, Equation 4.6b requires

$$x_1 = 1 - x_3 \tag{4.8a}$$

and the cost function is

$$z=3(1 - x_3) + x_3 = 3 - 2x_3 \tag{4.8b}$$

resulting in the cost being reduced with the increase of x_3. The decision to increase x_3 instead of x_2 is obvious. Equation 4.8a is then used to determine how much to increase x_3 in order to arrive at a corner of the feasible set. If x_3 is increased to 1, x_1 is reduced to zero and the point $\vec{\mathbf{x}} = [0 \quad 0 \quad 1]^T$, labelled R in Figure 4.3, is the neighboring corner selected by simplex. Since the only corners neighboring R represent higher costs, point R is the optimal solution to the linear programming problem presented by Equation 4.6.

4.3.2 Upper Bounding Simplex for Actuator Selection

Since there are upper limits to the amount a control actuator can be employed (i.e., an aerosurface can only be deflected a limited number of degrees, and 100% is the maximum duty cycle of an RCS jet) the decisions variables x_j are upper bounded, and simplex must not select decision variables above their limits. A modified, upper bounding simplex method is, therefore, required [21]. As with the basic simplex method, this modified method begins with a nonoptimal solution to the linear program with m nonzero components of $\vec{\mathbf{x}}$ representing the use of m actuators for the solution. An m by m matrix $\mathbf{B}$, whose columns consist of the activity vectors $\vec{\mathbf{a}}_j$

associated with the m chosen actuators, is considered the basis. For three dimensional attitude control, m =3 and upper bounding simplex begins with a 3-jet solution with the basis **B** a 3 by 3 matrix containing the activity vectors of the jets chosen for the solution.

Simplex then considers one of the $n - m$ unused actuators and increases its associated decision variable until one of three possibilities occurs. The first possibility is that one of the original decision variables will go to zero. When this happens, if the cost is lowered, the activity vector associated with the new nonzero decision variable is "pivoted" into the basis in place of the activity vector associated with the decision variable driven to zero. This occurrence is the equivalent of a single step of the general simplex method.

The second possibility during consideration of the new actuator is that either one of the original nonzero decision variables or the new nonzero decision variable reaches its upper bound before one of the decision variables is driven to zero. The resulting solution for consideration then consists of m decision variables at less than their upper bounds with their associated activity vectors making up the new basis **B**, and one (or more after consideration of several actuators) decision variable at its upper bound. In equation form

$$\mathbf{B}\vec{\mathbf{x}}_B + \sum_{k=1}^{p} \vec{\mathbf{a}}_k u_k = \Delta\mathbf{R} \tag{4.9}$$

where

B = m by m basis matrix consisting of the m activity vectors with decision variables that are nonzero and below their upper bounds

$\vec{\mathbf{x}}_B$ = vector of the m decision variables whose associated activity vectors are in the basis

p = total number of decision variables at their upper bounds

$\vec{a}_k$ = activity vector with associated decision variable u_k at its upper bound

$\Delta \mathbf{R} = [\dot{p}_c \ \dot{q}_c \ \dot{r}_c]^T$ = commanded angular accelerations.

If this resulting solution provides a lower overall cost, the solution is saved and the modified simplex method selects another actuator for consideration.

The third possibility can occur when the currently saved solution already has decision variables at their upper bounds as in Equation 4.9. As a new actuator is considered, the increase of its associated decision variable may drive a decision variable at its upper bound toward zero. The new decision variable is increased until a new solution of the form of Equation 4.9 is found. Decision variables at their upper bounds may drop out of the solution, they may become a decision variable whose activity vector is in the basis, or decision variables associated with basis activity vectors may be driven to their upper bounds. All actuators are considered until the optimal solution of the form of Equation 4.9 is found.

Chapter 5

Mass Property Identification

5.1 Introduction

From Chapter 4 it is obvious that the linear programming algorithm used for jet selection requires accurate mass property estimates to properly choose which jets to fire. In particular, activity vectors specifying the acceleration provided by each jet depend directly on accurate knowledge of the vehicle inertia matrix, the location of the jet with respect to the vehicle center of mass, and the thrust vector (i.e., thrust level and direction) for each jet. For the purposes of this thesis, the location on the vehicle and the thrust vector for each jet are assumed known, while the vehicle inertia matrix and location of the center of mass must be estimated.

For a mission like the AFE in which mass properties remain nearly constant and accurate estimates are known a priori, the initial estimates are valid throughout the mission and updated estimates are not required. For the more general case in which mass properties may be unknown a priori or may change significantly during the mission, accurate and timely estimates are essential. For many potential missions, updates of mass property estimates from the control centers on the ground are not feasible. For an aerocapture mission at Mars, for example, the time required to transmit data from Earth makes timely updates of mass property

estimates impossible. An in-flight mass property estimation capability is, therefore, required.

One approach to updating mass property estimates is to begin with initial accurate measurements of the desired mass properties of both the vehicle and the payload. Using onboard fuel gauges to measure fuel expenditure, updated estimates can then be generated by monitoring the mass of the fuel consumed along with the fuel's location in the vehicle. Since accurate knowledge of the payload mass properties is required, this approach is not feasible for the example system of this thesis in which unknown payload mass properties are possible. An estimation algorithm that doesn't require prior mass property knowledge is needed.

Section 5.2 describes a nonlinear filter design that is used to generate estimates of the vehicle inertia matrix and location of center of mass, without prior knowledge of these properties, based on noisy measurements of the vehicle angular rate changes due to jet firings. A strategy to select the jet firings that provide the most information to the filter during times dedicated to mass property identification is outlined in Section 5.3.

5.2 Estimation of Vehicle Inertia Matrix and Center of Mass Location

A standard Kalman filter is used to estimate system unknowns based on a linearized model of the system, while an extended Kalman filter is used for estimation when the more general nonlinear system model must be retained [34]. The model of the dynamics of a spacecraft (i.e., Equation 3.33) is nonlinear. As will be shown below,

the full nonlinear model must be used in order to make estimates of all the unknown mass properties (i.e., inertia matrix and location of center of mass). The mass property estimator is, therefore, a nonlinear filter design resembling a second-order, extended Kalman filter and is of the form first presented in references [22,23,24]. A model of the rigid spacecraft dynamics is used with the current mass property estimates to predict the output of the spacecraft's rate gyros due to jet firings. The filter compares these predictions with the measured values and makes revisions to its mass property estimates based on this comparison. The following outlines the filter design of [23,24].

In Chapter 3, a model of the dynamics of a rigid aerocapture spacecraft was developed and expressed in terms of the velocity angles and rates. A similar model in terms of the body referenced angular rates can be expressed by the equation

$$\mathbf{I}\dot{\vec{\omega}} = -\left(\vec{\omega} \times \mathbf{I}\vec{\omega}\right) + \vec{\tau} + \vec{\mathbf{d}} \qquad (5.1)$$

where

$\mathbf{I}$ = the vehicle inertia matrix
$\vec{\tau}$ = applied torques
$\vec{\mathbf{d}}$ = the sum of all disturbance torques
$\dot{\vec{\omega}}$ = angular accelerations
$\vec{\omega}$ = angular rates

Assuming mass properties and jet thrust are constant over the interval Δt and that $\dot{\vec{\omega}} = \Delta\vec{\omega}/\Delta t$ where $\Delta\vec{\omega}$ is the change in angular rate, Equation 5.1 can be rewritten as

$$\Delta\vec{\omega} = \mathbf{I}^{-1}\left[-\left(\vec{\omega}\times\mathbf{I}\vec{\omega}\right)+\sum_{j}\left(\vec{r}_j\times\vec{T}_j\right)+\vec{d}\right]\Delta t \qquad (5.2)$$

where $\vec{T}_j$ is the known thrust of jet #j, $\vec{r}_j$ is the displacement of jet #j from the center of mass (i.e., the lever arm), and Δt is the time step. Since the location of the center of mass is not known, $\vec{r}_j$ is not known. The displacement of jet #j from the center of mass can be expressed as

$$\vec{r}_j = \vec{r}_j' - \vec{r}_{cm} \qquad (5.3)$$

where $\vec{r}_j'$ is the known location on the vehicle of jet #j, and $\vec{r}_{cm}$ is the location of the center of mass which is to be estimated.

The spacecraft used for this example aerocapture mission is assumed to have a maximum allowable roll rate of 20 deg/sec. With a roll rate near this limit, the rate change due to the torque from the dynamic coupling (i.e., $\vec{\omega}$ x $\mathbf{I}\vec{\omega}$) is significant and must be considered. Ignoring this term for now in order to put Equation 5.2 in a form more suitable for filter design, an estimate of this dynamic coupling term based on rate measurements and the current inertia matrix estimate will later be subtracted from the difference (i.e., the residual) between the measured and predicted rate change.

Without dynamic coupling, Equation 5.2 can be rewritten to give the rate changes experienced by a spacecraft due to jet firings as

$$\Delta\vec{\omega} = \mathbf{I}^{-1}\vec{\alpha} - \mathbf{I}^{-1}\left(\vec{r}_{cm} \times \vec{\lambda}\right) + \vec{d}\Delta t \qquad (5.4)$$

where

$$\vec{\lambda} = \left(\sum_j \vec{T}_j\right)\Delta t \qquad (5.5)$$

is defined as the linear impulse due to all jet forces and

$$\vec{\alpha} = \left(\sum_j \vec{r}_j' \times \vec{T}_j\right)\Delta t \qquad (5.6)$$

is the angular impulse of the vehicle about the defined vehicle origin due to jet firings. The disturbance term in Equation 5.4 consists of the rate changes due to the aerodynamic forces, the unmodelled dynamics, and the difference between the actual dynamic coupling and the estimated dynamic coupling. The spacecraft is assumed to operate at altitudes high enough that the magnitudes of the aerodynamic torques are small compared to the torques applied by the RCS jets. Since the unmodelled dynamics and the difference between the actual and estimated dynamic coupling terms are also considered small, the last term of Equation 5.4 can be considered a noise signal

$$\vec{v}' = \vec{d}\Delta t \qquad (5.7)$$

With known jet positions and thrust levels, the only unknowns in Equation 5.4 other than the noise are the vehicle's location of

center of mass, $\vec{r}_{cm}$, and the inverse inertia matrix. These are the mass properties required by the actuator selection algorithm to calculate the activity vectors for each jet. With a noisy system like that expressed by Equation 5.4, an estimator such as a Kalman filter is required to generate accurate parameter estimates in the presence of noise.

The second-order filter designed in references [23,24] was derived in order to estimate these mass properties in the presence of noise. The filter contains the system model represented by Equation 5.2 which it uses to predict the output of rate gyros, $\Delta\vec{\omega}_p$. The predicted output is then used in comparison with the actual measured output, and revisions to the mass property estimates are made accordingly.

Since the filter compares measured angular rate changes to predicted angular rate changes at discrete times, the measured angular rate changes must first be expressed as a discretized function of the mass properties to be estimated. A state vector $\vec{y}$ whose elements are the mass properties to be estimated is defined as

$$\vec{y} = \left[I^{-1}_{11}, I^{-1}_{22}, I^{-1}_{33}, I^{-1}_{23}, I^{-1}_{13}, I^{-1}_{12}, r_{cm_1}, r_{cm_2}, r_{cm_3}\right]^T \qquad (5.8)$$

where $I^{-1}{}_{ij}$ is the element in the i^{th} row and j^{th} column of the inverse inertia matrix, and r_{cmi} is the i^{th} element of $\vec{r}_{cm}$. Rearranging Equation 5.4, a change in the vehicle's angular rates can be expressed in terms of $\vec{y}$ as

$$\Delta\vec{\omega} = \vec{h}(\vec{y}) + \vec{v} \qquad (5.9)$$

where

$$\vec{h}(\vec{y}) = A\vec{y} + \frac{1}{2}\sum_{i=1}^{3} \vec{\Phi}_i \vec{y}^T \Lambda_i \vec{y} \tag{5.10}$$

In Equation 5.10, **A** is a 3 x 9 matrix satisfying

$$A\vec{y} = I^{-1}\vec{\alpha} \tag{5.11}$$

while each Λ_i is a symmetric 9 x 9 matrix satisfying

$$\frac{1}{2}\vec{y}^T \Lambda_i \vec{y} = \left[I^{-1}\left(\vec{r}_{cm} \times \vec{\lambda}\right)\right]_i \tag{5.12}$$

for each vector component i = 1, 2, 3, and the $\vec{\Phi}_i$ are the natural basis vectors

$$\vec{\Phi}_1 = \begin{bmatrix} 1 \\ 0 \\ 0 \end{bmatrix}, \vec{\Phi}_2 = \begin{bmatrix} 0 \\ 1 \\ 0 \end{bmatrix}, \vec{\Phi}_3 = \begin{bmatrix} 0 \\ 0 \\ 1 \end{bmatrix} \tag{5.13}$$

used to create a vector out of the scalar terms, $\vec{y}^T \Lambda_i \vec{y}$. The matrices **A** and Λ_i are found to be:

$$A = \left[\begin{array}{ccc|ccc|ccc} \alpha_1 & 0 & 0 & 0 & \alpha_3 & \alpha_2 & 0 & 0 & 0 \\ 0 & \alpha_2 & 0 & \alpha_3 & 0 & \alpha_1 & 0 & 0 & 0 \\ 0 & 0 & \alpha_3 & \alpha_2 & \alpha_1 & 0 & 0 & 0 & 0 \end{array}\right] \tag{5.14}$$

$$\Lambda_1 = \begin{bmatrix} 0 & 0 & 0 & 0 & 0 & 0 & 0 & -\lambda_3 & \lambda_2 \\ 0 & 0 & 0 & 0 & 0 & 0 & 0 & 0 & 0 \\ 0 & 0 & 0 & 0 & 0 & 0 & 0 & 0 & 0 \\ 0 & 0 & 0 & 0 & 0 & 0 & 0 & 0 & 0 \\ 0 & 0 & 0 & 0 & 0 & 0 & -\lambda_2 & \lambda_1 & 0 \\ 0 & 0 & 0 & 0 & 0 & 0 & \lambda_3 & 0 & -\lambda_1 \\ 0 & 0 & 0 & 0 & -\lambda_2 & \lambda_3 & 0 & 0 & 0 \\ -\lambda_3 & 0 & 0 & 0 & \lambda_1 & 0 & 0 & 0 & 0 \\ \lambda_2 & 0 & 0 & 0 & 0 & -\lambda_1 & 0 & 0 & 0 \end{bmatrix} \quad (5.15a)$$

$$\Lambda_2 = \begin{bmatrix} 0 & 0 & 0 & 0 & 0 & 0 & 0 & 0 & 0 \\ 0 & 0 & 0 & 0 & 0 & 0 & \lambda_3 & 0 & -\lambda_1 \\ 0 & 0 & 0 & 0 & 0 & 0 & 0 & 0 & 0 \\ 0 & 0 & 0 & 0 & 0 & 0 & -\lambda_2 & \lambda_1 & 0 \\ 0 & 0 & 0 & 0 & 0 & 0 & 0 & 0 & 0 \\ 0 & 0 & 0 & 0 & 0 & 0 & 0 & -\lambda_3 & \lambda_2 \\ 0 & \lambda_3 & 0 & -\lambda_2 & 0 & 0 & 0 & 0 & 0 \\ 0 & 0 & 0 & \lambda_1 & 0 & -\lambda_3 & 0 & 0 & 0 \\ 0 & -\lambda_1 & 0 & 0 & 0 & \lambda_2 & 0 & 0 & 0 \end{bmatrix} \quad (5.15b)$$

$$\Lambda_3 = \begin{bmatrix} 0 & 0 & 0 & 0 & 0 & 0 & 0 & 0 & 0 \\ 0 & 0 & 0 & 0 & 0 & 0 & 0 & 0 & 0 \\ 0 & 0 & 0 & 0 & 0 & 0 & -\lambda_2 & \lambda_1 & 0 \\ 0 & 0 & 0 & 0 & 0 & 0 & \lambda_3 & 0 & -\lambda_1 \\ 0 & 0 & 0 & 0 & 0 & 0 & 0 & -\lambda_3 & \lambda_2 \\ 0 & 0 & 0 & 0 & 0 & 0 & 0 & 0 & 0 \\ 0 & 0 & -\lambda_2 & \lambda_3 & 0 & 0 & 0 & 0 & 0 \\ 0 & 0 & \lambda_1 & 0 & -\lambda_3 & 0 & 0 & 0 & 0 \\ 0 & 0 & 0 & -\lambda_1 & -\lambda_2 & 0 & 0 & 0 & 0 \end{bmatrix} \quad (5.15c)$$

If only the elements of the inverse inertia matrix were required, the linear portion of Equation 5.10 would suffice; however, the location of the center of mass is also needed. Since the third 3 x 3 block partition of **A** contains only zeros, the elements of $\vec{r}_{cm}$ do not contribute to the linear portion of Equation 5.10. The complete nonlinear model represented by Equation 5.10 must therefore be used in order to estimate $\vec{r}_{cm}$.

Neglecting the effects of dynamic coupling, the difference in the discrete measurements of the angular rates from time k-1 to time k is assumed to satisfy the stochastic equation

$$\Delta\vec{\omega}_m = \vec{h}(\vec{y}_k) + \vec{v}_k \quad (5.16)$$

where $\Delta\vec{\omega}_m$ is the measured output of the gyros, $\vec{h}(\vec{y}_k)$ is from Equation 5.10 at time k, and $\vec{v}_k$, consisting of both the disturbance noise $\vec{v}'$ and the sensor noise, is assumed to be a 3-dimensional white gaussian noise signal with zero mean and independent of $\vec{y}_k$ and all

forces and torques. This assumed gaussian distribution for the combined noise signal is considered reasonable since the sensor noise is assumed to dominate and common gyros, such as the DRIRU II [24], exhibit gaussian noise characteristics.

Successive updates to the mass property estimates are then generated by the estimator from

$$\vec{y}_k = \vec{y}_{k-1} + K_k\left[\Delta\vec{\omega}_m - \Delta\vec{\omega}_p - \hat{I}^{-1}\left(\vec{\omega}_m \times \hat{I}\vec{\omega}_m\right)\right] \qquad (5.17)$$

where K_k is a gain matrix calculated via equations 2-119 through 2-121 of reference [24] at each step and is a function of the error covariance, the jets being fired, and the noise characteristics of the sensors; $\Delta\vec{\omega}_m$ is the measured difference in angular rates from time k-1 to time k; $\Delta\vec{\omega}_p$ is the predicted angular rate change determined from the rigid spacecraft model of Equation 5.2; and $\hat{I}^{-1}\left(\vec{\omega}_m \times \hat{I}\vec{\omega}_m\right)$ is the estimated rate change due to the dynamic coupling effects.

5.3 Input Selection During Dedicated Mass Property Identification

The filter design described above generates mass property estimates based on the comparison of predicted and measured angular rate changes due to RCS jet firings. In order to rapidly converge to accurate estimates, however, these jet firings cannot be random. For example, little can be learned about a vehicle's roll inertia by firing only pitch or yaw jets. A jet selection strategy which chooses the jet firings that are most likely to maximize the

increase in knowledge of the estimated parameters was originally developed in reference [35]. This strategy is employed in the candidate design during the periods dedicated to mass property estimation.

The goal of this input selection strategy is to develop an analytical method to determine the maneuver (i.e., jet firings) that will maximize the increase in knowledge of the desired mass properties. To do so, the error covariance matrix propagation across a measurement is examined. The change in the covariance matrix due to a measurement at time k is given by

$$\Delta \mathbf{P}_k = \mathbf{K}_k \mathbf{H}_k \mathbf{P}_k(-) \qquad (5.18)$$

where $\mathbf{K}_k$ is the gain matrix at time k, $\mathbf{H}_k$ is the output matrix at time k, and $\mathbf{P}_k(-)$ is the error covariance matrix prior to the measurement. A detailed explanation of the terms in Equation 5.8 can be found in reference [24].

Equation 5.18 depends only on the old state estimate, the old error covariance matrix, the noise covariance matrix, and the current jet thrusts and positions (i.e., the applied torques). Since all of these are known or have estimates (whether accurate or not), Equation 5.18 can be evaluated prior to each step to determine the increase in accuracy of the mass property estimates due to the firing of a particular jet. A decrease in the trace of $\mathbf{P}$ represents an increase in accuracy of the mass property estimates. At each step, the jet which maximizes the increase in accuracy (i.e., maximizes the decrease in the trace of $\mathbf{P}$) is then chosen to be fired. The chosen jet firings

result in a sequence which maximizes the likelihood of rapid convergence of the mass property estimates, thus minimizing fuel consumption during the estimation process.

Chapter 6

System Integration

6.1 Introduction

Chapters 3, 4, and 5 presented the development of the three main elements of the candidate aerocapture attitude control system: the robust control law, the jet selection algorithm, and the mass property identification algorithm. When combining these elements into the final attitude control system structure first illustrated in Figure 2.1, several integration issues must be addressed. Such issues include the system cycling rates, the interaction of the main elements, and the timing of the mass property updates. The overall system cycling rate, and the cycling rates of each of the main elements, are discussed in Section 6.2. Section 6.3 describes the interaction of the control law and the jet selection algorithm along with the control law "tuning" required to make these elements work together. Section 6.4 describes how the mass property identification algorithm is employed to detect mass property changes and provide timely updates to the mass property estimates. A brief summary of the overall operation of the candidate aerocapture attitude control system is provided in Section 6.5. Section 6.6 outlines how the candidate attitude control system can be applied to attitude control for other aerocapture vehicles

6.2 System Cycling Rates

Since the candidate control system was designed for a mission and vehicle similar to the AFE, the decision as to what rates to cycle the overall attitude control system and its elements was based on cycling rates of the existing AFE DAP. Cycling rates of the control system for use in other aerocapture vehicles may vary and will usually be dictated by system specifications.

The AFE guidance law generates bank angle commands once per second (i.e., 1 hz). The existing AFE DAP operates at a 25 hz rate corresponding to the minimum RCS jet firing time of 40 msec. The AFE DAP's proportional control law and its table look-up jet selection algorithm are both cycled at this 25 hz rate. Each time the control law is cycled it generates angular acceleration commands which are used in the table look-up jet selection algorithm to determine which jets to fire.

For the candidate control system, the guidance is also assumed to provide bank angle commands at a 1 hz rate. Like the AFE DAP, the sliding mode control law is cycled at a 25 hz rate. The linear programming jet selection algorithm, however, is cycled at 2.5 hz. The reason for the lower rate is due to the fact that the solution of each linear program consists of the jet duty cycles required to provide the angular accelerations commanded by the control law. In implementation, the 400 msec between each solution to the linear program is divided into ten periods of 40 msec in length. Jets are fired for the fraction of these ten periods corresponding to their associated decision variables from the last solution of the linear

program. For example, if the last solution of the linear programming problem results in a decision variable (i.e., commanded duty cycle) of x_j=0.41 for jet #j, jet #j will be fired during four of the ten 40 msec time periods between solutions to the linear program.

To more evenly implement the commanded duty cycles over the ten periods between solutions to the linear program, a running ratio is calculated for each selected jet to determine if the jet should be fired during the present period [21]. The ratio is

$$R_j|_{N_t} = \frac{0.5 + \sum_{k=1}^{N_t} J_j(k)}{N_t} \tag{6.1}$$

where N_t is the number of periods that have elapsed since the last jet selection, and J_j is defined by

$$J_j(k) = \begin{cases} 1 & \text{if jet \#j was fired during time cycle \#k} \\ 0 & \text{otherwise} \end{cases} \tag{6.2}$$

A selected jet is fired for the current 40 msec time period if the following condition is true:

$$R_j|_{N_t} < x_j \tag{6.3}$$

Table 6.1 shows an example of how the condition 6.3 is used to evenly spread jet firings throughout the ten time periods between solutions of the jet selection linear program. The entries in the

second column of Table 6.1 represent the calculation of the ratio (Equation 6.1) for a jet with a selected decision variable of $x_j = 0.41$. The third column contains the decisions of whether or not to fire the jet based on Equation 6.3.

time step	R_j	fire jet ($R_j < x_j$)?
1	0.50	no
2	0.25	yes
3	0.50	no
4	0.38	yes
5	0.50	no
6	0.42	no
7	0.36	yes
8	0.44	no
9	0.39	yes
10	0.45	no

Table 6.1. Example of Firing of Jets Between Solutions of Jet Selection Linear Program ($x_j = 0.41$)

Jet #j is fired for four of the ten 40 msec periods between solutions of the linear programming problem.

Like the control law, the mass property identification algorithm is also cycled at 25 hz. Identification is performed on every jet firing, but updated mass property estimates are provided to the control law and jet selection algorithm only when needed. Section

6.4 outlines the scheme for determining when to provide these updates.

6.3 Control Law/Jet Selection Interaction

The ability of the jet selection algorithm to provide the angular accelerations commanded by the control law is limited by the control authority of the jets. Since the control law generates the inputs to the jet selection algorithm without knowledge of the limitations of the actuators, it is possible for the control law to command angular accelerations that the jet selection algorithm cannot provide. From the equations for the sliding surface (Equation 3.32) and the sliding condition (Equation 3.31), it is obvious the control law parameters λ_i and η_i determine how quickly the control law attempts to drive the vehicle to its desired state. If these parameters are chosen so that they dictate a response quicker than the vehicle is capable of providing, the control law may consistently command accelerations greater than the jet selection algorithm can provide. When this happens, the actual accelerations of the vehicle will lag the commanded accelerations and the vehicle will have difficulty in tracking the desired trajectory.

This problem is demonstrated in a simulation of the combined control law/jet selection algorithm. In Chapter 3, each λ_i was chosen from the rule of thumb

$$\lambda_i = \frac{\text{sampling rate}}{5} \tag{6.4}$$

to be 5. Since the only requirement on each η_i is that they be positive constants, let each η_i be chosen as 1. Figure 6.1 shows the bank angle tracking response of the nominal AFE vehicle using the new control law and jet selection algorithm during a simple 120 second simulation. The simulation is started with the vehicle at 0 deg bank and trim α and β. The commanded bank angle is initially 45 deg and varies sinusoidally during the simulation. A commanded bank reversal occurs 60 sec into the simulation.

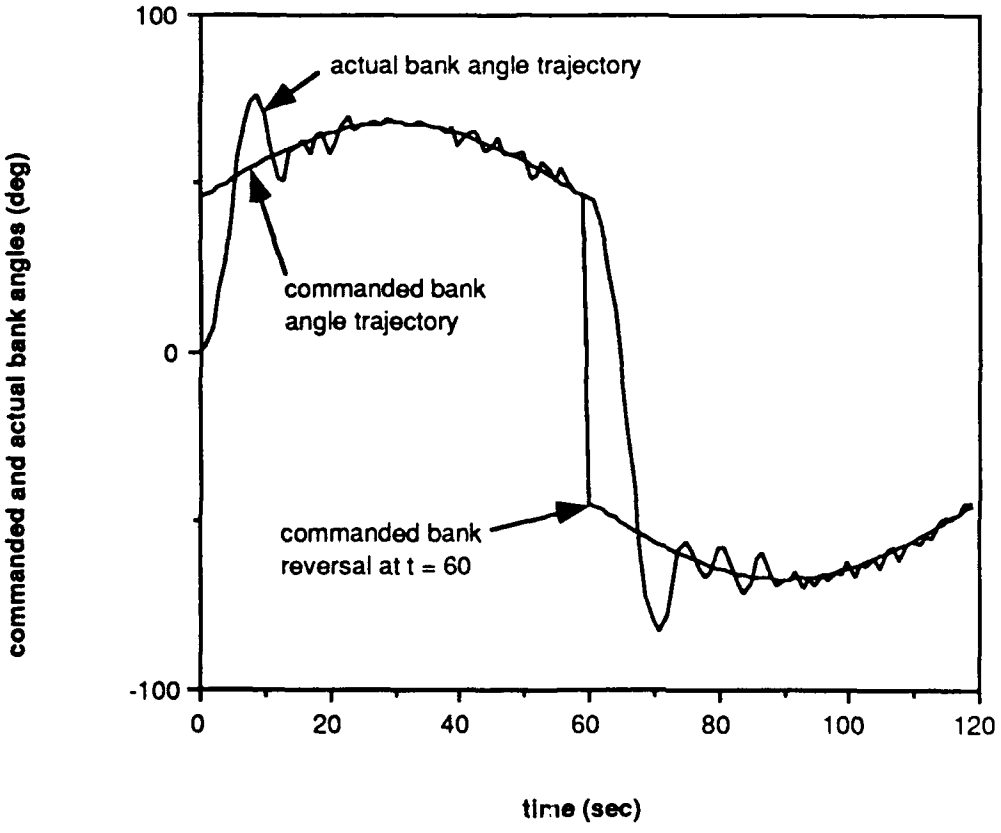

Figure 6.1. Bank Angle Tracking
(λ_i= 5.0, η_i = 1.0)

With $\lambda_i = 5$, $\eta_i = 1$ and an initial 45 deg offset, Equation 3.12 predicts that the sliding surface should be reached (resulting in tracking to within 2 deg) in a time less than

$$\frac{|s_i(\vec{x}(0), 0)|}{\eta_i} = \frac{|\lambda_i[\phi(0) - \phi_d(0)]|}{\eta_i} = \frac{5\left(45 \cdot \frac{\pi}{180}\right)}{1} \approx 3.9 \text{ sec} \qquad (6.5)$$

Figure 6.1 shows that the vehicle attempts to reach the desired bank angle trajectory rapidly, but is not able to do so as quickly as dictated by Equation 6.5 due to the limited authority of the RCS jets. Also, because of this limited control authority, the vehicle is not able to reverse its velocity as quickly as the control law dictates, and the vehicle overshoots the desired trajectory. When correcting the tracking error due to the overshoot, the vehicle again overshoots the desired trajectory in the other direction. Though the state initially reaches the sliding surface rapidly, it does not settle to the desired trajectory for another 30 seconds.

Since the jets cannot provide the needed control authority for the vehicle to react as fast as required by Equation 6.5, the control law must be "tuned" by altering the λ_i's and η_i's so that the control law does not consistently command angular accelerations the jet selection process cannot provide. Using the AFE DAP in the same simulation as above, the AFE vehicle is able to control to the desired trajectory with an initial 45 deg offset in approximately 10 sec. Using 10 sec as a goal, the simulation above was performed numerous times with various combinations of λ_i and η_i. Using this

trial-and-error approach, a combination of $\lambda_i = 1.0$ and $\eta_i = 0.1$ is found to give the desired response with a minimum of jet firings. With this combination, the sliding surface should be reached (resulting in tracking to within 2 deg) in a time less than

$$\frac{|s_i(\vec{x}(0), 0)|}{\eta_i} = \frac{1.0\left(45 \cdot \frac{\pi}{180}\right)}{0.1} \approx 8.0 \text{ sec} \qquad (6.6)$$

Figure 6.2 shows that, with the new parameters, the actual bank angle trajectory reaches to within 2 deg of the desired trajectory within 8.0 sec and that overshoot is eliminated. With $\lambda_i = 1.0$ and $\eta_i = 0.1$, the control law is properly tuned.

This control law tuning may also be required when using this candidate attitude control system design for other aerocapture vehicles. The actuator control authority of the particular vehicle will dictate the required tuning.

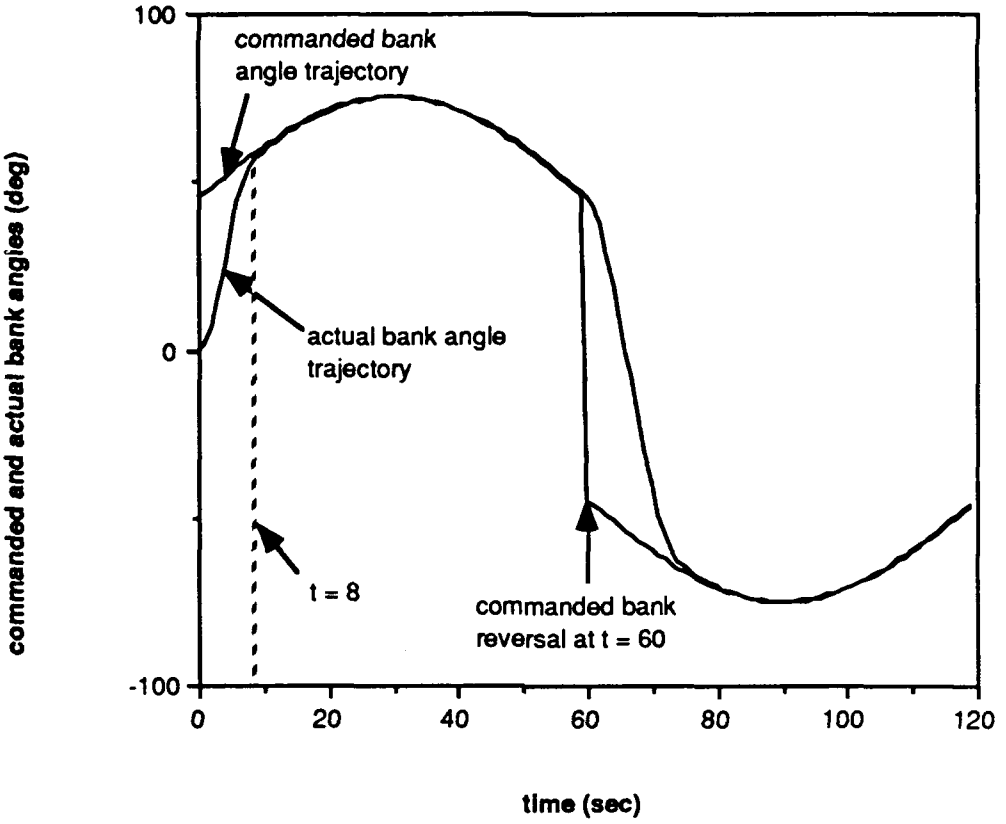

Figure 6.2. Bank Angle Tracking
(λ_i= 1.0, η_i = 0.1)

6.4 Mass Property Updates

From Chapter 4, the linear programming jet selection algorithm characterizes each jet available for selection by an activity vector (i.e., Equation 4.3) which represents the effect of firing the jet. Accuracy of the activity vectors is limited by errors in the estimates of the vehicle inertia matrix and center of mass location. The mass property identification algorithm must provide accurate initial estimates of these mass properties and must update the estimates if the mass properties change significantly during the mission. Failure

to provide accurate, timely estimates may result in the aerocapture attitude control system attempting to control a vehicle with mass properties outside the range for which it is robust. When this happens, the vehicle may become unstable. This section describes how the mass property identification algorithm is employed to provide both the initial mass property estimates, and any required updates.

6.4.1 Initial Estimation

The method of employing the mass property identification algorithm for the initial estimates is straight forward. The estimates of the mass properties to be identified are initially set to zero in the extended Kalman filter. For a period of 0.5 sec beginning at the point of atmosphere entry at an altitude of 400,000 feet, the control law and the jet selection algorithm are bypassed and vehicle motions are dedicated strictly to mass property identification. Operating at 25 hz, a sequence of 12 jet firings is generated by the selection strategy outlined in Section 5.3. Comparing the predicted angular rate changes to the measured rate changes due to these 12 firings, the estimator is able to converge to accurate mass property estimates by the end of the dedicated identification period. At the end of the initial identification period, the mass property estimates are supplied to both the control law and the jet selection algorithm. Activity vectors for each jet are calculated in the jet selection algorithm, and the control law and jet selection algorithm begin to implement the bank angle commands from the guidance law.

6.4.2 Detecting Mass Property Changes

The control law and jet selection algorithm alone represent a robust control system. Small mass property changes can be tolerated without adversely affecting the control system performance. Since the system may become unstable with large mass property changes, the control system must somehow detect significant changes in the mass properties. After detection, mass property identification can be performed to maintain stability.

What determines a "significant" mass property change? Any mass property change that puts the mass properties outside the range for which the control system is robust causing the vehicle to become unstable is certainly significant and must be detected. Additionally, for mass properties that change slowly, it is necessary to detect these changes before the vehicle becomes unstable.

During the normal operation of the attitude control system, the mass property identification algorithm continually monitors the effects of jet firings on the vehicle dynamics in order to detect significant mass property changes. For each jet firing, the estimator predicts the resulting angular rate changes using the last mass property estimates supplied to the control law and jet selection algorithm. When the magnitude of the residual (i.e., difference) between the estimated rate changes and the rate changes measured by the spacecraft gyros becomes large enough to indicate a significant mass property change, a flag is set signaling that updated mass properties estimates are required.

The residual value used to trigger the flag is found by assuming the control law/jet selection algorithm combination can tolerate up to a 40 inch displacement in the center of mass location with the associated change in the inertia matrix calculated as described in Appendix C (this assumption will be shown to be reasonable from the robustness test results presented in Chapter 7). With a 40 inch displacement, the center of mass is located at

$$\vec{r}_{cm} = \begin{bmatrix} 106.69 \\ 23.06 \\ 22.48 \end{bmatrix} \text{inches} \tag{6.7}$$

and the inertia matrix is calculated to be

$$\mathbf{I} = \begin{bmatrix} 4069.79 & -915.79 & -974.39 \\ -915.79 & 3280.79 & -889.79 \\ -974.39 & -889.79 & 3000.19 \end{bmatrix} \text{slugs}\cdot\text{ft}^2 \tag{6.8}$$

The residual between the measured and predicted angular rate change due to the firing of RCS jets is defined as

$$\vec{\mathbf{R}} = \Delta\vec{\omega}_m - \Delta\vec{\omega}_p \tag{6.9}$$

where

$\vec{\mathbf{R}}$ = the residual vector

$\Delta\vec{\omega}_m$ = measured angular rate changes

$\Delta\vec{\omega}_p$ = predicted angular rate changes

Using Equation 5.2 for the expression of the rate changes, the residual due to the firing of a single jet #j can be written as

$$\vec{R} = I^{-1}\left[\vec{\omega} \times I\vec{\omega} + (\vec{r}_j - \vec{r}_{cm}) \times \vec{T}_j + \vec{d}\right]\Delta t \qquad (6.10)$$
$$- \hat{I}^{-1}\left[\vec{\omega} \times \hat{I}\vec{\omega} + (\vec{r}_j - \hat{\vec{r}}_{cm}) \times \vec{T}_j + \vec{d}\right]\Delta t$$

The nominal AFE vehicle mass properties [36] are listed in Table 6.2 with the nominal inertia matrix calculated as in Appendix B relative to the body axes with origin at the vehicle center of mass. The position and thrust vector for each of the AFE's 16 RCS jets [31] are listed in Table 6.3 with the coordinate system used to specify the location of the center of mass illustrated in Figure 6.3.

inertia	$I = \begin{bmatrix} 2248.2 & -5.0 & -63.6 \\ -5.0 & 1459.2 & 21.0 \\ -63.6 & 21.0 & 1178.6 \end{bmatrix}$	slugs · ft^2
center of mass	$\vec{r}_{cm} = \begin{bmatrix} 83.6 \\ -0.03 \\ -0.61 \end{bmatrix}$	inches
mass	mass = 123.0	slugs

Table 6.2. Nominal Vehicle Mass Properties

Jet	Location (inches)			Thrust Vector (lbf)		
#	x	y	z	x	y	z
1	60.69	-6.5	-45.0	0	+30	0
2	60.69	+6.5	+45.0	0	-30	0
3	60.69	-45.0	-6.5	0	0	+30
4	60.69	+45.0	+6.5	0	0	-30
5	60.69	+3.5	+45.0	+30	0	0
6	60.69	-3.5	-45.0	+30	0	0
7	60.69	-45.0	-3.5	+30	0	0
8	60.69	+45.0	+3.5	+30	0	0
9	60.69	0	+41.5	+125	0	0
10	60.69	0	+48.5	+125	0	0
11	60.69	0	-41.5	+125	0	0
12	60.69	0	-48.5	+125	0	0
13	60.69	-41.5	0	+125	0	0
14	60.69	-48.5	0	+125	0	0
15	60.69	+41.5	0	+125	0	0
16	60.69	+48.5	0	+125	0	0

Table 6.3. Vehicle Jet Properties

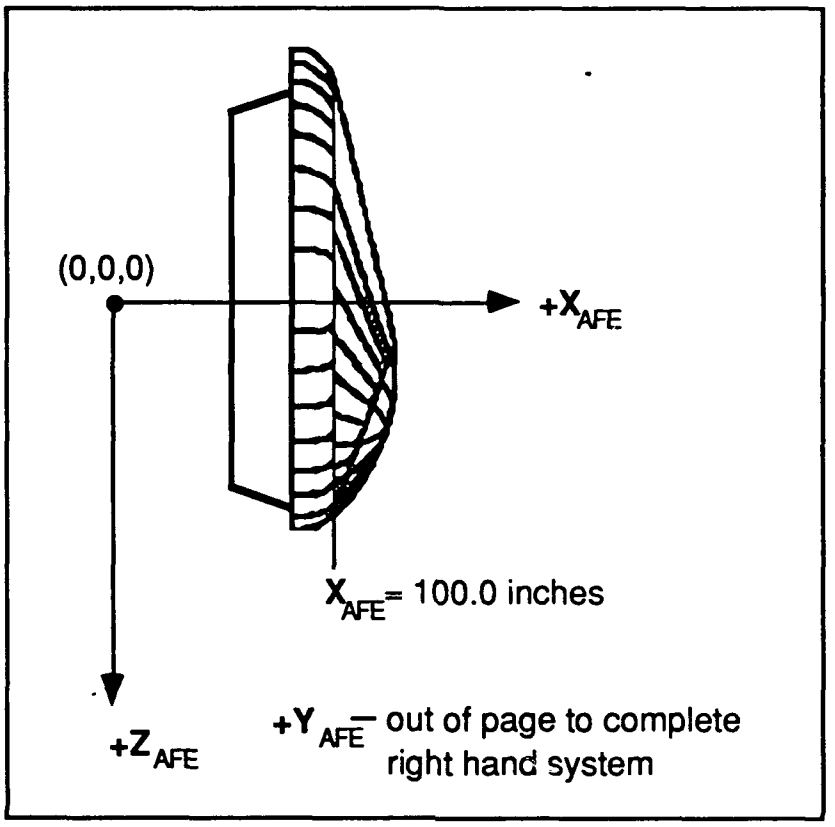

Figure 6.3. Body Referenced Coordinate System

The typical magnitude of the residual vector associated with the firing of a single jet is used as the trigger value. Since the majority of the jet firings commanded by the jet selection algorithm are roll jets, jet #4 is chosen to determine the typical residual vector magnitude. Assuming there are no disturbances or angular rates (i.e., $\vec{d} = \vec{\omega} = \vec{0}$), the estimated mass properties are the nominal values listed in Table 6.2, the actual mass properties are those for a 40 inch displacement given by Equations 6.7 and 6.8, and the thrust and position of jet #4 are as listed in Table 6.3, the residual vector due to a single firing of jet #4 is calculated from Equation 6.10 to be

$$\vec{\mathbf{R}} = \begin{bmatrix} 0.7768 \\ -0.4409 \\ -0.9179 \end{bmatrix} \times 10^{-3} \frac{\text{rads}}{\text{sec}} \qquad (6.11)$$

The magnitude of this residual vector is 1.3×10^{-3} rads/sec. To ensure a mass property change is detected before this large a change occurs, the detection trigger value is chosen to be 1.0×10^{-3} rads/sec. Using this approach, a trigger value based on the jet and mass properties of other vehicles can be calculated for other aerocapture missions.

As jets are fired, the residual vectors are calculated and the magnitudes are stored. To prevent triggering on a single residual measurement which may jump due to noise, the average of the last three residual magnitudes is calculated. The flag indicating that a significant mass property change has occurred is then set when this average becomes larger than the 1.0×10^{-3} rads/sec trigger value.

6.4.3 Updating Mass Property Estimates After a Change is Detected

When the detection flag is set, the extended Kalman filter is reinitialized, and the identification of the new mass properties is begun. New mass property estimates are not supplied to the control law and jet selection algorithm until the end of the new identification period. Unlike the initial dedicated identification period, the control law and jet selection algorithm are not bypassed after a change is

detected. Instead, in an effort to reduce the impact of the identification process on the attitude control task, the identification algorithm attempts to estimate the new mass properties based on the jet firings commanded by the jet selection algorithm.

Jet firings in addition to those commanded by the jet selection algorithm are required. The overall attitude control task is to track the bank angle trajectory commanded by the guidance law. Bank maneuvers are performed primarily by a combination of roll and yaw maneuvers; pitch jets are rarely commanded and little information about the inertia about the pitch axis can be gained. To alleviate this problem, the selection scheme used during the initial identification period is invoked during one out of every five cycles (i.e., 5 hz instead of 25 hz). The one jet chosen by this selection scheme is then fired along with any jets commanded by the jet selection algorithm.

The new identification period continues until the following two conditions are met. The first condition is that the filter estimates must improve the average residual magnitude by at least an order of magnitude (i.e., becomes less than 1.0×10^{-4} rads/sec). The second condition is that all the diagonal elements of the error covariance matrix **P** reduce to within an order of magnitude of what they were before the detected change. The first condition ensures a minimum acceptable accuracy of the estimates, while the second condition ensures the identification period is not ended while the filter is still converging rapidly to more accurate estimates.

Like any Kalman filter design, after several updates to the estimated state vector (i.e., Equation 5.17) the filter becomes optimistic and the information from later jet firings is weighed less than earlier firings. To prevent the filter from becoming optimistic, the elements of the error covariance matrix are set artificially high at the beginning of a new estimation period. As the information from more and more jet firings is extracted and the estimator converges to accurate estimates of the new mass properties, the elements of the error covariance matrix become smaller. By the time the elements of **P** become small enough to meet the second condition, little information can be extracted from additional jet firings and the filter should have converged to accurate estimates of the new mass properties.

Once the identification period ends, the new mass property estimates are supplied to the control law and the jet selection algorithm. New activity vectors for each jet are calculated in the jet selection algorithm, and the mass property identification algorithm again begins monitoring the magnitude of the residual vector to detect any further mass property changes.

6.5 Summary of Operation

Figures 6.4, 6.5, and 6.6 depict the operation of the candidate control system during the three main modes of employment. As Figure 6.4 illustrates, the control law and jet selection algorithm are bypassed during the initial dedicated mass property identification algorithm. During this first 0.5 sec of operation, which occurs at the

point of atmosphere entry, the motion of the vehicle is dedicated to mass property identification with the input selection scheme in the mass property identification algorithm commanding the jet firings needed to rapidly converge to accurate mass property estimates.

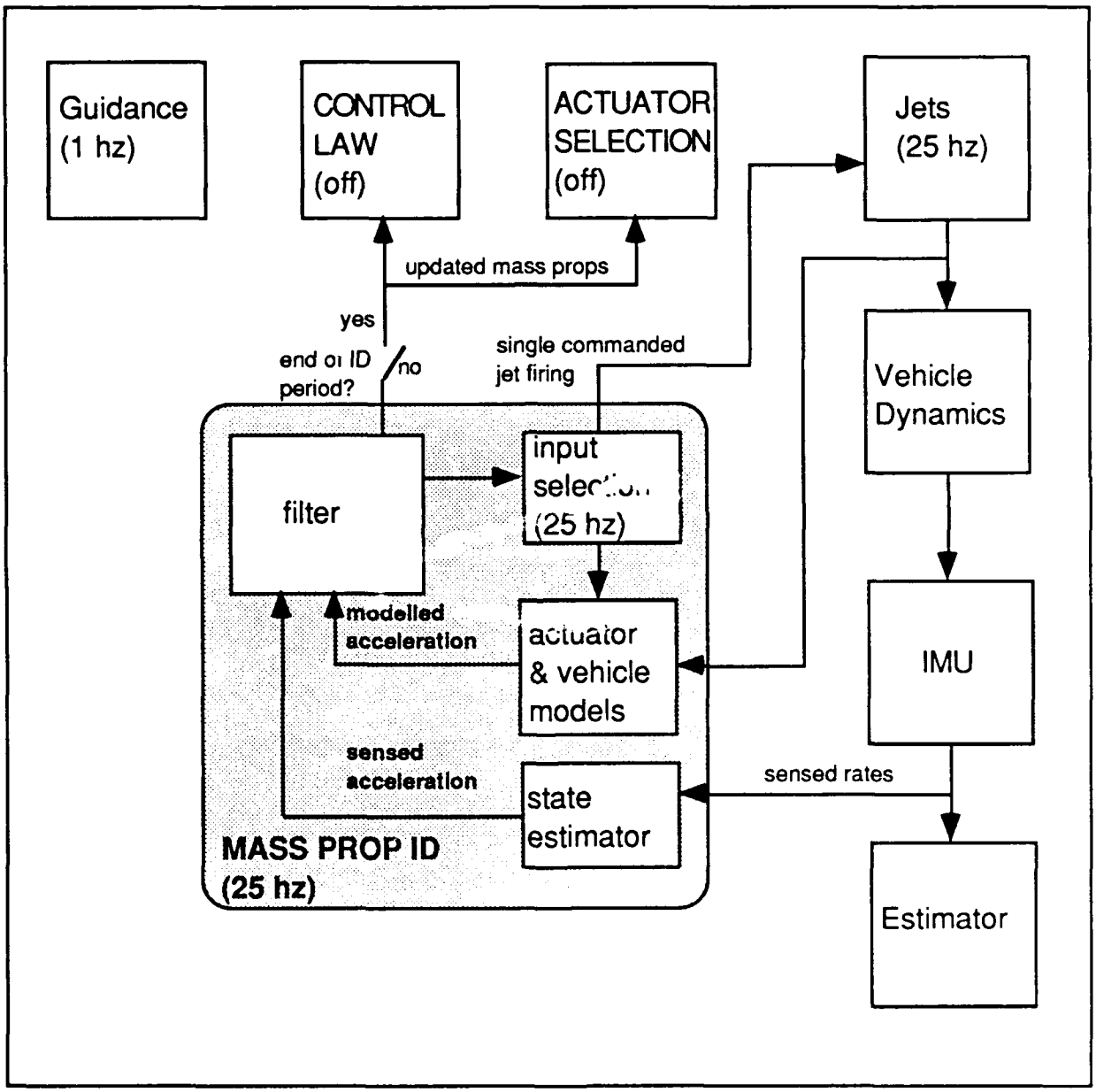

Figure 6.4. Dedicated Mass Property Identification Period (First 0.5 sec)

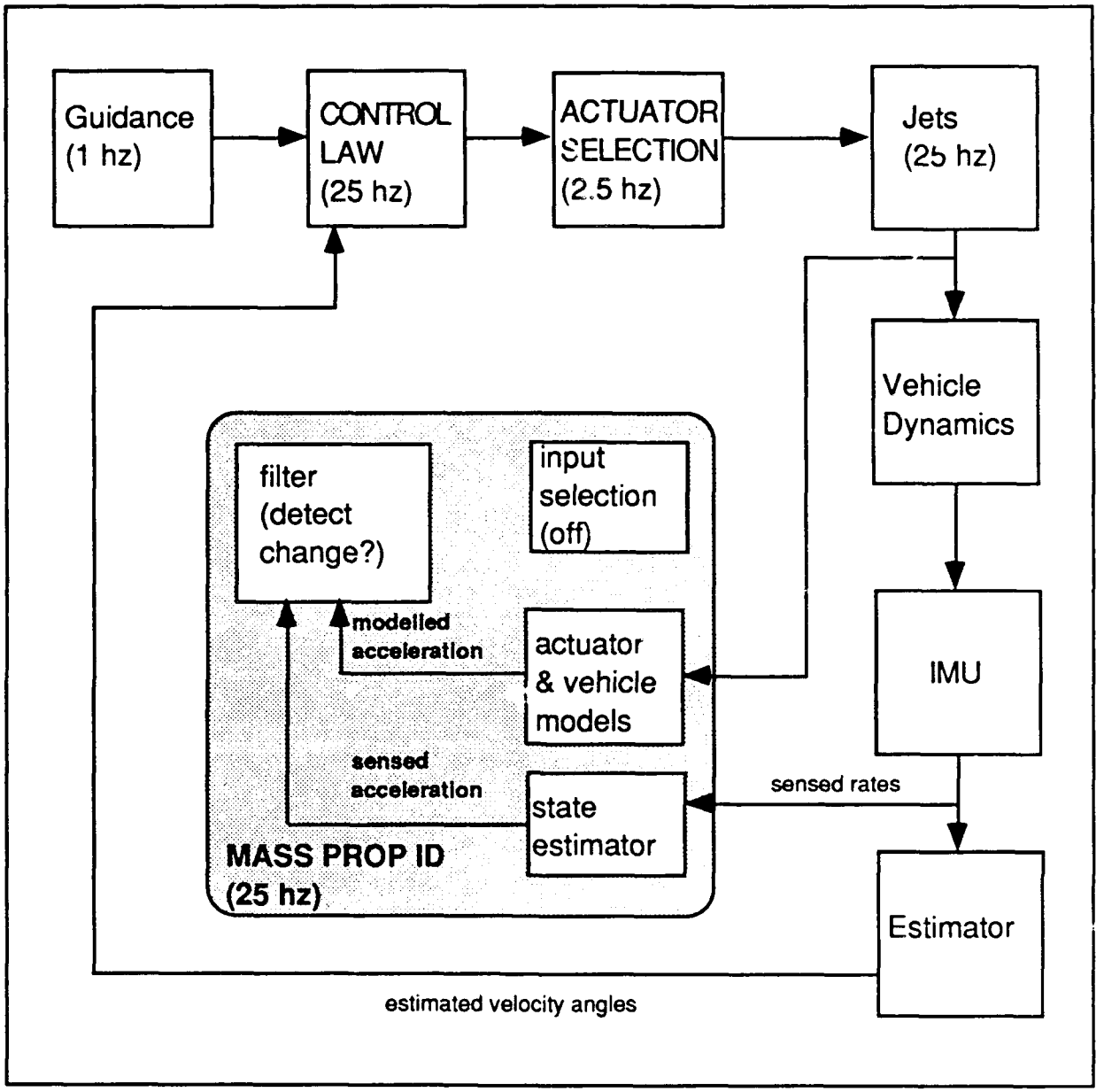

Figure 6.5. Normal Control System Operation

After the initial identification period, the control system begins its normal operation with the control law and the jet selection algorithm being used to implement the bank angle trajectory commanded by the guidance law (see Figure 6.5). The control law

operates at 25 hz, the linear programming jet selection problem is solved at 2.5 hz, and jets are commanded on or off at 25 hz to implement the solutions to the linear program. During this normal operation, the mass property identification algorithm monitors the effects of jet firings on the rate changes experienced by the vehicle and compares the measured rate changes to its predicted (i.e., modelled) rate changes. When the magnitude of the residual vector becomes larger than the trigger value of 1.0×10^{-3} rads/sec, a flag is set indicating a change in mass properties has been detected. When this flag is set, normal control system operation ends and a new mass property identification period begins.

During the new identification period, the control law and the jet selection algorithm continue their task of implementing the commanded bank angle trajectory. As Figure 6.6 illustrates, mass property identification is attempted based on the jet firings commanded by the jet selection algorithm. In addition to these jet firings, the input selection scheme described in Section 5.3 is invoked at a 5 hz rate and is used to choose a jet firing to help speed the convergence of the identification algorithm to accurate mass property estimates. This new identification period continues until the two conditions described in Section 6.4.3 are met.

At the end of the new identification period, the updated mass property estimates are supplied to the control law and the jet selection algorithm. New activity vectors based on the new mass property estimates are calculated in the jet selection algorithm, and the attitude control system returns to its normal operation with the

mass property identification algorithm monitoring the magnitude of the residual vectors for detection of additional mass property changes.

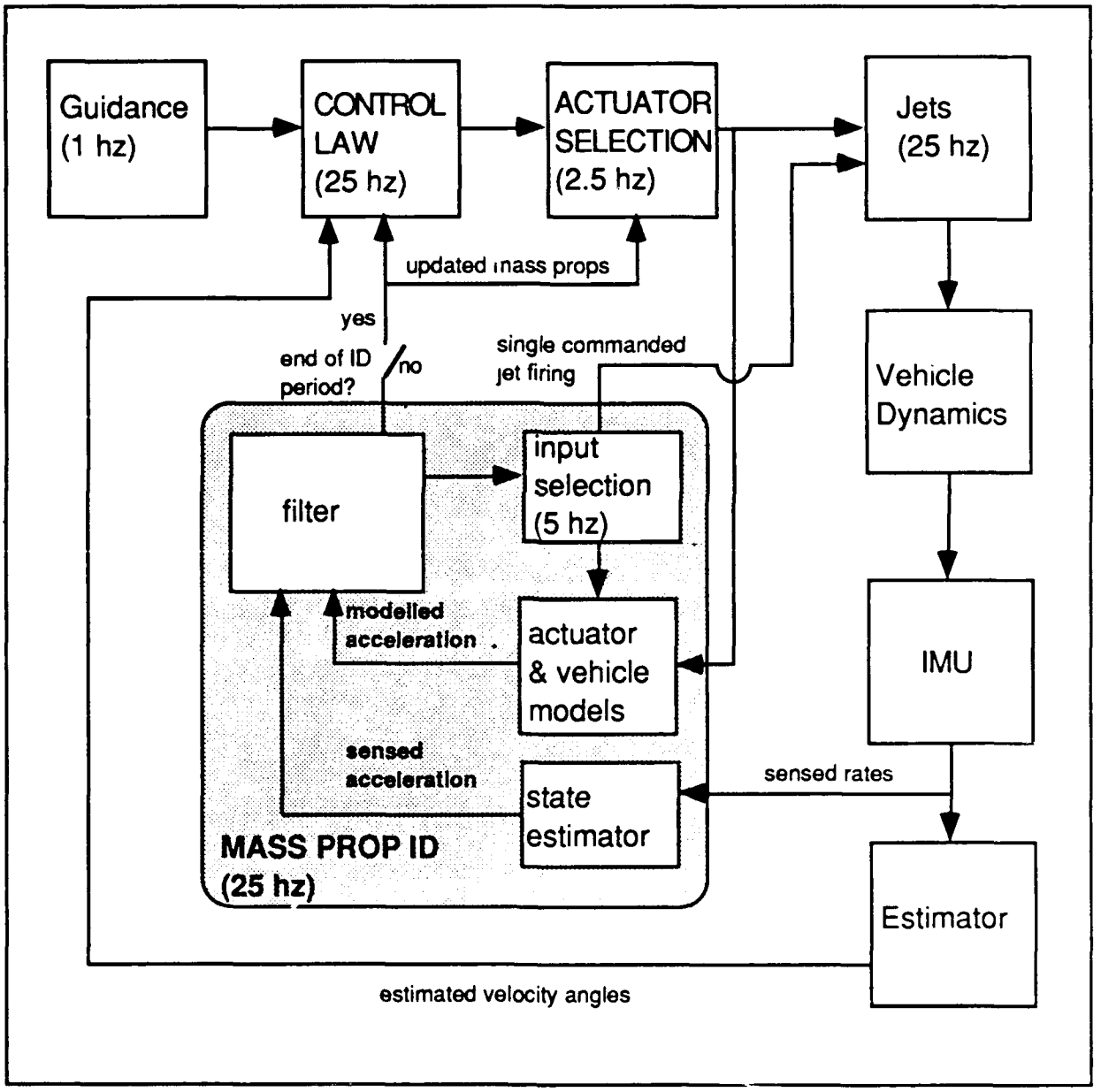

Figure 6.6. Operation After Detection of Mass Property Change

6.6 Application to Other Aerocapture Missions

The candidate aerocapture control system structure outlined in Figures 6.4, 6.5, and 6.6 was designed to be used for attitude control of any aerocapture vehicle or mission. The overall structure is also transportable to other missions or vehicles. The following mission and vehicle dependent issues, however, must be addressed:

A. Control Law

(1) The bounds on the unknowns in the system model (i.e., Equation 3.43) must be calculated as in Appendix B based on the vehicle mass and aerodynamic properties, along with the atmospheric properties expected during the mission.

(2) The choices of λ_i and η_i must be made based on the system cycling rates and the control authority of the vehicle's jets. Control law tuning, as discussed in Section 6.3, may be required.

B. Linear Programming Jet Selection

(1) Activity vectors for each jet (i.e., Equation 4.3) depend on the vehicle inertia matrix and center of mass location provided by the mass property identification algorithm. They also depend on the location and thrust vector of each jet. These jet properties must be provided for the vehicle to be used.

(2) The relative cost of using each jet must be specified based on their fuel consumption rates.

(3) A strategy, such as described in Section 6.2, for commanding jets on and off to implement the commanded duty cycles must be developed based on system cycling rates and minimum jet on times.

C. Mass Property Identification

(1) Measurement noise covariance must be determined as in reference [24] based on the noise characteristics of the vehicle sensors.

(2) The magnitude of the residual vector used to trigger the flag indicating detection of a mass property change must be calculated based on the vehicle mass and jet properties as in Section 6.4.2.

Chapter 7

Simulation Results

7.1 Introduction

The candidate aerocapture attitude control system has been tested in a computer simulation of an Earth aerocapture. Section 7.2 briefly describes the simulation developed for this effort. Results of testing to demonstrate the increased robustness of the new design over the existing AFE DAP design are included in Section 7.3. Section 7.4 presents results of tests demonstrating the ability of the candidate system to identify and adapt to changing mass properties. The tests described in Section 7.4 are performed without modelled aerodynamic forces and torques. Section 7.5 describes the effects aerodynamics have on these tests.

7.2 Simulation Description

A 6-DOF simulation of an earth aerocapture, written in FORTRAN, was developed for testing purposes and is hosted on a Macintosh IIcx personal computer. It simulates the actual AFE mission for a spacecraft similar to the AFE vehicle, but with a wider range of possible mass properties. For the purposes of this thesis, the AFE guidance has not been included in the simulation. Instead, simple bank angle commands mimicking the typical characteristics of

a trajectory commanded by the AFE guidance are generated and supplied to the attitude control system during simulation.

7.2.1 Initial Conditions

For each test, the simulated aerocapture maneuver begins with the spacecraft entering Earth's atmosphere with the following entry conditions matching those projected for the AFE mission [10]:

$$\begin{aligned}
&\text{altitude} = 400{,}000 \text{ ft} \\
&\text{latitude} = 0 \text{ deg} \\
&\text{longitude} = 0 \text{ deg} \\
&\text{velocity magnitude} = 33{,}820 \text{ ft/sec} \\
&\quad v_1 \text{ (North)} = 0 \\
&\quad v_2 \text{ (East)} = 33{,}716 \text{ ft/sec} \\
&\quad v_3 \text{ (toward center of Earth)} = 2{,}653 \text{ ft/sec} \\
&\text{flight path angle} = 4.5 \text{ deg below local horizontal}
\end{aligned} \tag{7.1}$$

At entry, the vehicle is in the following attitude:

$$\begin{aligned}
&\text{bank angle } (\phi) = 0 \text{ deg} \\
&\text{angle-of-attack } (\alpha) = 17.0 \text{ deg} \\
&\text{sideslip angle } (\beta) = 0 \text{ deg}
\end{aligned} \tag{7.2}$$

with $\phi = 0$ deg indicating full lift up (i.e., lift in the vertical plane only and directed away from the center of the Earth).

7.2.2 Vehicle Properties

For comparison purposes, simulations using the nominal mass properties listed in Table 6.2 are run with both the AFE DAP and the candidate attitude control system. Additional simulations are run with the vehicle mass properties varying from these nominal values. The methods used to vary the mass properties are described in Sections 7.3 and 7.4 below for each test.

The simulation assumes the test vehicle possesses the same configuration of RCS jets as the actual AFE vehicle. The simulation uses the jet properties listed in Table 6.3.

7.2.3 Equations of Motion

As the aerocapture vehicle descends deeper into the atmosphere, the aerodynamic forces and torques experienced by the vehicle increase. The aerodynamics are simulated using the aerodynamic properties of the actual AFE vehicle [37]. A simple exponential atmospheric model based on the 1962 U.S. Standard Atmosphere [6] is used to provide the atmospheric density encountered for each given altitude.

The overall simulation is cycled at 25 hz. The translational and rotational states of the aerocapture vehicle are specified at each step by the 12-element state vector

$$\overrightarrow{\text{state}} = [\, r_z \;\; \mu \;\; \zeta \;\; v_1 \;\; v_2 \;\; v_3 \;\; \theta \;\; \varphi \;\; \psi \;\; p \;\; q \;\; r \,]^T \qquad (7.3)$$

where

r_z = distance from the center of Earth
μ = latitude
ζ = longitude
v_1 = North component of velocity
v_2 = East component of velocity
v_3 = radial (toward center of Earth) velocity component
θ, φ, ψ = Euler angles relating the body axes to the velocity vector as described in Appendix A
p = roll rate
q = pitch rate
r = yaw rate

During each step, a first order differential equation for each of the elements in the state vector is calculated based on the jets fired and the aerodynamic forces and torques encountered. These equations of motion are then integrated using a fourth-order Runge-Kutta algorithm [38] to determine the new states at the end of each step. The current velocity angles are then calculated based on the velocity elements (i.e., v_1, v_2, and v_3) and the Euler angles.

7.3 Robustness Testing

The main objective of the candidate design was to integrate a mass property identification algorithm with a robust control law and an adaptable jet selection algorithm to extend the range of mass properties for which the attitude control system is robust. To demonstrate the improvement of the new design, robustness testing was conducted for the following three control system configurations:

1. AFE DAP [16]

2. new control law/jet selection algorithm with mass property estimates set to the nominal values (i.e., without the mass property identification algorithm)
3. complete candidate attitude control system design (i.e., employing the mass property identification algorithm)

Tests with the AFE DAP are performed only for comparison purposes. The range of mass properties to which the AFE DAP is subjected during these tests will not be encountered during the actual AFE mission. The AFE DAP is not designed nor required to be capable of providing attitude control over this range of mass properties.

For each configuration, a 60 sec simulation is repeatedly performed with the mass properties changed from one simulation run to the next. Figure 7.1 shows the results of a single run of the 60 sec simulation for the complete candidate control system (i.e., configuration #3) and a vehicle with the nominal mass properties. The commanded bank angle is initially 45 deg and then varies sinusoidally. The aerocapture vehicle begins with the initial conditions listed in Section 7.2.1, reaches the commanded trajectory in approximately 8 sec, and then begins tracking while maintaining the commanded α and β.

Nominal mass properties are used during the first run of the 60 sec simulation for each configuration. For each successive run, the center of mass location is moved 1 inch from the previous location (e.g., on the 10^{th} run, the center of mass is moved 9 inches from the nominal position). Each 1 inch move is achieved by moving the

center of mass an equal distance along the +x, +y, and +z axes (i.e., 0.58 inches along each axis). The inertia matrix is changed as described in Appendix C. This is done to simulate changes in both the center of mass location and the inertia matrix, the mass properties that affect performance of the control system.

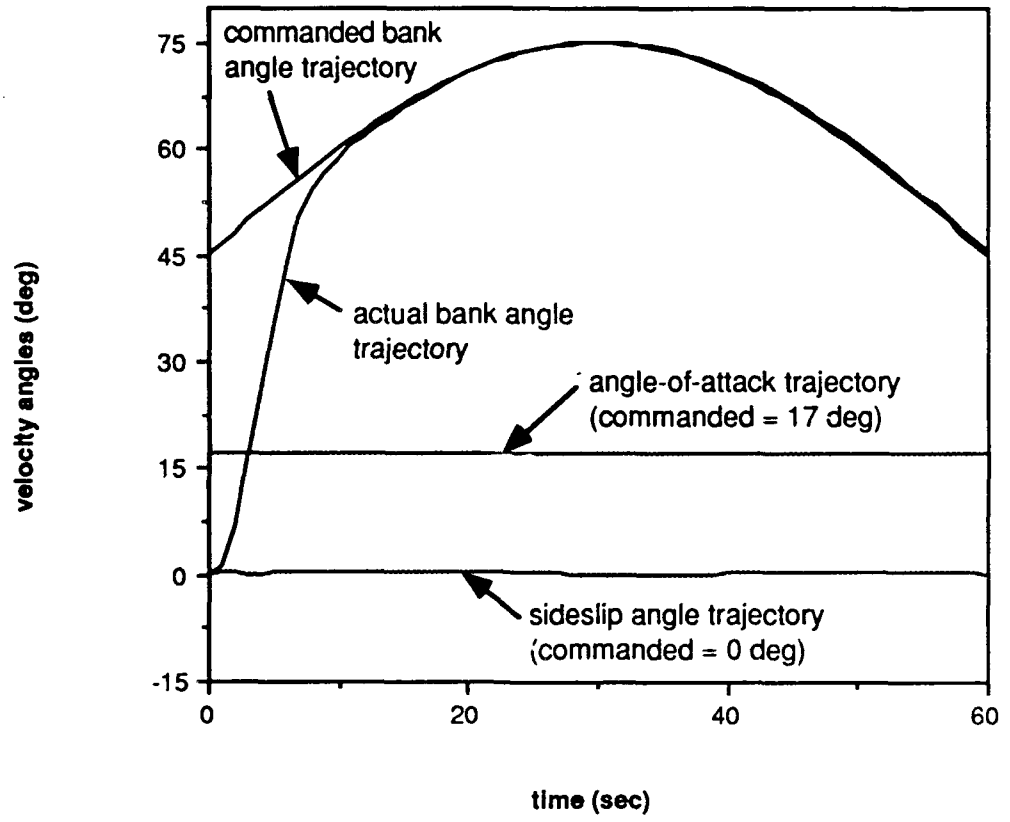

Figure 7.1. Velocity Angle Response of Typical 60 Sec Simulation

Figures 7.2 and 7.3 show the testing results for the three control system configurations. Figure 7.2 is a plot of the total number of jet firings required during each 60 sec simulation vs. the displacement of the center of mass location for each simulation.

Figure 7.3 shows the maximum bank angle tracking error, after the desired trajectory is reached, for each simulation.

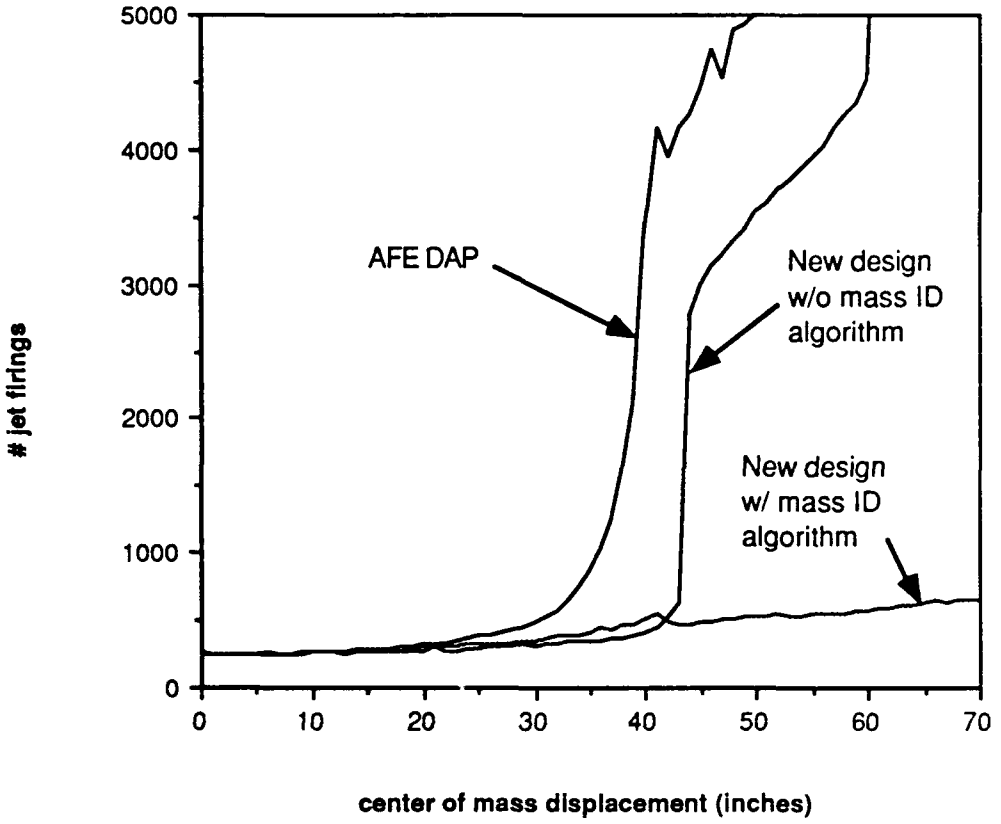

Figure 7.2. Jet Firings vs. Center of Mass Displacement

For the AFE DAP, the number of jet firings begins to increase rapidly when the center of mass location is displaced by more than 33 inches from the nominal location. The bank angle errors increase dramatically after about 40 inches of displacement. For the new design without the mass property identification algorithm (i.e., configuration #2), the number of jet firings increases rapidly at 44 inches of displacement while the maximum bank angle errors begin to increase rapidly after about 60 inches of displacement. For the new design employing the mass property identification algorithm

(i.e., configuration #3), bank angle errors do not increase significantly over the range of mass properties tested. The number of jet firings does slowly increase, however, as the center of mass is displaced further from the nominal location. This is expected since the magnitudes of the inertia matrix elements increase as the center of mass location is displaced further, requiring additional control activity to move the larger inertia.

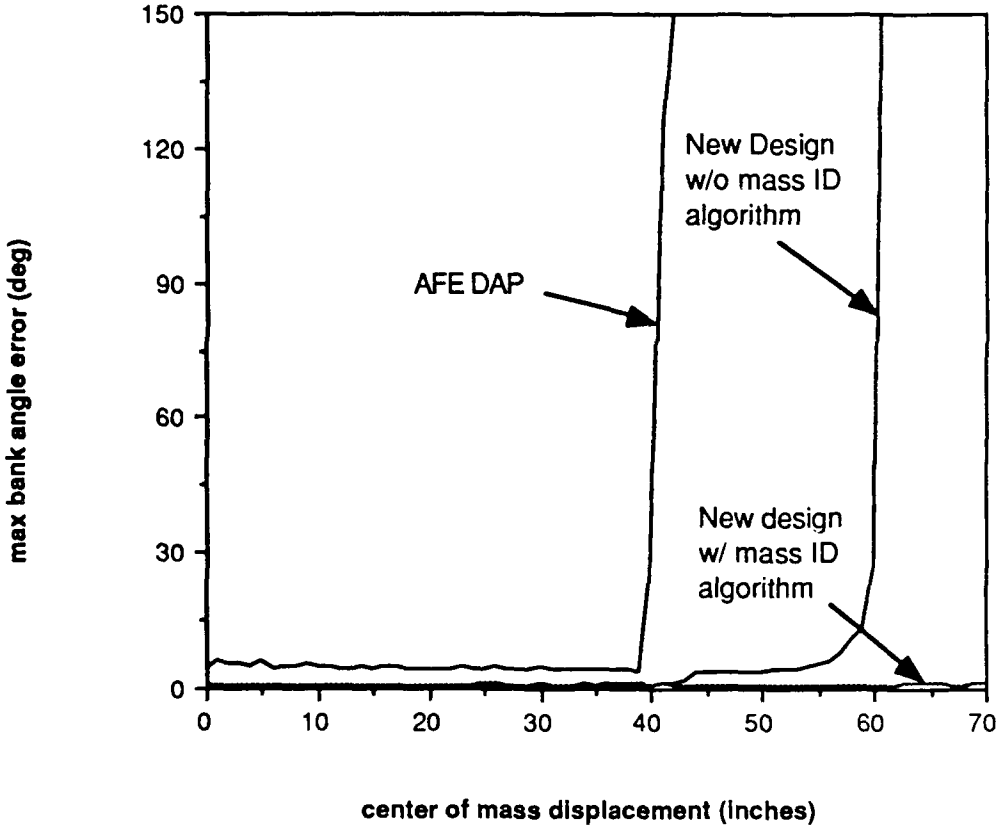

Figure 7.3. Max Bank Angle Error vs. Center of Mass Displacement

The displacements at which the bank angle errors rapidly increase can be considered the points at which the control system becomes unstable. The AFE DAP becomes unstable at a 40 inch

displacement of the center of mass location. The new design using the nominal values for mass property estimates becomes unstable at 60 inches of displacement, more robust than the AFE DAP, but not robust to the full range of mass properties tested. The complete design remains stable over the full range of mass properties, demonstrating the benefit of incorporating the mass property identification algorithm.

7.4 Performance of the Candidate Attitude Control System

Section 7.3 demonstrated the benefit of using a mass property identification algorithm to extend the range of mass properties for which a control system is robust. For each run of the 60 sec simulation, the actual mass properties were set as described above but remained constant during the simulation. The identification algorithm was able to accurately estimate the mass properties at the beginning of each simulation, and the control system was able to track the simple desired trajectory.

This section demonstrates the ability of the candidate control system to track a bank angle trajectory that includes a simulated commanded bank reversal, along with the ability to detect, identify, and adapt to mass properties that change during the simulation. Aerodynamic torques are not simulated during the tests described in this section, but are simulated during the tests presented in Section 7.5. Section 7.4.1 describes the performance of the candidate control system during tracking of the desired bank angle trajectory when the vehicle has the nominal mass properties. In Section 7.4.2, the

candidate control system tracks the desired trajectory while also detecting and adapting to large step changes in the vehicle mass properties. Finally, Section 7.4.3 shows the ability of the candidate control system to detect and adapt to gradual mass property changes.

The remaining tests use the same commanded bank angle trajectory. This trajectory was designed to mimic the main characteristics of an aerocapture bank angle trajectory commanded by the AFE guidance law. To provide maximum control margin, the in-plane portion of the AFE guidance commands most of the lift out of the desired vertical plane. If the aerocapture vehicle slows too quickly, guidance then can command more in-plane lift to pull the vehicle out of the atmosphere. If the vehicle does not decelerate quickly enough, more in-plane lift can be commanded to pull the vehicle deeper into the atmosphere increasing deceleration. Once the out-of-plane lift pulls the aerocapture vehicle out of the desired vertical plane, a bank reversal is commanded by the out-of-plane guidance to bring the vehicle back to the desired plane.

To simulate these characteristics, the desired bank angle trajectory calls for an initial bank angle of 75 deg. It then varies 30 deg sinusoidally around 90 deg bank until 60 sec into the simulation. At 60 sec, the mid point of the simulation, a bank angle reversal is commanded. The final 60 sec of the simulation calls for a sinusoidally varying trajectory centered at -90 deg bank.

7.4.1 Nominal Performance

Figure 7.4 illustrates the tracking performance of the candidate aerocapture attitude control system for a vehicle with the initial

conditions and the nominal, unchanging mass properties listed in Section 7.2. Even with the initial 0.5 sec mass property identification period when the control law and jet selection algorithm are bypassed, the desired bank angle trajectory is reached in under 13 sec, in agreement with Equation 3.12

$$\frac{|s_i(\vec{x}(0), 0)|}{\eta_i} = \frac{1.0\left(75 \cdot \frac{\pi}{180}\right)}{0.1} \approx 13.0 \text{ sec} \qquad (7.4)$$

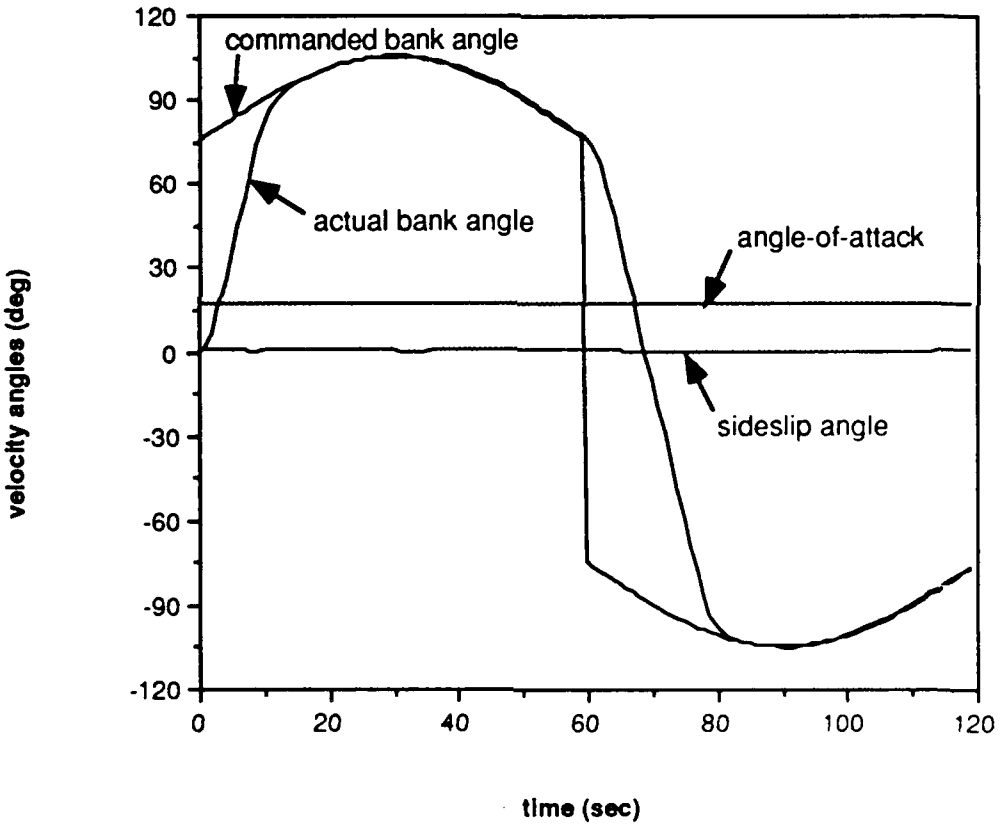

Figure 7.4. Velocity Angle Response - New Design (Nominal Mass Properties)

After the initial reach period, bank angle tracking precision is within the desired 2 deg until the commanded bank reversal when a

new reaching period is begun. During the entire simulation, α and β are precisely maintained at their commanded values.

Figure 7.5 shows the value of the sliding variable s_1 associated with the bank angle during the simulation. Initially, and at the point of the commanded bank reversal, the value of s_1 is off the sliding surface defined by $s_1(\vec{x},t)=0$. The sliding surface is reached and maintained to within the boundary layer Φ_1 in the time specified by Equation 3.12.

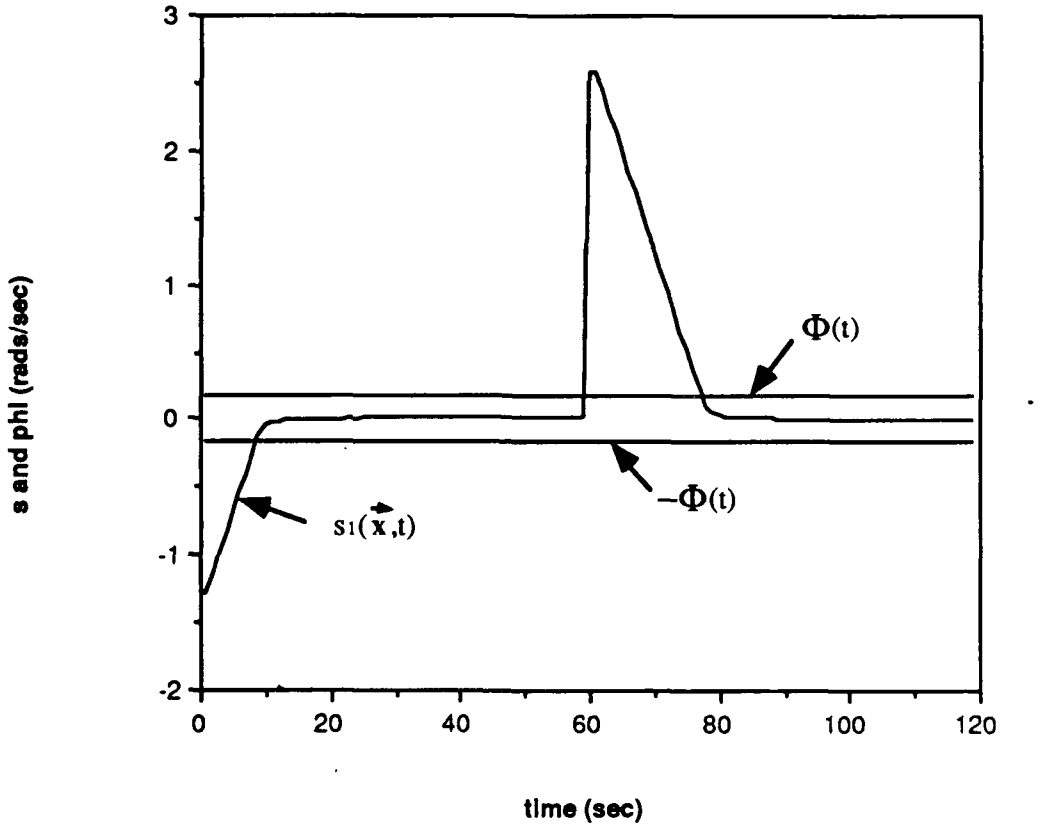

Figure 7.5. Sliding Variable and Boundary Layer (Nominal Mass Properties)

Table 7.1 shows additional results displayed to the screen during the simulation. At t=0.52 sec into the simulation, the estimated mass properties are reported and supplied to the control law and the jet selection algorithm. The mass property estimates are accurate to within 1% of the actual values. Table 7.1 also shows how often each jet is fired during the simulation. For the entire simulation, 554 jet firings, each of 40 msec duration, are performed to provide attitude control, while 12 jet firings, also of 40 msec duration, are used for mass property estimation.

Table 7.1 New Design (Nominal Simulation)

```
*** TIME =    .52 SEC ***

ACTUAL MASS PROPERTIES:
  INERTIA MATRIX IS:
       2248.20    -5.00   -63.60
         -5.00  1459.20    21.00
        -63.60    21.00  1178.60
  CENTER OF MASS IS:
        83.60
         -.03
         -.61

UPDATED MASS PROPERTY ESTIMATES:
  EST INERTIA MATRIX IS:
       2243.93    -4.97   -63.49
         -4.97  1459.20    21.03
        -63.49    21.03  1178.62
  ESTIMATED CENTER OF MASS IS:
        83.66
         -.03
         -.61
```

Table 7.1 (continued)

```
NUMBER OF JET FIRINGS COMMANDED BY CONTROL LAW/JET SELECTION:
   JET # 1:    99    JET # 9:     0
   JET # 2:   137    JET #10:     0
   JET # 3:   111    JET #11:     0
   JET # 4:   114    JET #12:     0
   JET # 5:    59    JET #13:     0
   JET # 6:     1    JET #14:     0
   JET # 7:    10    JET #15:     0
   JET # 8:    23    JET #16:     0

TOTAL # JET FIRINGS(CONTROL LAW/JET SELECT):  554


NUMBER OF JET FIRINGS COMMANDED BY MASS PROP ID:
   JET # 1:     1    JET # 9:     0
   JET # 2:     0    JET #10:     0
   JET # 3:     0    JET #11:     0
   JET # 4:     0    JET #12:     0
   JET # 5:     4    JET #13:     0
   JET # 6:     4    JET #14:     0
   JET # 7:     2    JET #15:     0
   JET # 8:     1    JET #16:     0

TOTAL # JET FIRINGS(MASS PROP ID):  12
```

For comparison purposes, the same simulation is performed with the AFE DAP. Figure 7.6 shows the tracking response to be similar to that for the candidate control system, but somewhat less precise. Table 7.2 indicates that the AFE DAP uses a total of 825 jet firings for attitude control for this simulation, nearly 50% more jet firings than the new design requires.

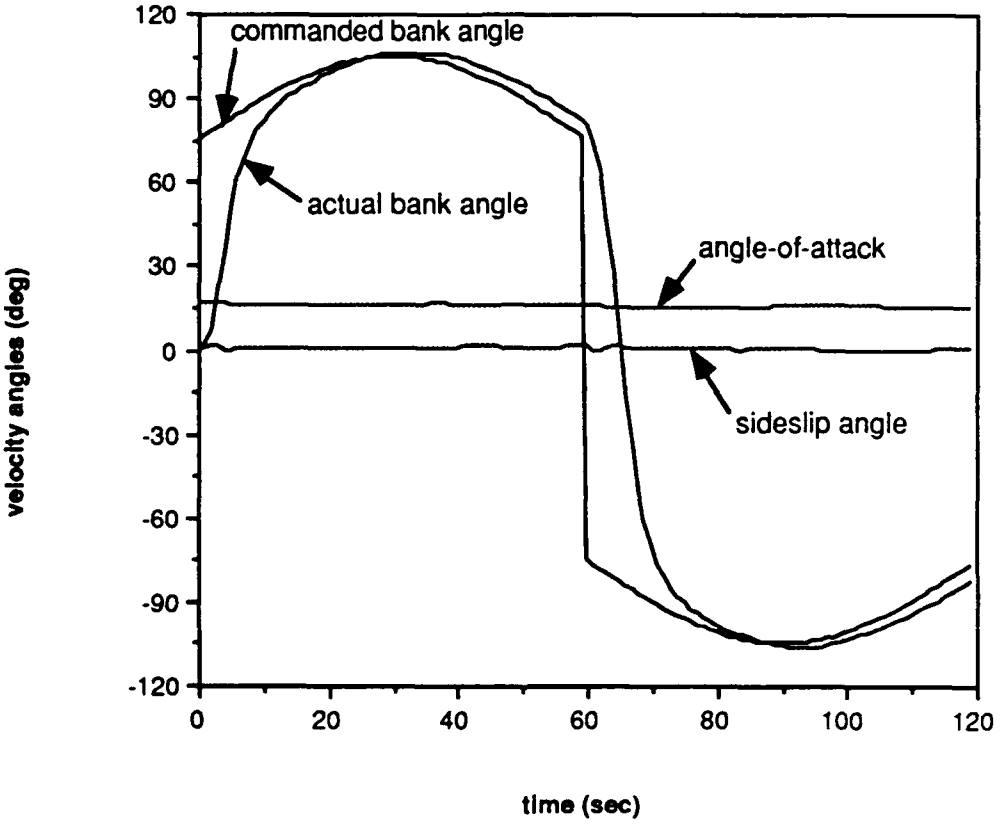

Figure 7.6. Velocity Angle Response - AFE DAP (Nominal Mass Properties)

Table 7.2 AFE DAP (Nominal Simulation)

```
*** TIME =    .52 SEC ***

ACTUAL MASS PROPERTIES:
  INERTIA MATRIX IS:
       2248.20    -5.00   -63.60
         -5.00  1459.20    21.00
        -63.60    21.00  1178.60
  CENTER OF MASS IS:
        83.60
         -.03
         -.61


NUMBER OF JET FIRINGS COMMANDED BY CONTROL LAW/JET SELECTION:
   JET # 1:   165   JET # 9:     0
   JET # 2:   165   JET #10:     0
   JET # 3:   159   JET #11:     0
   JET # 4:   159   JET #12:     0
   JET # 5:    81   JET #13:     0
   JET # 6:     2   JET #14:     0
   JET # 7:    52   JET #15:     0
   JET # 8:    42   JET #16:     0

TOTAL # JET FIRINGS(CONTROL LAW/JET SELECT):  825
```

7.4.2 Performance in the Presence of Large Step Changes to the Mass Properties

The above simulation was repeated with step changes in the mass properties to demonstrate the ability of the candidate control system to detect and adapt to large changes in the vehicle mass properties. The simulation begins with the vehicle having the nominal mass properties listed in Table 6.2. At t=30 sec, the center of mass is displaced 45 inches from its nominal location with the new inertia matrix calculated as in Appendix C. At t=90 sec, another step change is simulated by changing the mass properties back to the original nominal values.

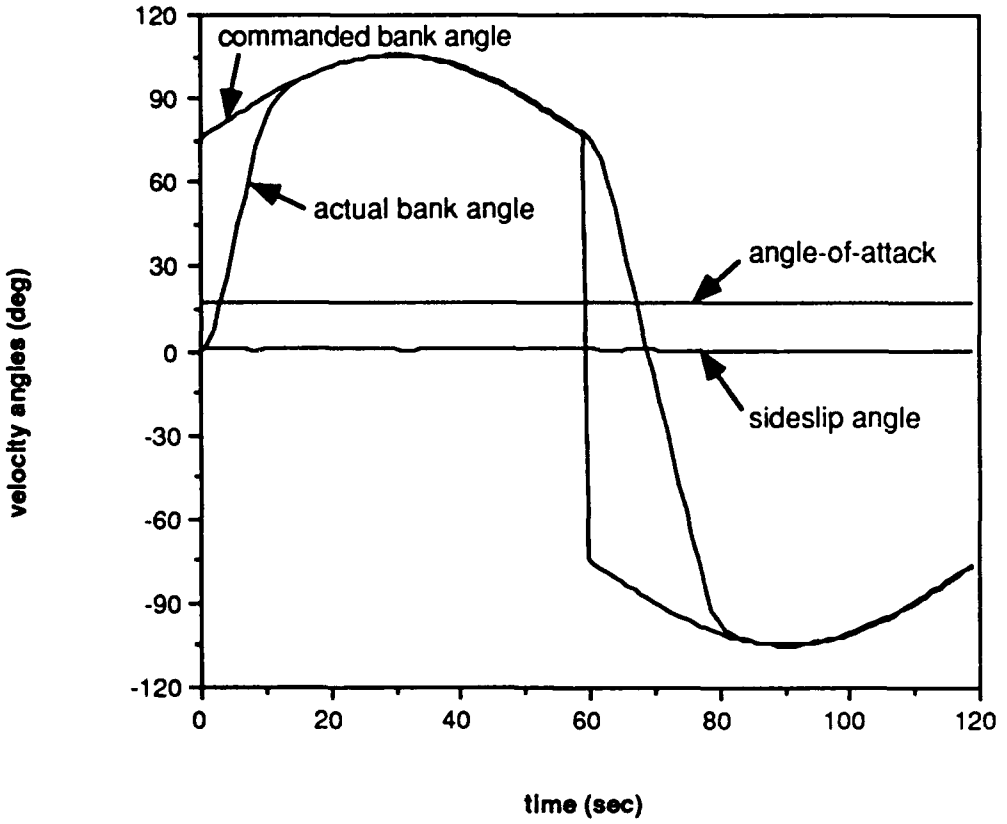

Figure 7.7. Velocity Angle Response - New Design (Large Step Changes in Mass Properties)

Figure 7.7 shows the tracking response of the candidate control system. Comparing to Figure 7.4, little change in tracking performance is discernable. Table 7.3 lists the significant results of this test. The initial mass property estimates at t=0.52 sec are the same as the initial estimates found in Table 7.1 for the nominal simulation. At t=32.08 sec, the first step change is detected. After 14 jet firings commanded by the special input selection scheme in the mass property identification algorithm, the mass property estimates are updated and supplied to the control law and jet selection algorithm at t=34.92 sec. The second mass property change is detected at t=91.72 sec. After 5 jet firings commanded by the

mass property identification algorithm, the identification period ends, and an accurate update to the mass property estimates occurs at t=92.76 sec.

Table 7.3 New Design (Step Changes in Mass Properties)

```
*** TIME =     .52 SEC ***

ACTUAL MASS PROPERTIES:
  INERTIA MATRIX IS:
       2248.20     -5.00    -63.60
         -5.00   1459.20     21.00
        -63.60     21.00   1178.60
  CENTER OF MASS IS:
        83.60
         -.03
         -.61

UPDATED MASS PROPERTY ESTIMATES:
  EST INERTIA MATRIX IS:
       2243.93     -4.97    -63.49
         -4.97   1459.20     21.03
        -63.49     21.03   1178.62
  ESTIMATED CENTER OF MASS IS:
        83.66
         -.03
         -.61


MASS PROPERTY CHANGE DETECTED AT T =  32.08 SEC

JET FIRINGS COMMANDED BY MASS PROP ID
     JET # 7 AT T =  32.20 SEC
     JET # 5 AT T =  32.40 SEC
     JET # 5 AT T =  32.60 SEC
     JET # 7 AT T =  32.80 SEC
     JET # 2 AT T =  33.00 SEC
     JET # 6 AT T =  33.20 SEC
     JET # 5 AT T =  33.40 SEC
     JET # 1 AT T =  33.60 SEC
     JET # 5 AT T =  33.80 SEC
     JET # 4 AT T =  34.00 SEC
     JET # 2 AT T =  34.20 SEC
     JET # 5 AT T =  34.40 SEC
     JET # 6 AT T =  34.60 SEC
     JET # 5 AT T =  34.80 SEC
```

Table 7.3 (continued)

```
*** TIME =  34.92 SEC ***

ACTUAL MASS PROPERTIES:
  INERTIA MATRIX IS:
       4554.31 -1158.06 -1216.66
      -1158.06  3765.31 -1132.06
      -1216.66 -1132.06  3484.71
  CENTER OF MASS IS:
       109.58
        25.95
        25.37

UPDATED MASS PROPERTY ESTIMATES:
  EST INERTIA MATRIX IS:
       4554.30 -1158.20 -1216.74
      -1158.20  3765.62 -1132.00
      -1216.74 -1132.00  3484.70
  ESTIMATED CENTER OF MASS IS:
       109.58
        25.95
        25.37


MASS PROPERTY CHANGE DETECTED AT T =  91.72 SEC

JET FIRINGS COMMANDED BY MASS PROP ID
     JET # 5 AT T =  91.80 SEC
     JET # 7 AT T =  92.00 SEC
     JET # 8 AT T =  92.20 SEC
     JET # 8 AT T =  92.40 SEC
     JET # 5 AT T =  92.60 SEC

*** TIME =  92.76 SEC ***

ACTUAL MASS PROPERTIES:
  INERTIA MATRIX IS:
       2248.20    -5.00   -63.60
         -5.00  1459.20    21.00
        -63.60    21.00  1178.60
  CENTER OF MASS IS:
        83.60
         -.03
         -.61

UPDATED MASS PROPERTY ESTIMATES:
  EST INERTIA MATRIX IS:
       2248.21    -4.97   -63.58
         -4.97  1459.02    21.05
        -63.58    21.05  1178.57
  ESTIMATED CENTER OF MASS IS:
        83.60
         -.03
         -.61
```

Table 7.3 (continued)

```
NUMBER OF JET FIRINGS COMMANDED BY CONTROL LAW/JET SELECTION:
   JET # 1:   315   JET # 9:     0
   JET # 2:   108   JET #10:     0
   JET # 3:   287   JET #11:     0
   JET # 4:    85   JET #12:     0
   JET # 5:    55   JET #13:     0
   JET # 6:    27   JET #14:     0
   JET # 7:    56   JET #15:     0
   JET # 8:    63   JET #16:     1

TOTAL # JET FIRINGS(CONTROL LAW/JET SELECT):  997

NUMBER OF JET FIRINGS COMMANDED BY MASS PROP ID:
   JET # 1:     2   JET # 9:     0
   JET # 2:     2   JET #10:     0
   JET # 3:     0   JET #11:     0
   JET # 4:     1   JET #12:     0
   JET # 5:    11   JET #13:     0
   JET # 6:     6   JET #14:     0
   JET # 7:     5   JET #15:     0
   JET # 8:     3   JET #16:     0

TOTAL # JET FIRINGS(MASS PROP ID):  30
```

For comparison, the AFE DAP is run against this simulation and the tracking results are shown in Figure 7.8. The initial tracking response is good, but the vehicle becomes unstable when the AFE DAP attempts to implement the bank reversal after the first step change in the mass properties. Even after the mass properties return to their nominal values at t=90 sec the AFE DAP cannot recover before the end of the simulation.

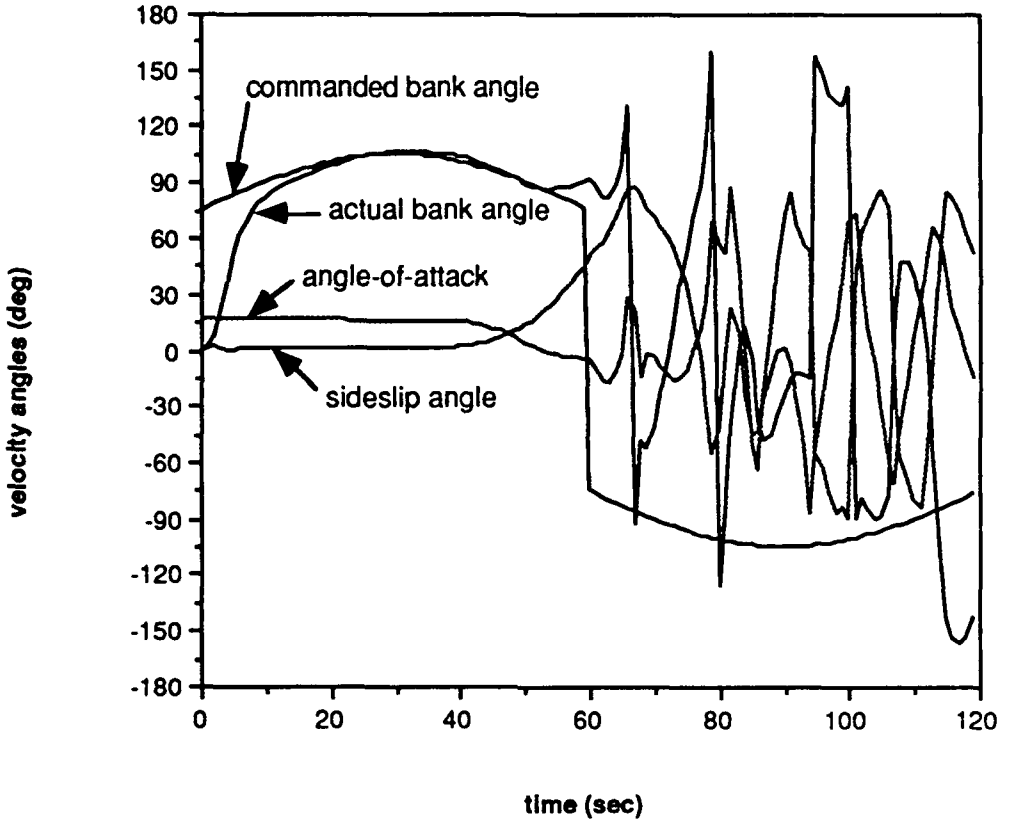

Figure 7.8. Velocity Angle Response - AFE DAP (Large Step Changes in Mass Properties)

7.4.3 Performance in the Presence of Gradually Changing Mass Properties

To demonstrate the ability of the candidate control system to identify and adapt to gradual changes in mass properties, the simulation was again repeated but with the center of mass continually moving. Beginning with the nominal mass properties, the center of mass is moved 0.5 inches/sec throughout the full simulation. As in the testing above, each 0.5 inch move is achieved by moving the center of mass an equal distance along the +x, +y, and +z axes. At the end of the 120 sec simulation, the center of mass

location is displaced a total of 60 inches from the nominal location at the coordinates

$$\vec{r}_{cm}(120\ \text{sec}) = \begin{bmatrix} 118.24 \\ 34.61 \\ 34.03 \end{bmatrix} \text{inches} \tag{7.5}$$

Throughout the simulation, the inertia matrix remains equal to the nominal inertia matrix.

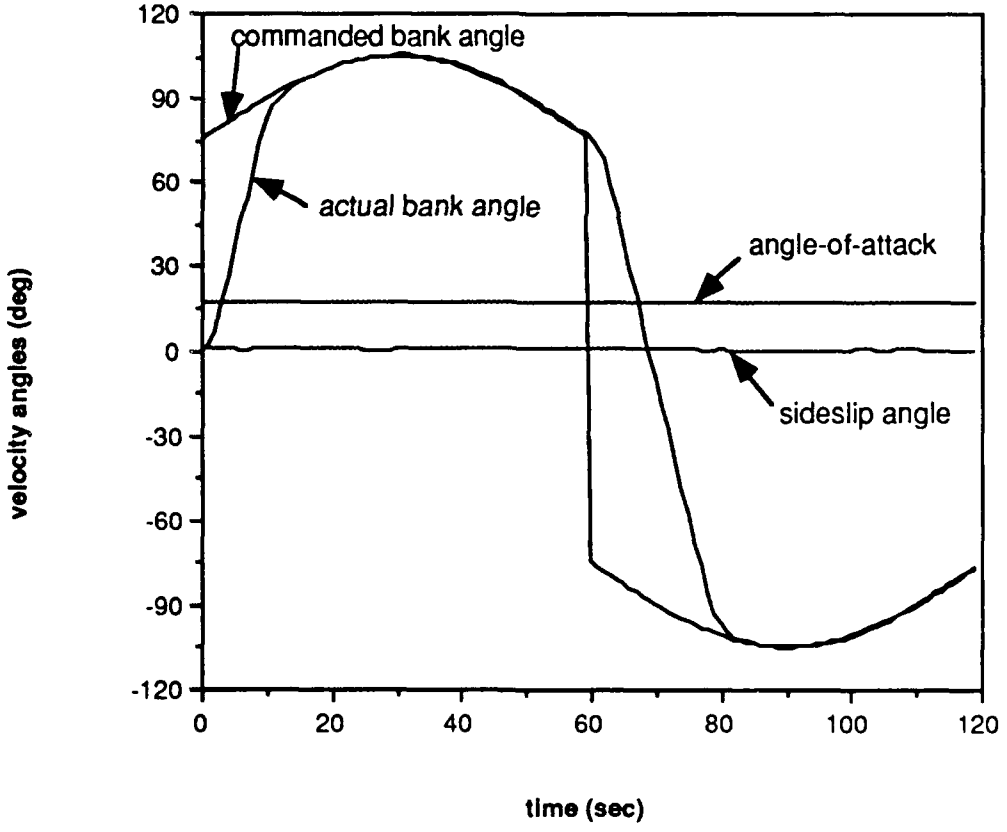

Figure 7.9. Velocity Angle Response - New Design (Slow, Continual Mass Property Changes)

Figure 7.9 shows the tracking response of the candidate control system for this test. Again comparing to Figures 7.4 and 7.7, no change in tracking performance is discernable. Table 7.4 lists the main events during this test. The initial mass property estimates are supplied by the identification algorithm at t=0.52 sec. At t=37.32 sec, the first detection of a mass property change occurs. Mass property identification is performed while control is maintained, and accurate, updated mass property estimates are supplied at t=38.68 sec. The center of mass continues to be moved, and at t=69.92 sec, the flag is set indicating another mass property change has been detected. The new identification period lasts until t=71.16 sec when the new estimates are supplied. A final change is detected at t=109.52 sec with updated mass property estimates supplied at t=110.80 sec. The simulation ends before another mass property change is detected.

Table 7.4 New Design
(Slow, Continual Changes in Mass Properties)

```
*** TIME =    .52 SEC ***

ACTUAL MASS PROPERTIES:
  INERTIA MATRIX IS:
       2248.20    -5.00   -63.60
         -5.00  1459.20    21.00
        -63.60    21.00  1178.60
  CENTER OF MASS IS:
        83.75
          .12
         -.46
```

Table 7.4 (continued)

```
UPDATED MASS PROPERTY ESTIMATES:
  EST INERTIA MATRIX IS:
       2243.42    -4.97   -63.48
         -4.97  1459.14    21.07
        -63.48    21.07  1178.54
  ESTIMATED CENTER OF MASS IS:
        83.66
          .04
         -.54


MASS PROPERTY CHANGE DETECTED AT T =  37.32 SEC

JET FIRINGS COMMANDED BY MASS PROP ID
     JET # 7 AT T =  37.40 SEC
     JET # 1 AT T =  37.60 SEC
     JET # 2 AT T =  37.80 SEC
     JET # 5 AT T =  38.00 SEC
     JET # 7 AT T =  38.20 SEC
     JET # 3 AT T =  38.40 SEC
     JET # 6 AT T =  38.60 SEC

*** TIME =  38.68 SEC ***

ACTUAL MASS PROPERTIES:
  INERTIA MATRIX IS:
       2248.20    -5.00   -63.60
         -5.00  1459.20    21.00
        -63.60    21.00  1178.60
  CENTER OF MASS IS:
        94.77
        11.14
        10.56

UPDATED MASS PROPERTY ESTIMATES:
  EST INERTIA MATRIX IS:
       2247.74    -4.78   -63.59
         -4.78  1457.49    21.56
        -63.59    21.56  1178.72
  ESTIMATED CENTER OF MASS IS:
        94.62
        11.04
        10.46
```

Table 7.4 (continued)

```
MASS PROPERTY CHANGE DETECTED AT T =  69.92 SEC

JET FIRINGS COMMANDED BY MASS PROP ID
     JET # 7 AT T =  70.00 SEC
     JET # 7 AT T =  70.20 SEC
     JET # 6 AT T =  70.40 SEC
     JET # 5 AT T =  70.60 SEC
     JET # 6 AT T =  70.80 SEC
     JET # 4 AT T =  71.00 SEC

*** TIME =  71.16 SEC ***

ACTUAL MASS PROPERTIES:
  INERTIA MATRIX IS:
       2248.20    -5.00   -63.60
         -5.00  1459.20    21.00
        -63.60    21.00  1178.60
  CENTER OF MASS IS:
       104.14
        20.51
        19.93

UPDATED MASS PROPERTY ESTIMATES:
  EST INERTIA MATRIX IS:
       2265.55     2.38   -58.89
          2.38  1395.09    30.76
        -58.89    30.76  1119.01
  ESTIMATED CENTER OF MASS IS:
       101.80
        20.29
        20.51


MASS PROPERTY CHANGE DETECTED AT T = 109.52 SEC

JET FIRINGS COMMANDED BY MASS PROP ID
     JET # 7 AT T = 109.60 SEC
     JET # 1 AT T = 109.80 SEC
     JET # 2 AT T = 110.00 SEC
     JET # 2 AT T = 110.20 SEC
     JET # 6 AT T = 110.40 SEC
     JET # 5 AT T = 110.60 SEC
```

Table 7.4 (continued)

```
*** TIME = 110.80 SEC ***

ACTUAL MASS PROPERTIES:
  INERTIA MATRIX IS:
       2248.20    -5.00   -63.60
         -5.00  1459.20    21.00
        -63.60    21.00  1178.60
  CENTER OF MASS IS:
       115.59
        31.96
        31.38

UPDATED MASS PROPERTY ESTIMATES:
  EST INERTIA MATRIX IS:
       2247.80    -4.05   -63.83
         -4.05  1458.48    20.70
        -63.83    20.70  1176.29
  ESTIMATED CENTER OF MASS IS:
       115.46
        31.79
        31.29


NUMBER OF JET FIRINGS COMMANDED BY CONTROL LAW/JET SELECTION:
   JET # 1:   131   JET # 9:     0
   JET # 2:   125   JET #10:     0
   JET # 3:   133   JET #11:     0
   JET # 4:   108   JET #12:     0
   JET # 5:    87   JET #13:     0
   JET # 6:     2   JET #14:     0
   JET # 7:     8   JET #15:     0
   JET # 8:    51   JET #16:     0

TOTAL # JET FIRINGS(CONTROL LAW/JET SELECT):  645


NUMBER OF JET FIRINGS COMMANDED BY MASS PROP ID:
   JET # 1:     3   JET # 9:     0
   JET # 2:     3   JET #10:     0
   JET # 3:     1   JET #11:     0
   JET # 4:     1   JET #12:     0
   JET # 5:     7   JET #13:     0
   JET # 6:     8   JET #14:     0
   JET # 7:     7   JET #15:     0
   JET # 8:     1   JET #16:     0

TOTAL # JET FIRINGS(MASS PROP ID):  31
```

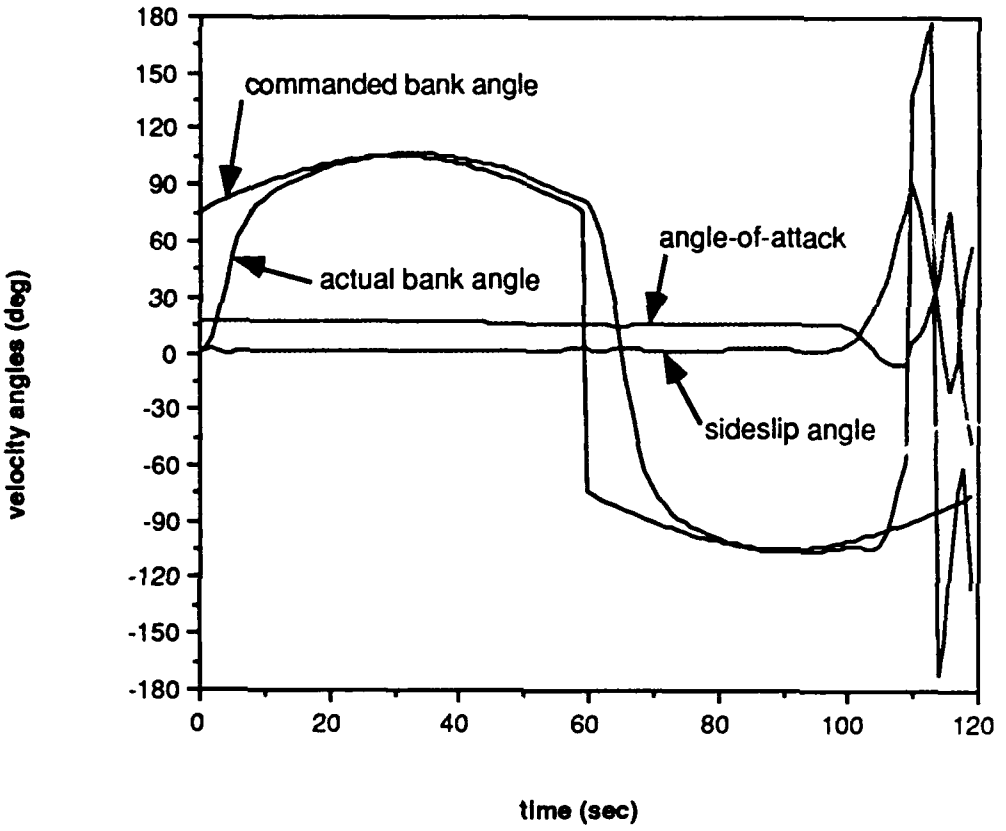

Figure 7.10. Velocity Angle Response - AFE DAP (Slow, Continual Mass Property Changes)

Figure 7.10 shows the tracking response of the AFE DAP run against this simulation. At the midpoint (i.e., t=60 sec) the center of mass has only been moved 30 inches. The AFE DAP is still stable with this amount of displacement and is able to implement the bank reversal. At roughly t=100 sec, the limits of stability have been exceeded, and the system becomes unstable.

7.5 Effects of Aerodynamics

In Section 1.5.2 the assumption was made that the aerodynamic torques experienced by the vehicle during the

aerocapture maneuver are small compared to the torques applied by the RCS jets. The control law was designed to be robust to the aerodynamic torques, and the candidate attitude control system should be robust to the disturbances caused by the aerodynamic torques. The tests performed in Section 7.4 were repeated with the aerodynamic torques simulated to verify these assumptions. The results presented below show that the control system is indeed robust to these aerodynamic disturbances. The results also show, however, that the mass property identification algorithm has difficulty in converging to accurate estimates when the vehicle is at its deepest points in the atmosphere where the magnitudes of the aerodynamic torques are at their greatest. This is not surprising since in Section 5.2 for the filter design for mass property estimation, the additional assumption was made that the aerodynamic torques were small enough to be treated as noise to the rate change measurements. The mass property identification algorithm design has not yet been extended to accurately estimate mass properties in the presence of significant aerodynamic disturbances.

7.5.1 Nominal Performance

For a vehicle with the nominal, unchanging mass properties, the response of the candidate control system is very similar to the response described in Section 7.4.1. The tracking response is almost identical, and Table 7.5 shows that the initial mass property estimates are nearly the same as the initial estimates listed in Table 7.1. The number of jet firings commanded by the jet selection has risen slightly, from 554 to 586, to counter the aerodynamic torques.

Table 7.5 New Design w/ Aerodynamics (Nominal Simulation)

```
*** TIME =     .52 SEC ***

ACTUAL MASS PROPERTIES:
  INERTIA MATRIX IS:
       2248.20     -5.00    -63.60
         -5.00   1459.20     21.00
        -63.60     21.00   1178.60
  CENTER OF MASS IS:
        83.60
         -.03
         -.61

UPDATED MASS PROPERTY ESTIMATES:
  EST INERTIA MATRIX IS:
       2243.57     -4.97    -63.47
         -4.97   1459.19     21.04
        -63.47     21.04   1178.61
  ESTIMATED CENTER OF MASS IS:
        83.66
         -.03
         -.62

NUMBER OF JET FIRINGS COMMANDED BY CONTROL LAW/JET SELECTION:
   JET # 1:     97    JET # 9:      0
   JET # 2:    145    JET #10:      0
   JET # 3:    120    JET #11:      0
   JET # 4:    111    JET #12:      0
   JET # 5:     84    JET #13:      0
   JET # 6:      1    JET #14:      0
   JET # 7:      6    JET #15:      0
   JET # 8:     22    JET #16:      0

TOTAL # JET FIRINGS(CONTROL LAW/JET SELECT):  586


NUMBER OF JET FIRINGS COMMANDED BY MASS PROP ID:
   JET # 1:      1    JET # 9:      0
   JET # 2:      0    JET #10:      0
   JET # 3:      0    JET #11:      0
   JET # 4:      0    JET #12:      0
   JET # 5:      4    JET #13:      0
   JET # 6:      4    JET #14:      0
   JET # 7:      2    JET #15:      0
   JET # 8:      1    JET #16:      0

TOTAL # JET FIRINGS(MASS PROP ID):  12
```

7.5.2 Performance in the Presence of Large Step Changes to the Mass Properties

Figure 7.11 shows the altitude of the vehicle throughout each simulation.

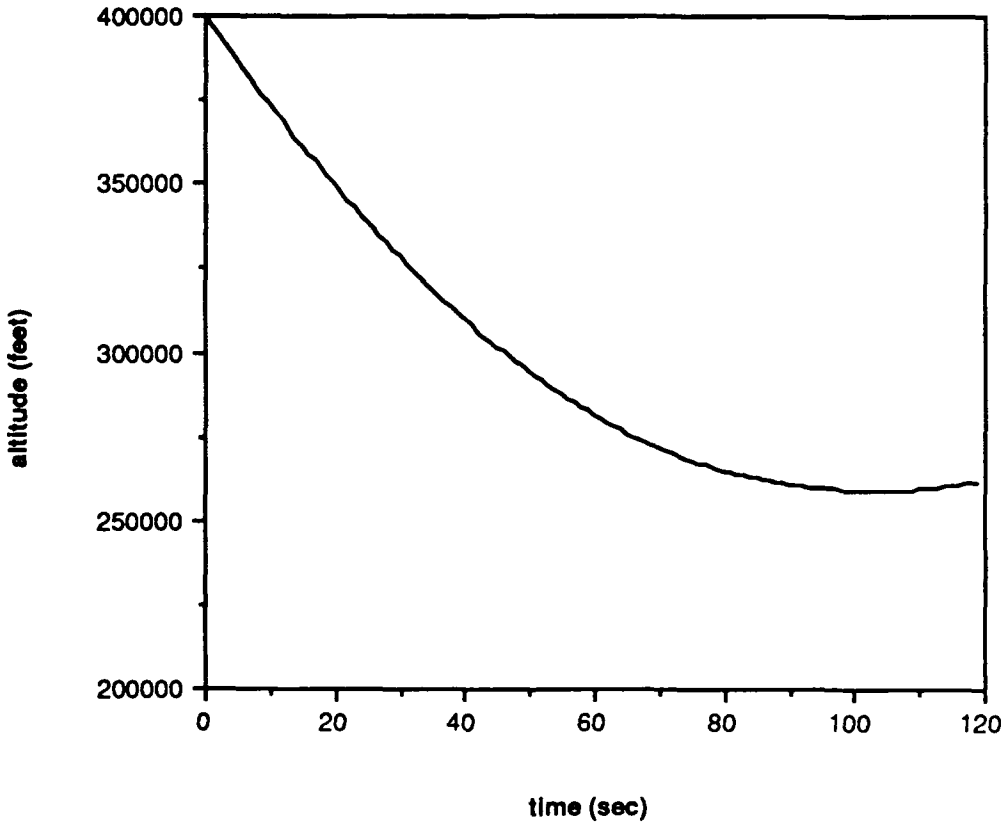

Figure 7.11. Altitude vs. Time

The aerodynamic torques do have a significant impact during the test in which large step changes in the mass properties are simulated. Table 7.6 shows that the candidate system is still able to identify and adapt to the first change at t=30 sec. The change is detected at t=33.76 sec and the updated mass property estimates are supplied at t=36.08 sec. These estimates, however, are not as accurate as the first updated estimates listed in Table 7.3. The

aerodynamic torques become larger as the vehicle descends through the atmosphere and begin degrading the accuracy of the mass property estimates.

Table 7.6 New Design w/ Aerodynamics (Step Changes in Mass Properties)

```
*** TIME =     .52 SEC ***

ACTUAL MASS PROPERTIES:
  INERTIA MATRIX IS:
       2248.20     -5.00    -63.60
         -5.00   1459.20     21.00
        -63.60     21.00   1178.60
  CENTER OF MASS IS:
        83.60
         -.03
         -.61

UPDATED MASS PROPERTY ESTIMATES:
  EST INERTIA MATRIX IS:
       2243.57     -4.97    -63.47
         -4.97   1459.19     21.04
        -63.47     21.04   1178.61
  ESTIMATED CENTER OF MASS IS:
        83.66
         -.03.
         -.62


MASS PROPERTY CHANGE DETECTED AT T =  33.76 SEC

JET FIRINGS COMMANDED BY MASS PROP ID
     JET # 7 AT T =  33.80 SEC
     JET # 5 AT T =  34.00 SEC
     JET # 3 AT T =  34.20 SEC
     JET # 7 AT T =  34.40 SEC
     JET # 8 AT T =  34.60 SEC
     JET # 4 AT T =  34.80 SEC
     JET # 5 AT T =  35.00 SEC
     JET # 3 AT T =  35.20 SEC
     JET # 8 AT T =  35.40 SEC
     JET # 4 AT T =  35.60 SEC
     JET # 7 AT T =  35.80 SEC
     JET # 2 AT T =  36.00 SEC
```

Table 7.6 New Design w/ Aerodynamics (Step Changes in Mass Properties)

```
*** TIME =  36.08 SEC ***

ACTUAL MASS PROPERTIES:
  INERTIA MATRIX IS:
       4554.31 -1158.06 -1216.66
      -1158.06  3765.31 -1132.06
      -1216.66 -1132.06  3484.71
  CENTER OF MASS IS:
       109.58
        25.95
        25.37

UPDATED MASS PROPERTY ESTIMATES:
  EST INERTIA MATRIX IS:
       4506.64 -1135.88 -1205.18
      -1135.88  3779.37 -1138.18
      -1205.18 -1138.18  3467.13
  ESTIMATED CENTER OF MASS IS:
       109.49
        24.55
        24.97

MASS PROPERTY CHANGE DETECTED AT T =  90.36 SEC

 JET FIRINGS COMMANDED BY MASS PROP ID
     JET # 5 AT T =  90.40 SEC
     JET # 7 AT T =  90.60 SEC
     JET # 5 AT T =  90.80 SEC
   . JET # 5 AT T =  91.00 SEC
     JET # 5 AT T =  91.20 SEC
     JET # 6 AT T =  91.40 SEC
     JET # 8 AT T =  91.60 SEC
     JET # 5 AT T =  91.80 SEC
     JET # 5 AT T =  92.00 SEC
     JET # 6 AT T =  92.20 SEC
     JET # 8 AT T =  92.40 SEC
     JET # 8 AT T =  92.60 SEC
     JET # 8 AT T =  92.80 SEC
     JET # 8 AT T =  93.00 SEC
     JET # 8 AT T =  93.20 SEC
     JET # 5 AT T =  93.40 SEC
     JET # 5 AT T =  93.60 SEC
     JET # 5 AT T =  93.80 SEC
     JET # 5 AT T =  94.00 SEC
     JET # 8 AT T =  94.20 SEC
     JET # 8 AT T =  94.40 SEC
     JET # 5 AT T =  94.60 SEC
     JET # 8 AT T =  94.80 SEC
     JET # 5 AT T =  95.00 SEC
```

Table 7.6 (continued)

```
      JET # 5 AT T =  95.20 SEC
      JET # 8 AT T =  95.40 SEC
      JET # 5 AT T =  95.60 SEC
      JET # 5 AT T =  95.80 SEC
      JET # 8 AT T =  96.00 SEC
      JET # 5 AT T =  96.20 SEC
      JET # 8 AT T =  96.40 SEC
      JET # 8 AT T =  96.60 SEC
      JET # 5 AT T =  96.80 SEC
      JET # 8 AT T =  97.00 SEC
      JET # 5 AT T =  97.20 SEC
      JET # 4 AT T =  97.40 SEC
      JET # 5 AT T =  97.60 SEC
      JET # 8 AT T =  97.80 SEC
      JET # 5 AT T =  98.00 SEC

*** TIME =  98.20 SEC ***

ACTUAL MASS PROPERTIES:
  INERTIA MATRIX IS:
       2248.20    -5.00   -63.60
         -5.00  1459.20    21.00
        -63.60    21.00  1178.60
  CENTER OF MASS IS:
        83.60
         -.03
         -.61

UPDATED MASS PROPERTY ESTIMATES:
  EST INERTIA MATRIX IS:
       2481.96    34.35    -1.22
         34.35  1414.26     1.85
         -1.22     1.85  1146.97
  ESTIMATED CENTER OF MASS IS:
        79.67
         3.46
         3.22


NUMBER OF JET FIRINGS COMMANDED BY CONTROL LAW/JET SELECTION:
   JET # 1:   360   JET # 9:     0
   JET # 2:   110   JET #10:     0
   JET # 3:   333   JET #11:     0
   JET # 4:    75   JET #12:     0
   JET # 5:    85   JET #13:     0
   JET # 6:    47   JET #14:     0
   JET # 7:    57   JET #15:     0
   JET # 8:    61   JET #16:     0

TOTAL # JET FIRINGS(CONTROL LAW/JET SELECT):  1128
```

Table 7.6 (continued)

```
NUMBER OF JET FIRINGS COMMANDED BY MASS PROP ID:
   JET # 1:      1    JET # 9:      0
   JET # 2:      1    JET #10:      0
   JET # 3:      2    JET #11:      0
   JET # 4:      3    JET #12:      0
   JET # 5:     23    JET #13:      0
   JET # 6:      5    JET #14:      0
   JET # 7:      6    JET #15:      0
   JET # 8:     18    JET #16:      0

TOTAL # JET FIRINGS(MASS PROP ID):  59
```

Table 7.6 also shows that the second mass property change is detected at t=90.36 sec. This time numerous jet firings are required before the filter can converge to mass property estimates accurate enough to end the identification period. After the first few jet firings, the input selection scheme in the mass property identification algorithm commands mainly jets #5 and #8. This is an indication that the filter has become optimistic (i.e., the trace elements of **P** have decreased nearly to their values before the identification period began). Little information is extracted from these later jet firings and the filter has difficulty in converging to accurate estimates. Finally, at t=98.20 sec, the two criteria described in Section 6.4.3 are met and updated mass property estimates are supplied. Though the accuracy has been degraded by the aerodynamic torques, the estimates are accurate enough for the control system to track the desired trajectory.

7.5.3 Performance in the Presence of Gradually Changing Mass Properties

Table 7.7 shows the impact of the aerodynamic torques on the ability of the mass property identification algorithm to accurately estimate gradually changing mass properties. During the identification period starting at t=70.36 sec, the filter becomes optimistic and is unable to converge to accurate estimates.

Table 7.7 New Design w/ Aerodynamics (Slow, Continual Changes in Mass Properties)

```
*** TIME =     .52 SEC ***

ACTUAL MASS PROPERTIES:
  INERTIA MATRIX IS:
       2248.20     -5.00    -63.60
         -5.00   1459.20     21.00
        -63.60     21.00   1178.60
  CENTER OF MASS IS:
        83.75
          .12
         -.46

UPDATED MASS PROPERTY ESTIMATES:
  EST INERTIA MATRIX IS:
       2243.05     -4.97    -63.47
         -4.97   1459.14     21.07
        -63.47     21.07   1178.50
  ESTIMATED CENTER OF MASS IS:
        83.67
          .04
         -.54


MASS PROPERTY CHANGE DETECTED AT T =  41.32 SEC

JET FIRINGS COMMANDED BY MASS PROP ID
     JET # 7 AT T =  41.40 SEC
     JET # 1 AT T =  41.60 SEC
     JET # 5 AT T =  41.80 SEC
     JET # 7 AT T =  42.00 SEC
     JET # 6 AT T =  42.20 SEC
     JET # 2 AT T =  42.40 SEC
     JET # 1 AT T =  42.60 SEC
     JET # 6 AT T =  42.80 SEC
```

Table 7.7 (continued)

```
     JET # 6 AT T =  43.00 SEC
     JET # 3 AT T =  43.20 SEC

*** TIME =  43.28 SEC ***

ACTUAL MASS PROPERTIES:
  INERTIA MATRIX IS:
       2248.20    -5.00   -63.60
         -5.00  1459.20    21.00
        -63.60    21.00  1178.60
  CENTER OF MASS IS:
        96.09
        12.46
        11.88

UPDATED MASS PROPERTY ESTIMATES:
  EST INERTIA MATRIX IS:
       2233.49     6.89   -54.45
          6.89  1457.09    27.34
        -54.45    27.34  1186.85
  ESTIMATED CENTER OF MASS IS:
        96.37
        10.97
        11.36

MASS PROPERTY CHANGE DETECTED AT T =  70.36 SEC

JET FIRINGS COMMANDED BY MASS PROP ID
     JET # 7 AT T =  70.40 SEC
     JET # 1 AT T =  70.60 SEC
     JET # 2 AT T =  70.80 SEC
     JET # 2 AT T =  71.00 SEC
     JET # 1 AT T =  71.20 SEC
     JET # 6 AT T =  71.40 SEC
     JET # 6 AT T =  71.60 SEC
     JET # 1 AT T =  71.80 SEC
     JET # 4 AT T =  72.00 SEC
     JET # 6 AT T =  72.20 SEC
     JET # 6 AT T =  72.40 SEC
     JET # 4 AT T =  72.60 SEC
     JET # 1 AT T =  72.80 SEC
     JET # 4 AT T =  73.00 SEC
     JET # 6 AT T =  73.20 SEC
     JET # 6 AT T =  73.40 SEC
     JET # 1 AT T =  73.60 SEC
     JET # 4 AT T =  73.80 SEC
     JET # 6 AT T =  74.00 SEC
     JET # 4 AT T =  74.20 SEC
     JET # 6 AT T =  74.40 SEC
     JET # 1 AT T =  74.60 SEC
     JET # 4 AT T =  74.80 SEC

(Firings continue until end of simulation. No new mass property
estimates provided)
```

sliding mode control law/linear programming jet selection algorithm combination provides somewhat more precise tracking, while using less fuel (i.e., fewer jet firings), than the existing AFE DAP system consisting of a proportional control law and a table look-up jet selection algorithm. Also, even without employing the mass property identification algorithm, the new control law/jet selection algorithm is somewhat more robust than the AFE DAP. Second, the employment of the mass property identification algorithm greatly extends the range of vehicle mass properties over which the attitude control system is robust.

The results of the simulation tests described in Section 7.4 show the ability of the candidate control system to not only make very accurate initial mass property estimates, but to also detect and adapt to mass property changes that occur during the aerocapture maneuver that would normally cause the system to become unstable. The mass property identification algorithm can detect instantaneous or gradual mass property changes by comparing the measured rate changes due to the jet firings to predicted rate changes. After a change is detected, the operation scheme described in Chapter 6 allows the control system to continue to provide attitude control while mass property identification is performed. At the end of an identification period, the updated mass property estimates are provided to both the control law and the jet selection algorithm enabling the control system to continue to provide stable, efficient, attitude control.

Test results presented in Section 7.5 show that the control system is robust to the aerodynamic torques experienced by the

Chapter 8

Conclusions and Recommendations

8.1 Conclusions

The main objective of this research has been the design of a candidate control system capable of providing attitude control for an aerocapture vehicle with a wide range of possible mass properties. The task demanded of the attitude control system has been to track the desired bank angle trajectory commanded by the guidance law while maintaining trim angle-of-attack (α) and sideslip angle (β). Additionally, the control system was required to be able to perform this task over a wide range of vehicle mass properties.

The candidate control system consists of the following three main elements: a nonlinear sliding mode control law, an adaptable linear programming jet selection algorithm, and a mass property identification algorithm based on a second-order extended Kalman filter design. The jet selection and mass property identification algorithms have both been used previously in similar works [20,21,24]. The sliding mode control law, on the other hand, was designed for this effort, while the main contribution of this work has been the integration of these elements into the candidate design.

The integrated candidate control system design does meet the main objective described above. Two significant results were demonstrated in the simulation tests discussed in Section 7.3. First, the

vehicle during the aerocapture maneuver. As the spacecraft descends deeper into the atmosphere, however, the aerodynamic torques experienced degrade the accuracy of the mass property identification. At lower altitudes where the magnitude of the aerodynamic torques are greatest, the filter is not able to converge to accurate mass property estimates.

8.2 Recommendations for Future Work

Future work should address the effects of aerodynamic torques on the ability of the mass property identification algorithm to accurately estimate mass properties. Additionally, since this thesis addresses only a subset of the ultimate goal (described in Section 1.5) of a generic attitude control system for use with any aerocapture mission and any vehicle, future research should concentrate on achieving the ultimate goal. Specifically, the recommendations are:

(1) Develop an estimation algorithm to continually identify the aerodynamic forces and torques on the aerocapture vehicle. With this knowledge, the effects of these forces and torques can be subtracted out of the calculation of the residual vector so that the mass property identification algorithm can more accurately estimate the mass properties in the presence of significant aerodynamic torques.

(2) Extend the mass property identification algorithm to accommodate non-ideal attitude and rate measurements.

(3) Test the candidate system in a simulation with an advanced guidance law that varies both bank angle and angle-of-attack.

(4) Develop algorithms to identify failed jets, along with reduced or misaligned jet thrust.

(5) Develop an algorithm to identify the effectiveness of alternate types of control actuators (i.e., aerosurfaces and control moment gyros) so that the attitude control system structure can be applied to a vehicle employing blended control.

(6) Apply the candidate attitude control system to a vehicle performing a Martian aerocapture to ensure the candidate system is viable in greatly different environments.

Finally, this candidate control system structure is not limited to attitude control of aerocapture vehicles. It may be applicable to many types of control problems for which parameters impacting actuator effectiveness are not known and may vary significantly during system operation. Future work should investigate the benefits of applying this control system structure to other types of control problems.

Appendix A

Velocity Angles and the Body Axes

A.1 123 Axes, Body Axes, and Velocity Angles

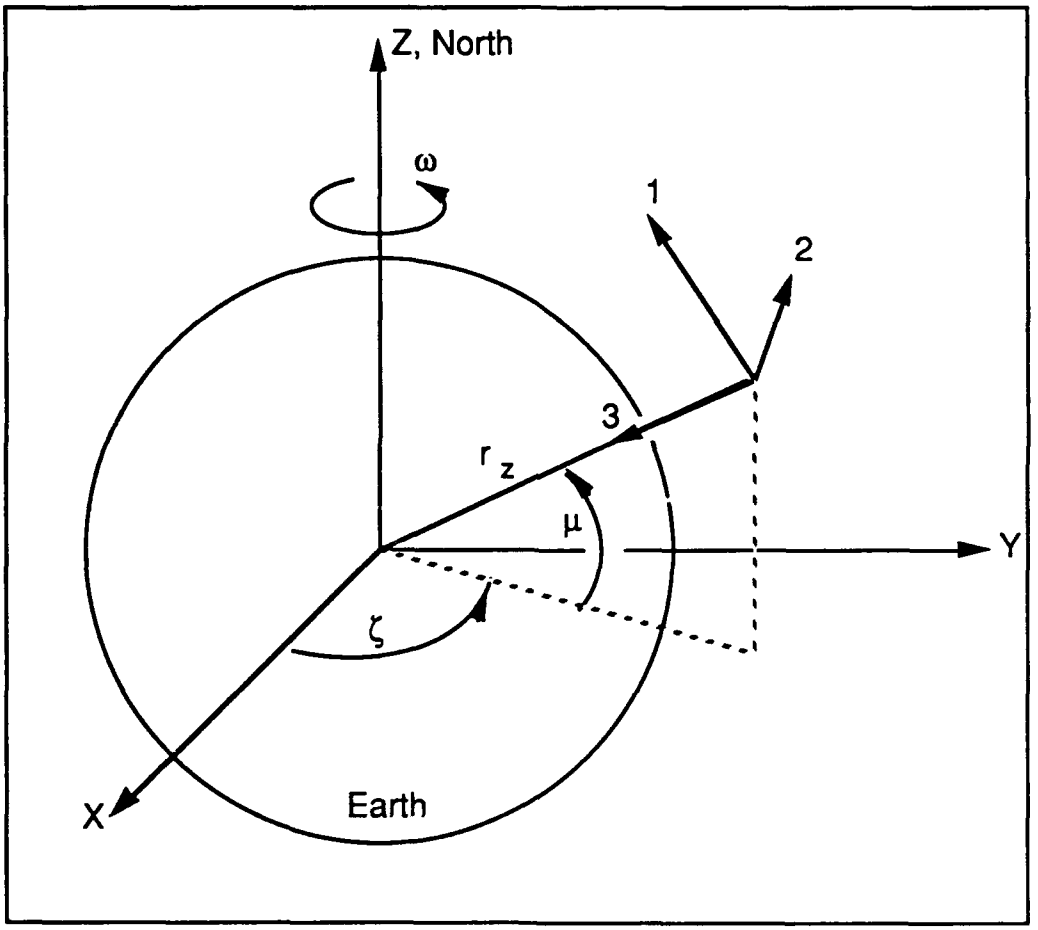

Figure A.1 123 Reference System

Figure A.1 illustrates the orientation of a local-vertical local-horizontal axes system denoted as 123 with respect to the Earth fixed axes XYZ. The angle of longitude ζ, the angle of latitude μ, and

the radial distance r_z from the center of Earth define the location of the center of the 123 axes system corresponding to the center of mass of the aerocapture vehicle. The 1 axis points towards the north, the 2 axis towards the east, and the 3 axis towards the center of Earth.

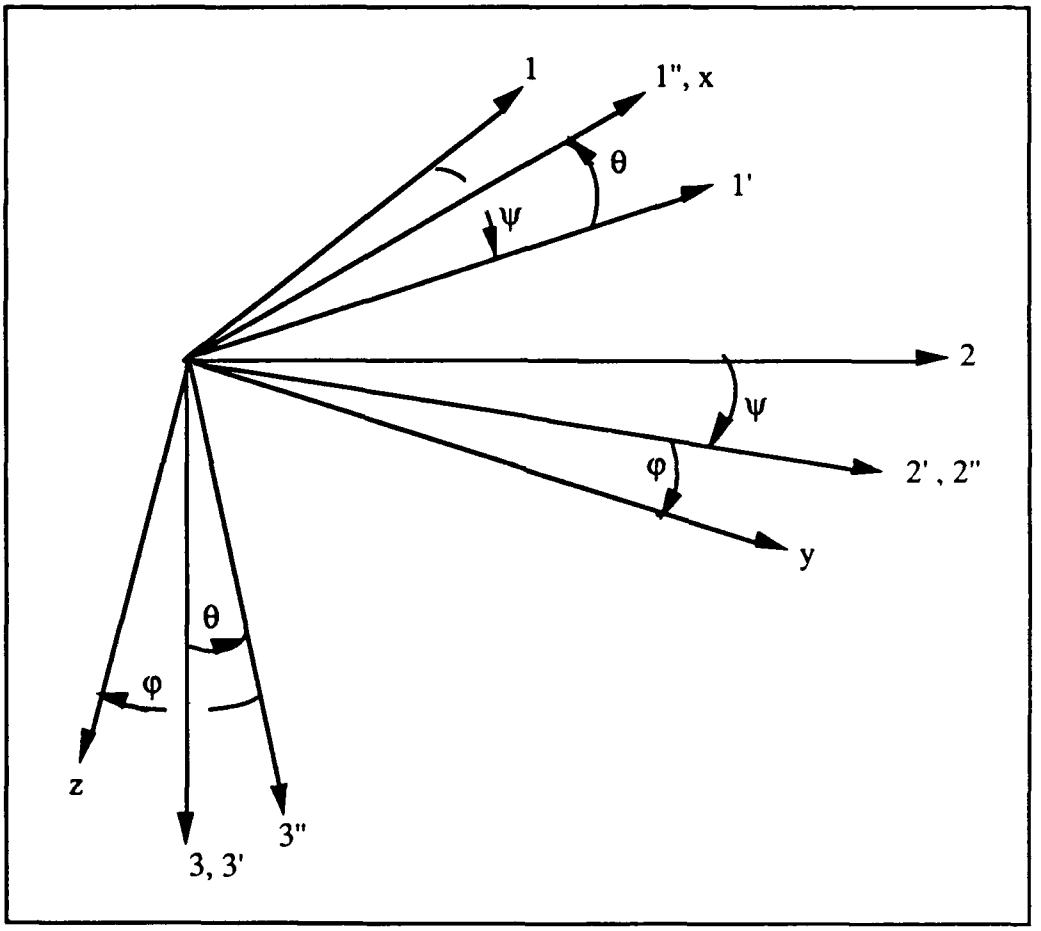

Figure A.2. Euler Angles

The Euler angles θ, φ, and ψ shown in Figure A.2 define the orientation of the xyz vehicle body axes with respect to the 123 axes. The order of rotations performed to achieve the body axes is:

ψ about the 3 axis

θ about the 2' axis

φ about the 1" axis

Bank angle, angle of attack, and sideslip angle (i.e., ϕ, α, and β) are considered the velocity angles. These angles determine the orientation of the body axes with respect to the velocity vector. Figure A.3 shows how the velocity angles are defined with respect to the body referenced axis system.

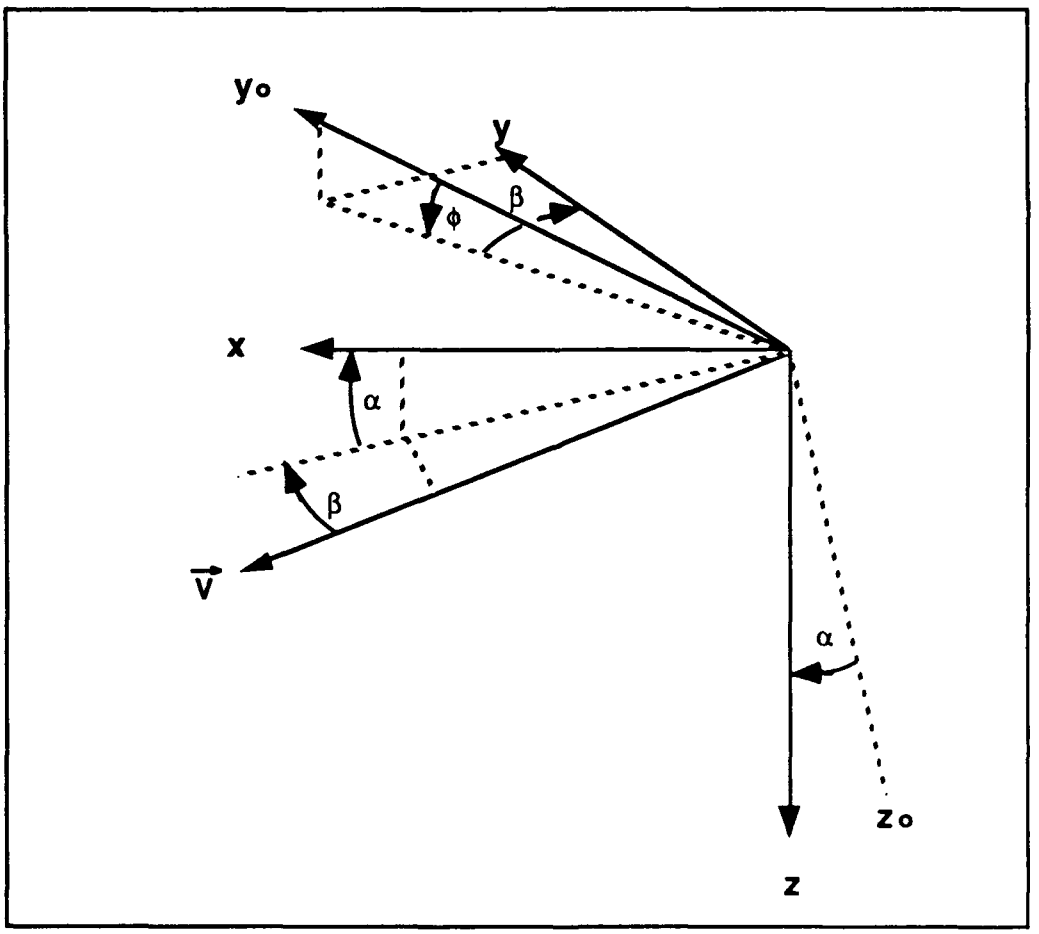

Figure A.3. Velocity Angles

The order of rotations required to orient the body axes with respect to the velocity vector is:

ϕ about $\vec{v}$
β about the z_o axis (other conventions use β about $-z_o$)
α about the y axis

A.2 Rotation Matrix for Conversion From Body Rates to Velocity Angle Rates

Following the examples in chapter 2 of reference [39], the rotation matrix required to convert body rates into velocity angle rates can be calculated with two rotations. The starting point is an axis system ABC with the A axis along the velocity vector. Since the velocity angles α and β are independent of the bank angle, the first step is to rotate an angle β about the C axis.

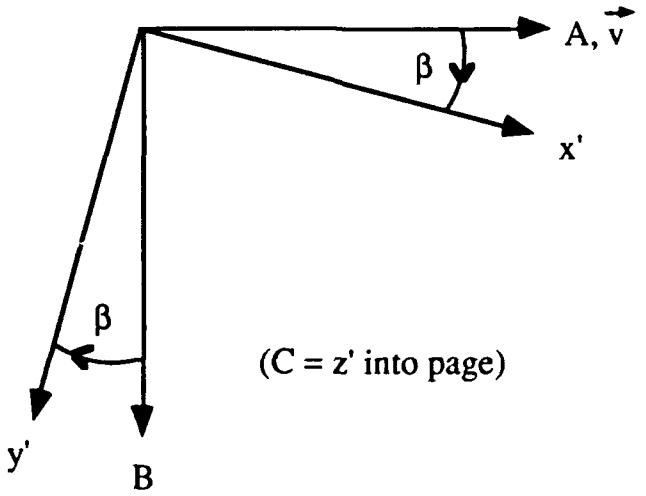

The ABC axis system can be written in terms of the new x'y'z' axis system by

$$\begin{bmatrix} A \\ B \\ C \end{bmatrix} = \begin{bmatrix} \cos\beta & -\sin\beta & 0 \\ \sin\beta & \cos\beta & 0 \\ 0 & 0 & 1 \end{bmatrix} \begin{bmatrix} x' \\ y' \\ z' \end{bmatrix} \qquad (A.1)$$

The x'y'z' axis system is now rotated about the y' axis through an angle of α and the x'y'z' can be written in terms of the body referenced axes xyz.

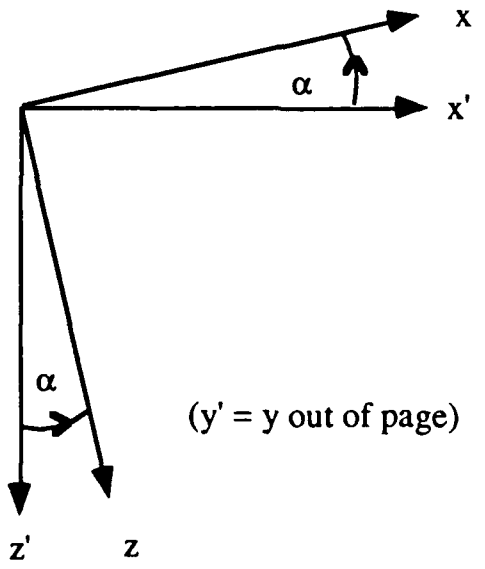

$$\begin{bmatrix} x' \\ y' \\ z' \end{bmatrix} = \begin{bmatrix} \cos\alpha & 0 & \sin\alpha \\ 0 & 1 & 0 \\ -\sin\alpha & 0 & \cos\alpha \end{bmatrix} \begin{bmatrix} x \\ y \\ z \end{bmatrix} \qquad (A.2)$$

Combining Equations A.1 and A.2, the ABC axis system can be written in terms of the body referenced system from

$$\begin{bmatrix} A \\ B \\ C \end{bmatrix} = \mathbf{R} \begin{bmatrix} x \\ y \\ z \end{bmatrix} \tag{A.3}$$

where the rotation matrix, **R**, is given by

$$\mathbf{R} = \begin{bmatrix} \cos\alpha\cos\beta & -\sin\beta & \sin\alpha\cos\beta \\ \cos\alpha\sin\beta & \cos\beta & \sin\alpha\sin\beta \\ -\sin\alpha & 0 & \cos\alpha \end{bmatrix} \tag{A.3}$$

The resulting rotation matrix can be used to express velocity angle rates in terms of body angle rates and vice versa. In equation form,

$$\begin{bmatrix} \dot{\phi} \\ \dot{\alpha} \\ \dot{\beta} \end{bmatrix} = \mathbf{R} \begin{bmatrix} p \\ q \\ r \end{bmatrix}$$

where p, q, and r are the roll rate (about the x axis), pitch rate (about the y axis), and yaw rate (about the z axis), respectively.

Appendix B

Estimates and Bounds for Control Law Design

B.1 Inertia Matrix

Reference [36] provides the mass properties of the AFE vehicle. At atmosphere entry, the inertia matrix is predicted to be

$$\mathbf{I} = \begin{bmatrix} 2290.7 & -5.0 & -63.6 \\ -5.0 & 1490.9 & 21.0 \\ -63.6 & 21.0 & 1189.5 \end{bmatrix} \text{ slugs} \cdot \text{ft}^2$$

and at atmosphere exit (after fuel consumption), **I** is predicted to be

$$\mathbf{I} = \begin{bmatrix} 2196.2 & -5.0 & -63.6 \\ -5.0 & 1420.4 & 21.0 \\ -63.6 & 21.0 & 1165.2 \end{bmatrix} \text{ slugs} \cdot \text{ft}^2$$

Assuming these estimates are accurate to within +/- 10%, the range on **I** for the nominal AFE vehicle is assumed to be

$$\begin{bmatrix} 1976.6 & -5.5 & -70.0 \\ -5.5 & 1278.4 & 18.9 \\ -70.0 & 18.9 & 1048.7 \end{bmatrix} \leq \mathbf{I} \leq \begin{bmatrix} 2519.8 & -4.5 & -57.2 \\ -4.5 & 1640.0 & 23.1 \\ -57.2 & 23.1 & 1308.5 \end{bmatrix} \qquad \text{(B.1)}$$

Taking the midpoint of the ranges for each element, the estimated inertia matrix to be used in the controller design is

$$\hat{\mathbf{I}} = \begin{bmatrix} 2248.2 & -5.0 & -63.6 \\ -5.0 & 1459.2 & 21.0 \\ -63.6 & 21.0 & 1178.6 \end{bmatrix} \text{ slugs} \cdot \text{ft}^2 \qquad \text{(B.2)}$$

B.2 Input Matrix

In order to calculate the estimate and bounds for the input matrix B defined by Equation 3.30, the bounds on the matrix D (defined in Equation 3.35) must first be found. Using the inertia matrix estimates and bounds found above and assuming the maximum value of the rotation matrix **R** defined by Equation A.3 is the 3 by 3 identity matrix, from Equation 3.45,

$$\begin{bmatrix} -0.1080 & -0.0004 & -0.0048 \\ -0.0005 & -0.1102 & 0.0001 \\ -0.0096 & 0.0003 & -0.0995 \end{bmatrix} \leq \Delta \leq \begin{bmatrix} 0.1380 & 0.0006 & 0.0076 \\ 0.0008 & 0.1414 & -0.0002 \\ 0.0153 & -0.0005 & 0.1244 \end{bmatrix} \qquad \text{(B.3)}$$

With $\hat{\mathbf{B}}$ equal to the 3 by 3 identity matrix as specified in Equation 3.45, the range on the input matrix is found from Equation 3.30,

$$\begin{bmatrix} 0.8920 & -0.0004 & -0.0048 \\ -0.0005 & 0.8898 & 0.0001 \\ -0.0096 & 0.0003 & 0.9005 \end{bmatrix} \leq \mathbf{B} \leq \begin{bmatrix} 1.1380 & 0.0006 & 0.0076 \\ 0.0008 & 1.1414 & -0.0002 \\ 0.0153 & -0.0005 & 1.1244 \end{bmatrix} \qquad \text{(B.4)}$$

B.3 Aerodynamic Disturbances

In Equation 3.34, the system of equations used to calculate the control law gains $\vec{k}$, d_{imax} is the maximum angular acceleration in the i^{th} dimension due to the unmodelled aerodynamic torques. Since α and β errors cause torques that drive the vehicle back to trim, the main aerodynamic acceleration of concern is the bank acceleration due to velocity angle errors.

Following the analysis provided in reference [37], β can be assumed small. The banking moment is then comprised of moments about the x and z body axes. A bank moment coefficient can be defined as

$$C_l' = C_n \sin\alpha + C_l \cos\alpha \qquad \text{(B.5)}$$

where

C_l' = bank moment coefficient
C_n = yaw moment coefficient
C_l = roll moment coefficient

Assuming α and β remain within 2 deg of their trim values, from reference [37]

$$\begin{aligned} C_{nmax} &= 0.00562 \\ C_{lmax} &= 0.00034 \end{aligned} \qquad \text{(B.6)}$$

The maximum bank moment coefficient is then calculated at α = 19 deg to be

$$\dot{C}_{l_{max}} = 0.0005 \tag{B.7}$$

The maximum bank moment τ_ϕ is calculated from

$$\tau_\phi = \dot{C}_l S b \bar{q} \tag{B.8}$$

where

S = reference area = 151.74 ft^2
b = reference length = 13.99 ft
$\bar{q}$ = dynamic pressure in lbs/ft^2

Dynamic pressure is a function of velocity and atmospheric pressure.

$$\bar{q} = \frac{1}{2} \rho v^2 \tag{B.9}$$

where ρ is the atmospheric density and v is the magnitude of the velocity. Figure B.1 is a plot of $\bar{q}$ vs. altitude during the simulation tests performed. Assuming a maximum $\bar{q}$ of 34.0 lbs/ft^2, from Equation B.8,

$$\tau_{\phi_{max}} = 36.08 \text{ lbs·ft} \tag{B.10}$$

The disturbance acceleration due to this aerodynamic bank moment is estimated to be

$$d_1 = \frac{\tau_{\phi_{max}}}{I_{xx_{min}}} = \frac{36.08}{1976.6} = 0.018 \frac{\text{rads}}{\text{sec}^2} \tag{B.11}$$

The maximum disturbance in each dimension is set to d_1,

$$d_{i_{max}} = 0.018 \frac{rads}{sec^2} \tag{B.12}$$

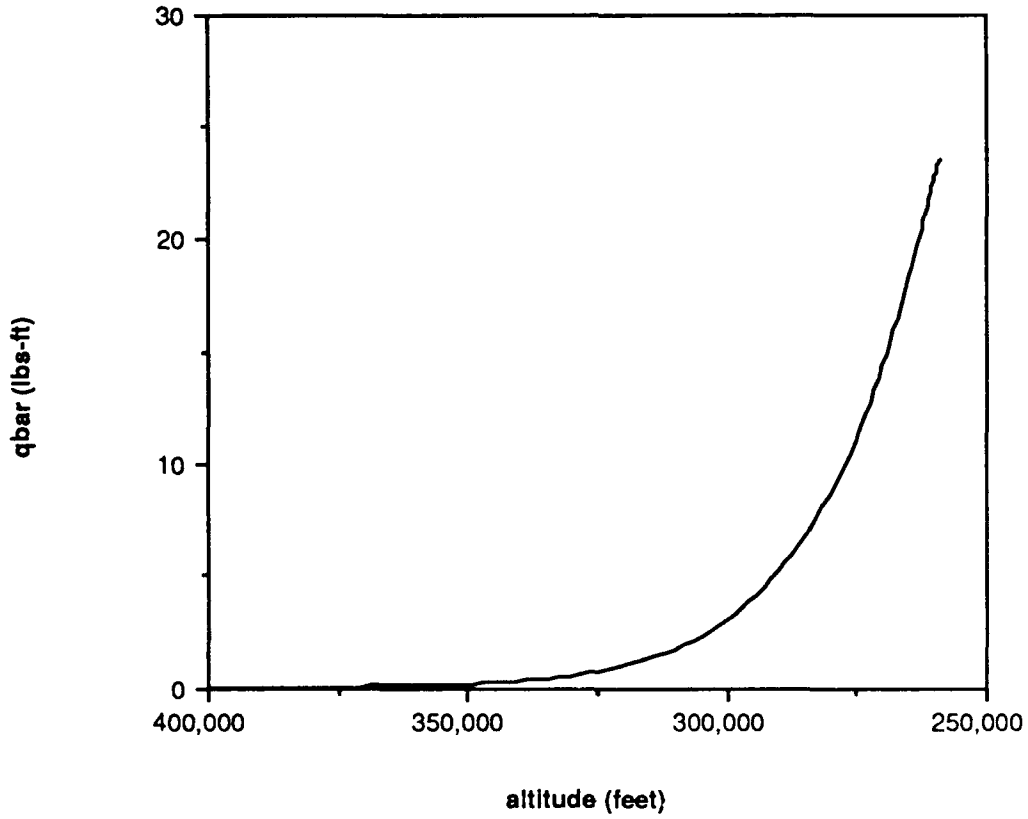

Figure B.1. Dynamic Pressure vs. Altitude

Appendix C

Simulated Changes to Vehicle Inertia Matrix

This appendix describes how inertia matrix changes due to movements of the center of mass location from its nominal position were calculated during simulation testing.

First, center of mass movements were simulated without adding mass to the vehicle. Assuming a point mass equal to half the vehicle mass exists at the nominal center of mass location, the desired displacement of the center of mass is achieved by moving the point mass to twice the desired displacement. The resulting center of mass is then at the desired location. For example, for the 45 inch center of mass displacement used in Section 6.4.2, half the vehicle mass was moved 90 inches from

$$\vec{r}_{cm_{nominal}} = \begin{bmatrix} 83.60 \\ -0.03 \\ -0.61 \end{bmatrix} \text{inches} \qquad \text{(C.1)}$$

to

$$\text{half mass position} = \begin{bmatrix} 135.56 \\ 51.93 \\ 51.35 \end{bmatrix} \text{inches} \qquad \text{(C.2)}$$

so that the new center of mass location is 45 inches from the nominal location at

$$\vec{r}_{cm_{new}} = \begin{bmatrix} 109.58 \\ 25.95 \\ 25.37 \end{bmatrix} \text{inches} \tag{C.3}$$

The new inertia matrix elements are calculated based on their definitions given in reference [30]:

$$I_{xx} = \sum_{i=1}^{N} m_i \left(y_i^2 + z_i^2\right) \tag{C.4}$$

$$I_{yy} = \sum_{i=1}^{N} m_i \left(z_i^2 + x_i^2\right)$$

$$I_{zz} = \sum_{i=1}^{N} m_i \left(x_i^2 + y_i^2\right)$$

$$I_{xy} = -\sum_{i=1}^{N} m_i \, x_i \, y_i$$

$$I_{xz} = -\sum_{i=1}^{N} m_i \, x_i \, z_i$$

$$I_{yz} = -\sum_{i=1}^{N} m_i \, y_i \, z_i$$

where the vehicle consists of N mass particles each with mass m_i and located at $x_i y_i z_i$. Since a point mass was removed from the nominal center of mass location, the inertia due to the remaining mass at this

point can be assumed to remain equal to the nominal inertia matrix. By adding half the mass at twice the desired displacement as described above (i.e., at the location given by Equation C.2 for the 45 inch displacement example), the new inertia matrix elements are calculated by:

$$I_{xx} = I_{xx_{nominal}} + \frac{m}{2}\left(y_m^2 + z_m^2\right) \qquad (C.5)$$

$$I_{yy} = I_{yy_{nominal}} + \frac{m}{2}\left(z_m^2 + x_m^2\right)$$

$$I_{zz} = I_{zz_{nominal}} + \frac{m}{2}\left(x_m^2 + y_m^2\right)$$

$$I_{xy} = I_{xy_{nominal}} - \frac{m}{2} x_m\, y_m$$

$$I_{xz} = I_{xz_{nominal}} - \frac{m}{2} x_m\, z_m$$

$$I_{yz} = I_{yz_{nominal}} - \frac{m}{2} y_m\, z_m$$

where m is the total vehicle mass and x_m, y_m, and z_m are the displacement in feet of the half mass from the nominal location (e.g., x_m = [135.56 - 83.6]/12.0 = 4.33 ft for the example above).

Using Equations C.5, the inertia matrix for a 45 inch center of mass displacement is

$$\mathbf{I} = \begin{bmatrix} 4554.31 & -1158.06 & -1216.66 \\ -1158.06 & 3765.31 & -1132.06 \\ -1216.66 & -1132.06 & 3484.71 \end{bmatrix} \text{slugs}\cdot\text{ft}^2 \qquad (C.6)$$

References

1. WALBERG, G.D., "A Review of Aeroassisted Orbit Transfer", AIAA Paper 82-1378, AIAA 9th Atmospheric Flight Mechanics Conference, San Diego, CA, August, 1982.

2. GAMBLE, J.D., CERIMELE, C.J., MOORE, T.E. and HIGGINS, J. "Atmospheric Guidance Concepts for an Aeroassist Flight Experiment", *The Journal of the Astronautical Sciences*, Vol 36, No.s 1/2, January - June 1988, pp. 45 - 71.

3. *Pioneering the Space Frontier - The Report of the National Commission on Space*, Bantam Books, New York, 1986.

4. "Report of the Advisory Committee on the Future of the U.S. Space Program", Washington, D.C., December, 1990.

5. "News Breaks", *Aviation Week & Space Technology*, March 25, 1991, p. 17.

6. *U.S. Standard Atmosphere, 1962*, NASA, USAF, U.S. Weather Bureau, Washington, D.C., December, 1962.

7. CERIMELE, C.J. and GAMBLE, J.D. "A Simplified Guidance Algorithm for Lifting Aeroassist Orbital Transfer Vehicles", AIAA Paper 85-0348, AIAA 23rd Aerospace Sciences Meeting, Reno, Nevada, January 1985.

8. HIGGINS, J.P. "An Aerobraking Guidance Concept for a Low L/D AOTV", OTV Memo No:10E-84-04, Charles Stark Draper Laboratory, Inc., Cambridge, MA, May 23, 1984.

9. FUHRY, D.P. "A Design Study of Onboard Navigation and Guidance During Aerocapture at Mars", CSDL-T-986, Master's Thesis, Charles Stark Draper Laboratory, Inc., Cambridge, MA, May 1988.

10. "Aeroassist Flight Experiment Mission Analysis Report", MSFC-RPT-1771, CDR issue, NASA, Marshall Space Flight Center, June 1990.

11. KWOK, J.H., and FIEDLANDER, A. "Mars Rover and Sample Return Mission Design", AAS 89-198, AAS/GSFC International

Symposium on Orbital Mechanics and Mission Design, Goddard Space Flight Center, Greenbelt, MA, 24-27 April, 1989.

12. BOURKE, R., KWOK, J., and FRIEDLANDER, A. "Mars Rover Sample Return Mission", AIAA Paper 89-0417, AIAA 27rd Aerospaces Sciences Meeting, Reno, Nevada, 9-12 January, 1989.

13. GAMBER, R., and ROGERS, L. "Aerocapture, Entry and Landing Systems for the Mars Rover Sample Return Mission", AIAA Paper 89-0422, AIAA 27rd Aerospaces Sciences Meeting, Reno, Nevada, 9-12 January, 1989.

14. LAWSON, S. "MRSR Aerocapture Configuration Design and Packaging Constraints", AIAA Paper 89-0631, AIAA 27rd Aerospaces Sciences Meeting, Reno, Nevada, 9-12 January, 1989.

15. WILLCOCKSON W.H. "L/D Requirements for the Mars Aerocapture Missions", AIAA Paper 90-2937, AIAA/AAS Astrodynamics Conference, Portland, OR, 20-22 August, 1990.

16. "Aeroassist Flight Experiment, AFESIM All-Digital Functional Simulator, Vol II, Flight Software Description", CSDL-R-1951, Charles Stark Draper Laboratory, Inc., Cambridge, MA, May15, 1987.

17. "Aeroassist Flight Experiment Attitude Control System Design Book", MSFC-RQMT-1743, CDR issue, NASA, Marshall Space Flight Center, June 29,1990.

18. ASADA, H. and SLOTINE, J.-J.E., *Robotic Analysis and Control*, John Wiley and Sons, New York, 1986.

19. SLOTINE, Jean-Jacques E. and LI, Weiping, *Applied Nonlinear Control*, Prentice Hall, Englewood Cliffs, NJ, 1991.

20. PARADISO, J., "A Highly Adaptable Steering/Selection Procedure for Combined CMG/RCS Spacecraft Control", CSDL-R-1835, March 1986.

21. PARADISO, J.A., "Application of Linear Programming to Coordinated Management of Jets and Aerosurfaces for

Aerospace Vehicle Control", CSDL-R-2065, Charles Stark Draper Laboratory, Inc., Cambridge, MA, November, 1988.

22. BERGMANN, E.V. and BLANCHARD, R.C. "In Flight Demonstration of Mass Property Identification on the Aeroassist Flight Experiment", Society of Allied Weight Engineers 49th Annual Conference, May 1989.

23. BERGMANN, E.V., WALKER, B.K., and LEVY, D.R. "Mass Property Estimation for Control of Asymmetrical Satellites", AIAA Paper 85-1857, Guidance, Navigation, and Control Conference and *Journal of Guidance, Control and Dynamics*, Vol. 10, #5, Sept. - Oct. 1987.

24. LEVY, D.R. "Mass Property Estimation with Jet Failure Identification for Control of Asymmetrical Satellites", CSDL-T-831, Master's Thesis, Charles Stark Draper Laboratory, Inc., Cambridge, MA, December, 1983.

25. MACIEJOWSKI, J.M., *Multivariable Feedback Design*, Addison-Wesley Publishing Company, Reading, MA, 1989.

26. DOYLE, J.C. "Analysis of Feedback Systems with Structured Uncertainties", *IEEE Proc.*, vol 129, pp. 242-250, 1982.

27. DOYLE, J.C. "Structured Uncertainty in Control System Design", *Proceedings of IEEE Conference on Design and Control*, pp. 260-265, December, 1985.

28. BERGMANN, E., CROOPNICK, S., and DALY, K. "RCS Architectural Issues for Space Vehicle Rendevous and Proximity Operations", CSDL-P-2007, presented to NASA Rendevous and Proximity Operations Workshop, NASA Johnson Space Center, February, 1985.

29. ATHERTON, D.P., *Stability of Nonlinear Systems*, Research Studies Press, New York, 1981.

30. CRANDALL, S.H., KARNOPP, D.C., KURTZ, E.F., Jr., PRIDMORE-BROWN, D.C., *Dynamics of Mechanical and Electromechanical Systems*, Robert E. Krieger Publishing Company, Malabar, FL, 1968.

31. "Analysis Reaction Control System (RCS) Aeroassist Flight Experiment (AFE)", EP53-ANAL-010, CDR issue, George C. Marshall Space Flight Center, June 29, 1990.

32. CRAWFORD, B.S. "Operation and Design of Multi-Jet Spacecraft Control Systems", M.I.T. Doctoral Thesis, CSDL-T-509, September 13, 1968.

33. STRANG, G., *Introduction to Applied Mathematics*, Wellesley-Cambridge Press, Wellesley, MA, 1986.

34. GELB, A. (editor), *Applied Optimal Estimation*, The M.I.T. Press, Cambridge, MA, 11th printing, 1989.

35. RICHFIELD, R.F., WALKER, B.K., and BERGMANN, E.V. "Input Selection and Convergence Testing for a Second Order Mass Property Estimator", AIAA 1986 Guidance, Navigation and Control Conference and *Journal of Guidance, Control, and Dynamics*, Vol. 11, #3, May - June 1988.

36. "Mass Properties Report, Aeroassist Flight Experiment", MSFC-RPT-1549, NASA, Marshall Space Flight Center, May 26,1989.

37. "Aerodynamic Issues for Aeroassist Flight Experiment (AFE) Aeropass Simulations", letter from ED3/Chairman, AFE Aerodynamics Chairman, ED3/8808-120, NASA, Lyndon B. Johnson Space Center, Houston, TX, August 25, 1988.

38. PRESS, W.H., FLANNERY, B.P., TEUKOLSKY, S.A., VETTERLING, W.T., *Numerical Recipes - The Art of Scientific Computing (FORTRAN) Version)*, Cambridge University Press, New York, 1990.

39. BATTIN, R.H., *An Introduction to the Mathematics and Methods of Astrodynamics, American Institute of Aeronautics and Astronautics*, Inc., New York, 1987.